

FIELD-SCALE EXPERIMENTS AND ANALYSIS OF TURBULENT FLOW STRUCTURES IN A RIVER REACH WITH GROYNES

FELDVERSUCHE AND ANALYSE VON TURBULENTEN STRÖMUNGSMUSTERN IN BUHNENFELDERN



Diplomarbeit

Verfasst und eingereicht von
Christine Anlanger

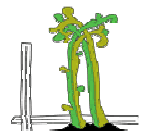
Wien, im Juni 2008

Betreuer:

O.Univ.Prof. Dr. Florin FLORINETH
Univ.Ass. Dipl.-Ing. Dr. Johann Peter RAUCH

**University of Natural Resources and Applied Life
Sciences, Vienna**

Department of Civil Engineering and Natural Hazards
Institute of Soil Bioengineering and Landscape Construction



ACKNOWLEDGMENTS

This master thesis evolved from a research project which consists of two experiments on shallow mixing layers and is entitled “Fluid Dynamics Laboratory in the Field”. The project is collaboration between the Leibniz-Institute of Freshwater Ecology and Inland Fisheries Berlin (IGB) and the Environmental Fluid Mechanics section of the TU Delft in the Netherlands. I participated in the second experimental program on groyne fields during summer 2007 and conducted the post-processing and analyse of the data during my stay at IGB.

The time during working on this master thesis has been interesting and challenging. Many people have, knowingly or unknowingly, contributed to the successful completion of my master's degree. Special thanks for their support go to the following people:

To my supervisors O.Univ.Prof. Dr. Florin Florineth and Univ.Ass. Dr. Johann Peter Rauch from the BOKU, Vienna, for their support and for the freedom they gave me to work on the topic and for making it possible to go to Berlin and stay at the IGB.

To Dr. Alexander Sukhodolov and Dr. Ingo Schnauder from the IGB in Berlin. They introduced me to all the measurement techniques we applied out in the field; they helped with the post-processing and analyse of the complex data set, they always took the time to answer all my questions and concerns and guided me through the whole thesis. Thank you!

To Achim Reiprich, Dr. Nils Rüter, Friederike Gabel, Bernhard Vowinckel, Dr.ir. W. Uijttewaal, Christiaan Erdbrink and Dr. Carsten Wirtz for the support during the extensive field campaign and for valuable comments. To Wernher Brevis helping out in the field and for providing the records with the PTV streaklines.

To my family who supported me patiently during the whole time of my studies. And to Mario who not only helped me with proof reading and the layout of the thesis but gave me the mental support, especially during the though last weeks before submission of the thesis.

ABSTRACT

The flow around groynes is controlled by many complex phenomena associated with turbulence – e.g. the occurrence and interaction of multiple mixing layers, which are created at the interface of flows of different velocities. Large-scale structures advected in the mixing layers have a significant influence on the dispersion of nutrients, pollutants and sediment transport. Thus, the aim of this thesis is to investigate mixing layer development and interaction in groyne fields.

The gap between detailed lab studies which are conducted under idealised flow conditions and large-scale field studies which provide realistic but coarse data gave the motivation to establish a “lab in the field” at the Leibniz-Institute of Freshwater Ecology and Inland Fisheries Berlin (IGB). Seven groynes were placed into a reach of the river Spree near Berlin and their effects on the mean and turbulent flow patterns were investigated for submerged and emerged conditions. Measurements were conducted with acoustic Doppler velocimeters (ADV) and coherent structures were additionally visualised by particle tracking experiments and uranin dye injections.

Mean velocity vector plots revealed differing flow structures for emerged and submerged conditions. Contrary, coherent structures advected in the global mixing layer (GML) which evolves from the horizontal mean velocity gradient between the main channel and the groyne fields are characterised by the same peak frequencies for both cases. These coherent structures are interacting with the flow inside the groyne field and dominating the instationary flow patterns. For the submerged case the imprints of those structures inside the groyne field were less pronounced but still recognisable. Furthermore the horizontal detached mixing layer (DML), which is created at each groyne tip, is interacting with a vertical DML at the lee-side of the groynes causing complex three-dimensional flow structures when groynes were submerged.

ZUSAMMENFASSUNG

Die Strömung in Buhnenfeldern ist geprägt von komplexen turbulenten Strömungsvorgängen. Im Grenzbereich zweier Strömungsschichten mit unterschiedlicher Geschwindigkeit bilden sich Mischungsschichten aus in denen sich großräumige kohärente Wirbelstrukturen bilden. Diese Strukturen tragen wesentlich zur Ausbreitung von Nähr- und Schmutzstoffen und zum Sedimenttransport bei. Das Ziel dieser Arbeit ist es, die Entstehung und die Interaktion dieser Mischungsschichten in Buhnenfeldern zu untersuchen.

Mit Laborversuchen können natürlichen Strömungsbedingungen nur bedingt wiedergegeben werden. Dies war die Motivation für das Leibniz-Institut für Gewässerökologie und Binnenfischerei Berlin (IGB) ein "Labor im Feld" zu etablieren. Sieben Buhnen wurden in einem Gewässerabschnitt der Spree, nahe Berlin, eingebaut, um die mittlere und turbulente Strömung unter um- sowie überströmten Verhältnissen zu untersuchen. Die Experimente wurden mit Hilfe akustischer Strömungsmessgeräte, "Particle Tracking" Methoden und Tracerversuchen durchgeführt.

Vektorgraphiken der mittleren Geschwindigkeiten ergaben unterschiedliche Strömungsmuster für um- und überströmte Buhnen. Im Gegensatz dazu zeigte sich, dass kohärente Strukturen in der globalen Mischungsschicht, welche aufgrund des Geschwindigkeitsgradienten zwischen der Strömung im Buhnenfeld und im Hauptgerinne entsteht, gleiche charakteristische Frequenzen aufwiesen. Diese Strukturen interagierten mit der Strömung im Buhnenfeld und dominierten die dortigen instationären Strömungsverhältnisse. Im überströmten Fall war diese Dominanz weniger ausgeprägt. Zusätzlich kam es im überströmten Fall zu einer Interaktion zwischen der Mischungsschicht, die durch die Ablösungserscheinungen an jedem Buhnenkopf hervorgerufen wird und einer vertikalen Mischungsschicht an der Lee Seite der Buhne. Daraus resultierten an dieser Stelle komplexe dreidimensionale Strömungsmuster.

TABLE OF CONTENTS

1	Introduction	1
2	State of the art and problem identification	3
2.1	General	3
2.1.1	History of groyne constructions	3
2.1.2	Function of groynes	4
2.1.3	Groyne types and classification	4
2.1.4	Design criteria for groynes	5
2.2	State of the art	7
2.2.1	Fundamentals of shallow mixing layer flows	7
2.2.2	Flow hydrodynamics under emerged conditions	11
2.2.3	Effect of aspect ratio	15
2.2.4	Effect of groyne orientation	15
2.2.5	Effect of the stage of submergence	16
2.2.6	Effect of groyne design	18
2.2.7	The role of groynes for ecology	18
2.3	Problem identification	20
2.4	Aim and objectives of the thesis	22
3	Material and methods	23
3.1	Experimental river reach	23
3.1.1	Geographical location	23
3.1.2	Hydraulic regime	24
3.1.3	Morphology	26
3.2	Groyne construction and experimental setup	28
3.3	Field experiments and measurements	30
3.3.1	ADV point measurements – short-term	30
3.3.2	ADV point measurements – long-term	38
3.3.3	Tracer studies	40
3.3.4	Visualisation technique – Dye Injections	41
3.3.5	Particle tracking velocimetry (PTV)	42
3.3.6	Water level readings	43
3.3.7	Topographical survey	43
3.4	Experimental program - overview	45
4	Experimental results and analysis	46
4.1	Mean velocity patterns	46
4.2	Turbulent kinetic energy (TKE) patterns	51
4.3	Stresses, bottom friction and shear velocity	55
4.4	Coherent structures and exchange processes	57
5	Discussion	63
5.1	Mean velocity patterns	63
5.2	Turbulent kinetic energy (TKE) patterns	69
5.3	Coherent structures and exchange processes	71
6	Summary and conclusions	76
7	Literature	79

TABLE OF FIGURES

Figure 1.1: Airborne photos of groynes at the river Elbe and at the river Danube	1
Figure 2.1: Design of a classical Dutch groyne and historical map of the Müggelspree with groynes, whose remnants can still be found today	3
Figure 2.2: Forward and backward inclined groynes and different plan view shapes of groynes ...	5
Figure 2.3: Kink groynes combining the positive effects of different inclination angles and a “slotted groyne” at the river Elbe	6
Figure 2.4: Development of a shallow mixing layer	7
Figure 2.5: Correlation of scaled mixing layer width and scaled distance between mixing layer beginning and point of interest in the mixing layer.	9
Figure 2.6: Different types of flow patterns in groyne fields	11
Figure 2.7: Particle trajectories using intermittent photography of floating candles, with the main flow direction from left to right	11
Figure 2.8: Mixing layer developing at the tip of the groyne	12
Figure 2.9: Mixing layer developing at the interface of the groyne field and the fast stream and eddies that are shed at the groyne tips, merge and grow in size during their travel downstream	13
Figure 2.10: Recirculation pattern depending on the aspect ratio	15
Figure 2.11: Groyne fields with different inclination angles and their influence on the development of the two gyre system	15
Figure 2.12: A sequence of backward inclined groynes at the river Elbe	16
Figure 3.1: Map of the federal states of Berlin, airborne pictures and a picture showing the location of the experimental river reach	24
Figure 3.2: Elevation of the water level calculated from water level readings from pressure loggers of IGB compared with water level readings at gauging poles during experiment 1 and 2; discharges according to mean cross section at Freienbrink and tracer experiments	25
Figure 3.3: Stage-discharge relation at the experimental river reach	26
Figure 3.4: Stage – discharge curve of the weir “Grosse Tränke” 2007	27
Figure 3.5: Riverbed elevation in May 2007 before the experiments	27
3 Figure 3.6: Riverbed elevation, and mean sediment particle diameter in 2005	28
Figure 3.7: Experimental setup, frame of fully shaped groynes with top up for emerged conditions, construction works	29
Figure 3.9: Experimental setup for ADV point measurements and positioning of probes.	30
Figure 3.10: ADV mounting system	31
Figure 3.11: Nortek Doppler Velocimeter	31
Figure 3.12: Sensor head of an NorTek Doppler Velocimeter	32
Figure 3.13: Schematic diagram of pulse-to-pulse coherent method	32
Figure 3.14: NorTek Vectrino Doppler Velocimeter	33
Figure 3.15: Stationary analysis for mean velocities and variances in the mixing layer	34
Figure 3.16: Stationary analysis for mean velocities and variances in the groyne field.	34
Figure 3.17: ExploreV with filtered time series, correlation and SNR scores and main statistical characteristics of measurement during submerged conditions in groyne field five	35
Figure 3.18: Power spectra for streamwise, transverse, and vertical components and statistics of the velocity distribution recorded during submerged conditions upstream near groyne 6 ..	36
Figure 3.19: ADV positions for long term measurements	38
Figure 3.20: Change of NDV probe orientation	38
Figure 3.21: Dye injection for tracer studies: uranin dye injected as a line source across the river	40
Figure 3.22: Distribution of uranin concentration over time for experiment 1 and experiment 2 ..	41

Figure 3.23: Dye injection: Dissolving of uranin dye, fixing of the injection tube, and injection.....	41
Figure 3.24: Experimental river reach with gauging stations (GS) 1 to 4.....	43
Figure 3.25: Topographical survey of river reach with groynes – measurement points.....	43
Figure 3.26: Points measured by total station for geographical coordinates of groynes and groyne fields.....	44
Figure 4.1: Vector plots of mean velocity for emerged conditions: near the bed, at groyne crest level, and near the surface.	47
Figure 4.2: Vector plots of mean velocity for emerged conditions in longitudinal sections	48
Figure 4.3: Vector plots of mean velocity for submerged conditions.....	50
Figure 4.4: Vector plots of mean velocity for submerged conditions in longitudinal sections.....	50
Figure 4.5: Mean velocity vector distributions in transverse sections through the groyne field during submerged condition.....	51
Figure 4.6: Turbulent kinetic energy distribution near the riverbed and near the flow surface in the groyne field during emerged condition	52
Figure 4.7: Turbulent kinetic energy distribution in longitudinal sections through the groyne field during emerged conditions.....	53
Figure 4.8: Turbulent kinetic energy distribution near the riverbed and near the flow surface in the groyne field during submerged condition.	54
Figure 4.9: Turbulent kinetic energy distribution in longitudinal sections through the groyne field during submerged conditions.....	55
Figure 4.10: Flow velocity record for transverse velocities in the mixing layer at position 6.....	57
Figure 4.11: ADV setup for long term measurements, and averaged auto-correlation spectrum for the transverse velocity component averaged for locations 3 and 6 in the GML.....	58
Figure 4.12: Time series of water level fluctuations in the groyne field at positions pos_4 and pos_5	59
Figure 4.13: Auto-spectra for water level fluctuations in the groyne field at positions pos_4 and pos_5.....	60
Figure 4.14: Cross-correlation function for the water level fluctuations measured synchronously at positions 4 and 5 and 4 and 6, respectively.....	60
Figure 4.15: Overview of measured time series used for auto-spectra for submerged conditions, and auto-spectra in the mixing layer during submerged conditions.....	61
Figure 4.16: Auto-spectra in the groyne field during submerged conditions at point D.....	62
Figure 5.1: Uranin dye visualisation of the emerged flow pattern; injection point at tip of groyne 5.....	63
Figure 5.2: PTV streaklines for emerged conditions; recorded area covers groyne field 5 and 6, and part of the main stream.	64
Figure 5.3: Mean flow patterns in groyne fields under emerged conditions: Lab: Sukhodolov et al. 2002, Weitbrecht et al. 2008; Numerics: McCoy et al. 2008, Kimura & Hosoda 1997; and Field: Engelhardt et al. 2004, and Fujita et al. 1998.....	65
Figure 5.4: Example of a PTV record from groyne field 5 during submerged conditions	66
Figure 5.5: Mean flow patterns in groyne fields under submerged conditions: Lab: Brevis et al. (2008), Uijttewaal (2005), Tominaga et al. (2001); Numerics: McCoy et al. (2007)	67
Figure 5.6: Channel flow with two submerged groynes used in a LES simulation	68
Figure 5.7: Flow patterns over rough surfaces, vertical plain; after Morris.....	69
Figure 5.8: Distribution of TKE in a groyne field during emerged conditions: Field: Engelhardt et al. 2004 (a); Numerics: McCoy et al. 2008; Lab: Yossef 2005, and Uijttewaal 2005.	70
Figure 5.9: Distribution of the TKE over a groyne field.....	71
Figure 5.10: Auto-spectra for transverse velocities in the GML: Lab: Yossef 2005; Field: Engelhardt et al. 2004; Numeric McCoy et al. 2008; this study	72

Figure 5.11: Standing wave with one overtone.....	73
Figure 5.12: Auto-spectra for transverse velocities during submerged conditions: at the lee-side of the groyne: lab experiments (Yossef 2005), and this study; in the downstream half of the groyne field: lab experiments (Yossef 2005), and this study.....	75

1 INTRODUCTION

Groynes are small dams which are constructed transverse to the main flow direction in rivers or along coastlines in maritime environment. They deflect the flow away from banks and shores and confine its lateral extent – with strong impact on sediment transport and deposition/erosion patterns. Groynes reduce the cross-sectional area for the free-flow and thus increase the main channel flow velocities. Higher flow velocities cause higher sediment transport rates and often lead to bed erosion which in turn increases water depths - a desirable aim for navigation and thus one of the main reasons for groyne constructions. Often groynes are constructed in sequences to maximise their effect. Furthermore, the groyne fields between the groynes have important effects. They are trapping sediments with significance for the overall sediment budget of the river and can provide valuable habitats for aquatic and terrestrial flora and fauna.



Figure 1.1: Airborne photos of groynes at the river Elbe close to Wittenberge, Germany and the at river Danube downstream of Vienna, Austria (images: Google earth)

Groynes were first built for the purpose of bank and shoreline protection and to maintain navigability during low-water periods. Many navigable rivers, like the river Elbe and parts of the river Danube are intensively equipped with groynes (Figure 1.1). These are subjected to destructive hydrodynamic forces during flood events and need maintenance and repair to guarantee their functioning. According to a resume of WIRTZ (2004) on the state of preservation of groynes in the river Elbe in 2002 (Elbe-kilometre 290.7 to 502.2, around the city of Magdeburg), 28% of 2967 existing groynes are defect while 1117 groynes have already been repaired since 1995. 74.5% of the defect groynes are subject to major damage, 19.5% are limited in their hydraulic function and 6% have no more hydraulic function at all (WIRTZ 2004). The report highlights the potential for alternative groyne design to lower the costs of maintenance as well as construction.

On top of the classical groyne concepts and functions, new aspects have evolved within the last decades and due to the rise of ecological issues - which has been legally manifested in the EU water framework directive in 2000. The WFD demands that the current ecological state of surface waters cannot be allowed to deteriorate and must be kept on a good level. In this context, an alternative and modern approach to groynes is an important step towards an improvement of the structural diversity of aquatic ecosystems. This potential has been identified at BOKU where groynes are constructed as morphologic and flow-diversifiers from living materials such as willows.

In order to plan and implement optimised and multi-functional groyne design, one has to understand the exchange and transport processes between the main channel of a river and the groyne field. The first step towards understanding those processes is to study flow and turbulence patterns and their effect on morphology. Although current hydraulic research improved the accuracy of predicting flows in simple conditions, natural geometries with mobile beds and at high Reynolds numbers are presently predicted with uncomfortable uncertainties. The situation arises from a gap between highly detailed but also highly idealised experiments in laboratory flumes or by means of numerical codes on one side and scarce, relatively uncontrolled and coarse field measurement on the other.

This thesis evolved from a research project aiming to bridge this gap and to expand the analysis of turbulent flow structures towards both, higher Reynolds numbers and realistic flow conditions. The currently still running project is entitled “Fluid Dynamics Laboratory in the Field” (2006-2009), and involves collaboration between the Leibniz-Institute of Freshwater Ecology and Inland Fisheries (IGB) and the Environmental Fluid Mechanics section of the TU Delft. The project consists of a study on shallow mixing layers at confluences and a study on recirculating flows around groyne fields - both based on field measurements conducted at the river Spree near Berlin, Germany. I participated in the second experimental program on groyne fields during summer 2007 and conducted the post-processing of the data during my stay at IGB - which forms the base for this work.

The thesis is structured into six parts, starting with a short introduction to the history and function of groynes in chapter one, followed by classification concepts of groynes and their most important design criteria. The second chapter will introduce the state of the art in literature concerning the flow hydrodynamics in groyne fields. Chapter three describes the measurement campaign including a detailed summary on methods and techniques employed, followed by a description on how data was collected and processed. The results and analysis of the field experiments are presented in chapter four including many graphs, tables and photographs. The fifth chapter is a discussion of the results in the frame of previous publications and the state-of-the-art on the topic. The thesis closes with a summary and conclusions in the final chapter six.

2 STATE OF THE ART AND PROBLEM IDENTIFICATION

The chapter starts with a brief summary of the history of groynes and their construction. This is followed by an overview on the functions of groynes and classification schemes of groynes - considering construction materials, stage of submergence, main effects on stream flow and shape. Design considerations for groynes are presented on the basis of this classification scheme

The second part of this chapter focuses on a review of published literature about flow structures and exchange processes in groyne fields including laboratory and field studies as well as numerical simulations. After a brief introduction of flow patterns in groyne fields, the state of the art of flow around a sequence of emerged groynes will be described. This will be followed by a review on literature dealing with effects of different aspect ratios, groyne orientation, stages of submergence, and groyne design. Finally, aspects of the role of groynes in ecohydraulics will be discussed. Based on this summary, a problem identification will be derived which then form the base for the aims and objectives of the experimental program and the thesis in general.

2.1 General

2.1.1 History of groyne constructions

The beginning of coastal engineering and construction of groynes was marked by the founder of coastal engineering in the Netherlands, Andries VIERLINGH (1507–1579). Around 1576, he wrote the first essay on groyne construction (“*Tractaet van Dyckagie*”) which was not published until 1920 (BIJKER 2007). Vierlingh described several groynes and their main purpose was to stimulate accretion in inter-tidal areas and shore protection against tidal currents. The essay contains extensive descriptions of the functioning of these groynes and incorporates groyne spacing and orientation.

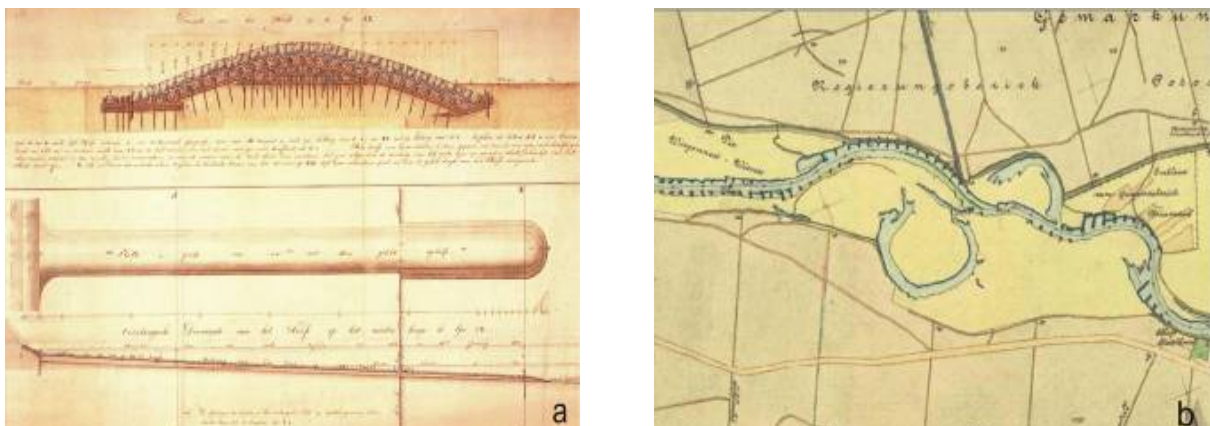


Figure 2.1: Design of a classical Dutch groyne from 1835: foundation of brushwood covered by stones (taken from VERHAGEN 2009) (a), historical map of the Müggelspree with groynes, whose remnants can still be found today (taken from KÖHLER et al. 2002) (b).

The prototypes of these groynes were simple, low crested structures constructed with wooden poles. Later, in the 18th century the design changed from a wooden structure to a stone structure, which was more resistant (Figure 2.1a). In Germany, in former Prussia, river engineering activities started under Emperor Friedrich Wilhelm (1620–1688). He built a navigation canal connecting the river Spree at Müllrose with the river Oder at Brieskow. With continuously increasing industrialisation and colonisation, shipping of goods to Berlin became more and more important and waterways had to be broadened and reinforced. Hence, an increasing number of groynes were built to assure sufficient water depths for navigation and to protect the banks against erosion at the beginning of the 18th century. Initially, single groynes were built for local deflection of the flow but soon whole sequences were constructed for better effectiveness (Figure 2.1b).

2.1.2 Functions of groynes

The main functions of river groynes are:

- Reduction of the cross section of the river or main channel,
- Increase of water levels by reducing the cross-sectional mean velocity,
- Variation of flow velocities in the cross section with increased velocities in the main channel and reduced velocities in the groyne fields,
- Increase erosion to clear the navigable main channel from sediments (and at the same time sediment deposition in the groyne fields),
- Prevention of bank erosion and protection of structures along the banks.

2.1.3 Groyne types and classification

The following types of groynes can be distinguished according to their construction, effects on stream flow and geometry (PRZEDWOJSKI et al. 1995):

Classification according to methods and materials of the construction:

Groynes can be constructed either permeable out of piles, bamboo or timbers or impermeable (also called solid groynes) using materials such as concrete, steel, rock, gravel, gabions etc. Impermeable groynes allow the water to flow through at reduced velocities causing less flow disturbance.

Classification according to submergence stage ($\zeta = \text{water depth } h / \text{groyne height } H_g$):

Groynes may be submerged or emerged. Groynes are emerged when their crest is higher than the water surface level and submerged when the flow is overtopping the crests. In the “natural” case of varying water levels between low flow and flood events, the degree of submergence also varies. Emerged groynes are typically realised as impermeable structures whereas submerged groynes are sometimes permeable to avoid strong acceleration of the flow over the top which enhances erosion.

Classification according to effects on stream flow:

Groynes may attract, repel or deflect the stream flow depending on their orientation relative to the main flow direction. Attracting groynes point downstream (forward inclined groynes, inclination angle α is bigger than 90°), they serve to attract the stream flow towards themselves and do not repel the

flow towards the other bank. Deflecting groynes are generally short ones and used of local protection. They serve to change the direction of the flow without repelling it. Repelling groynes point upstream (backward inclined groynes, inclination angle α is smaller than 90°). They serve to force the flow away from themselves.

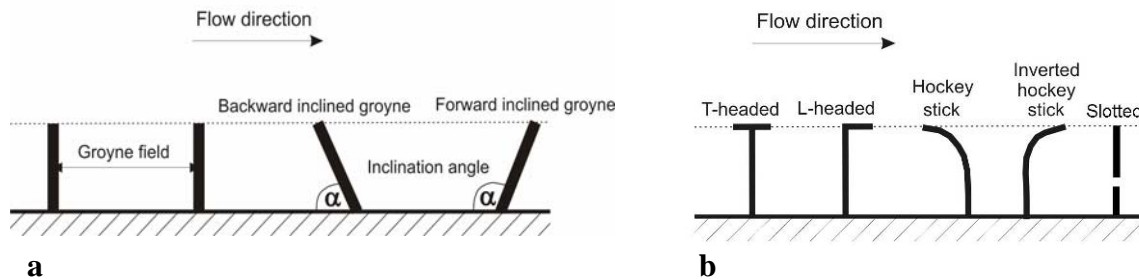


Figure 2.2: Forward and backward inclined groynes (a) and different plan view shapes of groynes (b).

Classification according to groyne plan view shape:

The plan view shape of groynes can be straight, T-headed or L-headed. Other examples are hockey stick and inverted hockey stick groynes or the recently developed slotted groynes (Figure 2.2b).

2.1.4 Design criteria for groynes

Groynes have proven to be effective to guarantee navigability in rivers. However, contemporary river management has to re-evaluate groyne design by taking into account new aspects. One of the most pressing aspects are highly variable stages of submergence due to dramatically increased extreme events or the ecological value as habitats due to plan view and cross sectional shape, length and spacing, as well as construction materials.

The new context comprises contradictory demands to the submergence stage. Groynes should reduce the cross section of the main channel to provide sufficient water depths for navigation during low water on one hand side, but their retarding effect on the flow should be minimised during flood events on the other. Implications for design are that too high groynes cause unnecessary high flow resistance during floods while too low groynes decrease the effect to confine the flow at mean water levels (UIJTTEWAAL 2005). The standard compromise for this problem is to design the groyne crest height to reach up to mean water levels (MQ). This means that during periods with higher discharges such groynes are fully submerged.

The geometry (plan view and cross sectional shape) and the quantity of groynes in a sequence should effectively reduce the flow velocity close to the banks to ensure bank protection but should also be economically convenient. Groynes are aligned either at an angle or perpendicular to the flow. Experience showed that repelling groynes are more effective in terms of bank protection (RIEPE 1930). During periods of high discharges, forward inclined groynes function like weirs and the

overflowing water is directed to the adjacent river bank and causes erosion (LANGE & LECHER 1989). During lower discharges they are efficient in trapping fine sediments and organic matter. In recent investigations, the positive effects of forward and backward inclined groynes were combined by using groynes with a kink (HENTSCHEL & ANLAUF 2002) as shown in Figure 2.3a.

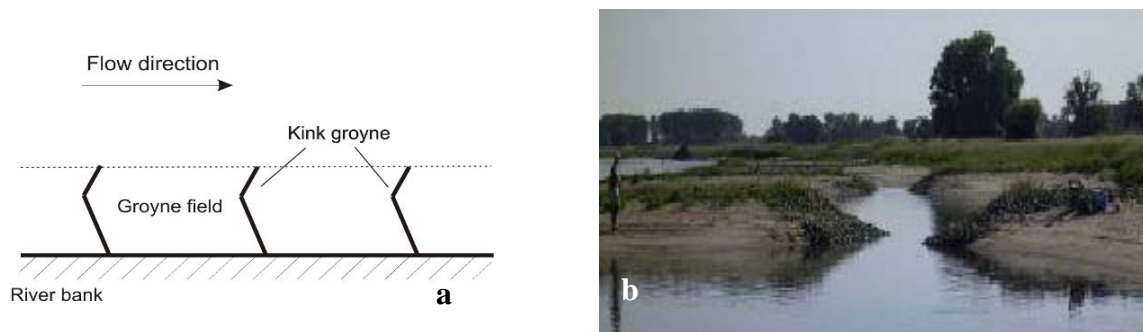


Figure 2.3: Kink groynes combining the positive effects of different inclination angles (a), and a “slotted groyne” at the river Elbe (b).

Another alternative groyne design are slotted groynes which exhibit a V-shaped opening close to the bank (Figure 2.3b). These groynes provide improved ecological value in terms of biodiversity and are an easily realisable “bio-upgrade” of already existing standard groynes, while other parameters (bank protection, flood safety and main channel velocities) are not negatively affected.

Groyne crests may be either at the same level or sloped downwards from the bank towards the groyne head. For bank protection, sloping-crested groynes are recommended by ALVAREZ (1989). Sloping-crested groynes have the advantage of reducing scour at the groyne tip, requiring less material for construction and accelerate the deposition of sediment between them. Groynes of that kind work best perpendicular to the flow or backward inclined. For navigation channel control, groynes with constant crest height work best perpendicular or forward-inclined relative to the main flow direction (RICHARDSON et al. 1975).

In a system of a sequence of groynes, the groyne length “ L_g ” (m) depends on its location and the streamwise spacing “ L_f ” (m). The spacing is the distance to the subsequent groyne downstream. The aspect ratio L_g / L_f determines the overall flow patterns in a groyne field. RICHARDSON et al. (1975) recommends an aspect ratio of 0.5 to 0.7 for a well-defined deep navigation channel, whereas for bank protection the ratio should range from 0.5 to 0.2. If the distance between groynes is too large, a meander loop may form between groynes resulting in channel degradation and local bank erosion which will hinder navigation. If the distance between groynes is too small, construction costs will increase while the effectiveness of the sequence will decrease.

Considering groyne design in terms of permeability it has to be mentioned that permeable groynes allow the water to flow through at reduced velocities. Thus, permeable groynes filter the passing water and simultaneously provide habitat for aquatic organisms. However, permeable groynes are less robust

than solid groynes and may afford more maintenance (ZUISEN et al. 2007). Furthermore, fully submerged permeable groynes are relatively ineffective and maintain a high conveyance capacity of the river section (UIJTTEWAAL 2005).

2.2 State of the art

2.2.1 Fundamentals of shallow mixing layer flows

Shallow flows exist where the horizontal length scales of the flow domain are much larger than the depth. This is the case for many large rivers, estuaries or coastal areas. Also the lowland river Spree with a width to depth ratio of about $b/h = 20$ belongs to this class. Shallow flows are vertically confined between the bed and the water surface and large coherent structures can only grow in horizontal direction. This is why they are considered quasi two-dimensional in shallow flows. Another characteristic of shallow flows is that the turbulent boundary layer extends over the entire water depth. The bottom roughness imposes shear stresses on the water body which causes energy dissipation and production of bottom turbulence. This bed-generated shear and bottom friction plays a major role in shallow flows which will be summarised in the following subchapters.

Shallow mixing layers

Mixing layers develop where two flows with different velocities merge, e.g. at river confluences, harbour entrances, between groyne fields or floodplains and the main channel or at the borders of recirculation zones. Mixing layers control the exchange of momentum and mass, including all dissolved substances, suspended particles and sediment transported in the river.

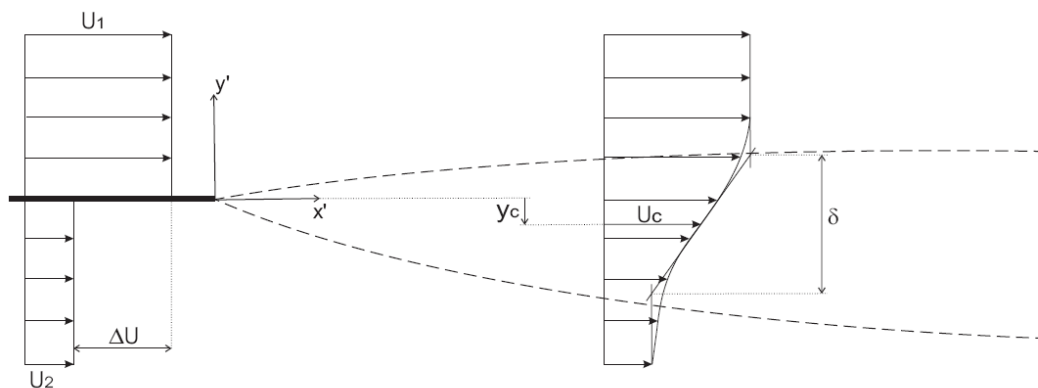


Figure 2.4: Development of a shallow mixing layer

In general, shallow mixing layers are characterised by coherent structures of two length scales. First, there are bed-shear generated vertical structures with a characteristic length scale of order magnitude of the water depth. Second, horizontal structures are generated by the shear due to the horizontal velocity difference. These structures can only grow horizontally and are characterised by the mixing layer width δ (m) which often is one order of magnitude larger than the water depth. The origin of mixing layers are Kelvin-Helmholtz instabilities in the shear plain which grow with downstream

distance into alternating roller-type structures. These rollers merge and pair (“vortex pairing”) and grow in size. This process is associated with the inverse energy-cascade. The presence of these two types of structures and their interaction are the characteristic features of shallow mixing layers and still challenges hydraulic and turbulence research.

Spreading rate and mixing layer width δ

CHU & BABARUSI (1988) first investigated the transverse spreading rate of a shallow mixing layer in a flume by initially separating the part-streams by a splitter plate. The spreading rate is defined

$$\frac{d\delta}{dx} = \alpha \frac{\Delta U(x)}{U_{c,0}}$$

where $\Delta U(x)$ is the velocity difference at the apex of the splitter plate and $U_{c,0}$ is the average velocity across the mixing layer at the apex and α the (initial) entrainment coefficient. The factor α was determined to be 0.18 (CHU & BABARUTSI 1988) which was twice as large as for free mixing layers. Chu & Babarutsi concluded that the layer grows until the stabilising influence of the bed friction dominates and the structures start to dissipate. This mechanism was incorporated in their definition of the entrainment coefficient by introducing a stability number S . This number is defined as the ratio between the stabilizing effect of bed friction and the destabilizing effect of transverse shear. For the shallow mixing layer, the bed-friction number is defined as (CHU & BABARUTSI 1988):

$$S = \frac{c_f \delta U_{c,0}}{2h \Delta U}$$

where c_f is the bottom friction factor which is defined as $c_f = 2(u_* / U)^2$ (with u_* as the bottom shear velocity), and h is the water depth. At some point downstream this parameter reaches a critical value S_c associated with dissipation of structures. For $S < S_c$ the bottom friction has a negligible effect and the growth of the instabilities in the mixing layer is not hindered. In case $S > S_c$ the growth of instabilities is constricted by bottom friction. From their experimental data, CHU & BABARUTSI (1988) determined S_c to a value of 0.09. With this concept, CHU & BABARUTSI (1988) introduced scaling parameters for the downstream distance and width of the mixing layer:

$$\delta^* = f(x^*), \quad \delta^* = \frac{c_f \delta}{\lambda_0 h}, \quad x^* = 2c_f \frac{x}{h}, \quad \text{and} \quad \lambda_0 = \frac{\Delta U}{U_1 + U_2} = \frac{\Delta U}{2U_{c,0}}$$

where δ^* and x^* are the scaled width and length of the mixing layer, u_1 is the velocity in the fast stream and u_2 is the mean velocity in the slower stream.

This scaling was also used in a later study by UIJTTEWAAL & BOOIJ (2000) but revealed an initial growth rate of the shallow mixing layer in agreement with free mixing layers - 0.09 instead of 0.18. UIJTTEWAAL & BOOIJ (2000) suggested that the flow in CHU & BABARUTSI’s experiments was not fully developed due to a relatively short inflow and splitter section. In Figure 2.5, scaled data of both studies are compared with the shallow mixing layer experiments at IGB in 2006 (experiments 1-

3). Additional PIV data were taken from UIJTTEWAAL & BOOIJ (2000) and V. PROOIJEN & UIJTTEWAAL (2002). The figure points out that the bottom friction coefficient is a valid parameter to scale studies from lab and field. Furthermore, the field study at IGB supports UIJTTEWAALS & BOOIJ's hypothesis of the initial spreading rate and shows that in the field experiments the inflow was fully developed.

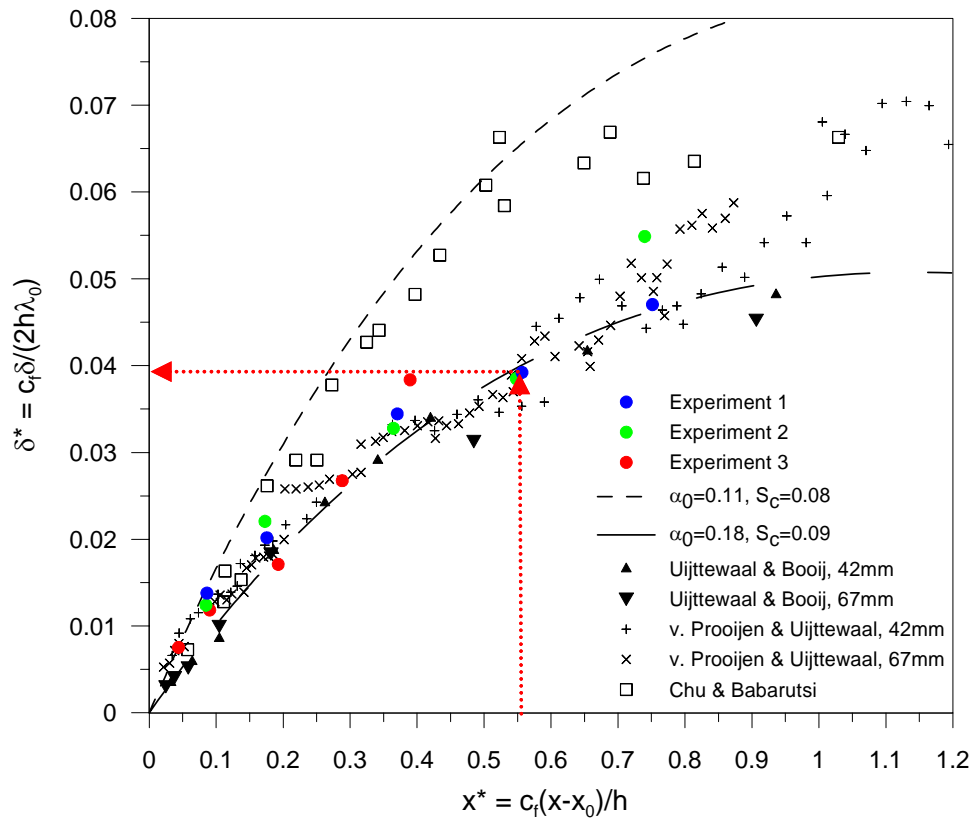


Figure 2.5: Correlation of scaled mixing layer width δ^* and scaled distance between mixing layer beginning and point of interest in the mixing layer x^* (unpublished data, IGB).

Even though the discussed papers do give some insight on the interaction between small-scale bed-generated turbulence and large-scale horizontal structures, the whole extent of this interaction is not fully understood yet – but also plays a role in groyne field hydrodynamics. However, the bottom friction factor is an important scaling parameter which will be used later in this thesis.

Frequency of coherent structures

SUKHODOLOV & SUKHODOLOVA (2007) conducted field experiments on vertical mixing layers above submerged aquatic macrophytes. From theoretical considerations, they derived an analytical model relating the eddy turnover time to the length scale of structures and the mean dissipation rate. Applied to their field data, the predicted frequencies agreed well with the measured ones. In a second step, the model was applied to shallow mixing layers (see SCHNAUDER et al. 2008) – incorporating characteristic scales and velocities of the mixing layer as well as the bottom friction coefficient. This resulted in the following Strouhal-number for shallow mixing layer structures:

$$f = \frac{U_c}{\gamma \delta} \left(\frac{2}{c_f} \frac{U_c}{\Delta U} \right)^{-1/3}$$

where γ is a coefficient of proportionality. Predictions of the equation were compared with lab and field data of shallow mixing layers and proved to be reasonably accurate. The formula will be applied to groyne field hydrodynamics later in this thesis (see Chapter 5.3) to compare and interpret structures of the DML and GML.

Flow patterns in groyne fields

The studies and publications on groyne field hydrodynamics which will be introduced in this subchapter are summarised in Table 2.1 below. The table differentiates field studies, laboratory experiments and numerical computations (ADV - measurements with acoustic Doppler velocimetry, PIV - particle image velocimetry, PTV - particle tracking velocimetry, dye injections, LDV - Laser Doppler velocimetry, EMF - electromagnetic flowmeters, LES - Numerical Large Eddy Simulations). Furthermore, basic experimental conditions are presented for comparison (h = water depth in the main channel, U = mean streamwise velocity, L_f = spacing between two subsequent groynes, L_g = groyne length, H_g = groyne height, Reynolds numbers are calculated according to $Uh(\nu)^{-1}$ where ν = kinematic viscosity of water). Finally, the shape, design and quantity of the groynes in a sequence are listed.

Table 2.1: Overview on studies described in this chapter which are dealing with flow hydrodynamics in groyne fields.

Authors		method	h [m]	U [m/s]	Re - Number	L_g / L_f	h / H_g	shape	design	g. fields
Engelhardt et al. (2004)	field	ADV	2.8, 1.7	0.80, 0.70	2.2×10^6 , 1.2×10^6	0.6, 0.4	1.0	natural/sloping	riprap	1
McCoy et al. (2007)	numerics	LES	0.1	0.14*	1.9×10^4	0.5	1.4	rectangular	imper.	1
McCoy et al. (2008)	numerics	LES	0.1	0.35*	3.5×10^4	0.5	1.0	rectangular	imper.	6
Muto et al. (2002)	field	PIV	2.8	0.32	10^6	0.3	1.0	natural/sloping	rock	3
	lab	PIV	0.038	0.11	4.3×10^4	0.3	1.0	rectangular	imper.	3
Sukhodolov et al. (2002)	field	ADV	1.50, 1.70	0.90, 0.70	1.3×10^6 , 1.1×10^6	0.7, 0.4	1.0	natural/sloping	riprap	1
Tominaga et al. (2001)	lab	PIV	0.08	0.17	1.4×10^4	0.6	1.0 - 4.0	rectangular	imper.	1
Uijtewaai et al. (2001)	lab	dye, PTV	0.1	0.35*	$4.0 \times 10^{3\circ}$	0.3, 0.7	1.0	rec/sloping	imper.	5, 10
Uijtewaai (2005)	lab	PTV, LDV	0.25, 0.30, 0.35	0.35*	$6.0 \times 10^{4*}$, $10^{5\circ}$	0.4	1.0 - 1.3	varying	varying	5
Weitbrecht et al. (2008)	lab	PIV, LDV, dye	0.46	0.16*	7.4×10^4	0.35 - 3.35	1.0, slightly subm.	rectangular	imper.	multiple
Yossef (2005)	lab	EMF, PTV, PIV	0.25, 0.30, 0.35	0.30*	$6.0 \times 10^{4*}$, $10^{5\circ}$	0.4	1.0 - 1.4	sloping	imper.	4
this study	field	ADV, dye, PTV	0.94, 1.14	0.30	$1.7 \times 10^{3*}$, $2.5 \times 10^{3*}$	0.7	1.0, 1.6	sloping	imper.	6

*main channel, °groyne field

Flow patterns in groyne fields differ depending on how the flow in the main channel is directed relative to the groynes and can be classified according to Figure 2.6:

- Type 1: The main flow is completely deflected outside the groyne field and a single gyre develops in the groyne field. The main flow is not entering the groyne field and is thus favourable for navigation purposes.
- Type 2: The main flow is completely deflected outside the groyne field and two gyres develop in the groyne field.

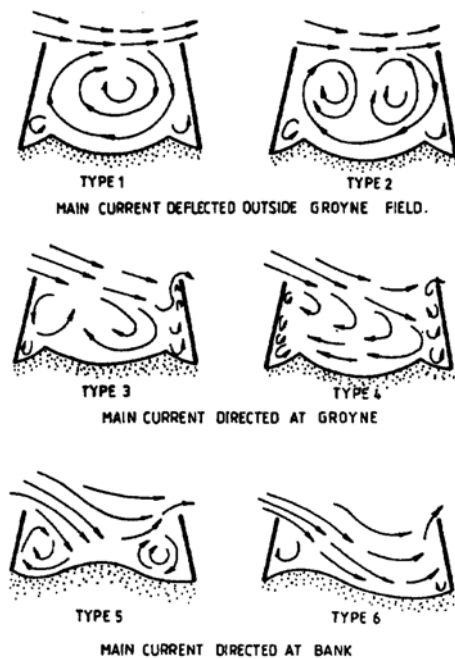


Figure 2.6: Different types of flow patterns in groyne fields (taken from KLINGELMAN et al. 1984).

- Type 3: The main flow enters the groyne field due to a larger spacing between groynes. Two gyres of opposite direction develop where the one near the upstream groyne is much stronger.
- Type 4: The main flow enters the groyne field and a single strong gyre occurs.
- Type 5: The main flow enters the groyne field just behind the upstream groyne and is directed towards the bank. Two smaller gyres develop on each side of the flow assuring some bank protection.
- Type 6: The main flow enters the groyne field and reaches the shore as spacing of groynes is further increased. The flow from the main stream is now directly attacking the bank.

2.2.2 Flow hydrodynamics under emerged conditions

When the flow is hitting the first groyne it separates at the tip of the groyne and is deflected towards the main channel. At the interface of the main channel and the groyne field a shear layer is developing. Considering only stationary flow patterns the water masses inside the groyne field are following a big horizontal gyre which is driven by the shear forces from the shear layer. Turbulence is furthermore causing instationary exchange processes between the main channel and the groyne field over the shear layer. Patches of the flow from the main channel are diverted into the groyne field. Generally these patches are entering the groyne field at the downstream third of the groyne field, enhancing the recirculating flow and eventually leaving the field again at the downstream side of the upstream

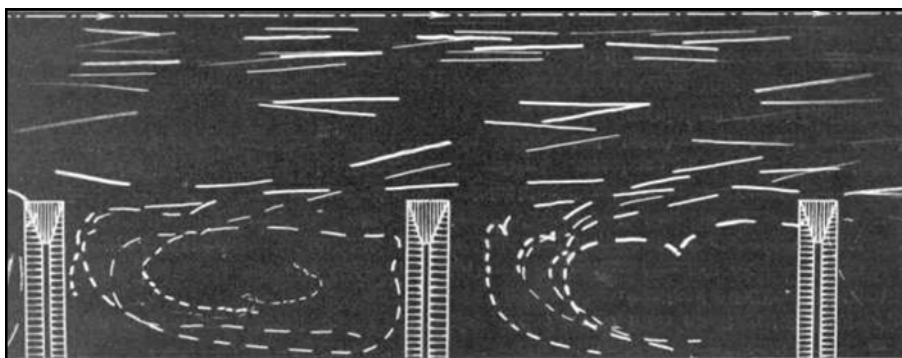


Figure 2.7: Particle trajectories using intermittent photography of floating candles, with the main flow direction from left to right (REHBOCK 1926).

groyne. This flow pattern was first described by REHBOCK (1926) who used floating candles to visualise the recirculation gyre (Figure 2.7).

At the interface between the main channel with higher velocities and the flow in the groyne fields with much slower velocities shear evolves and a mixing layer is created. Individual local mixing layers are generated at each groyne tip (Figure 2.8).

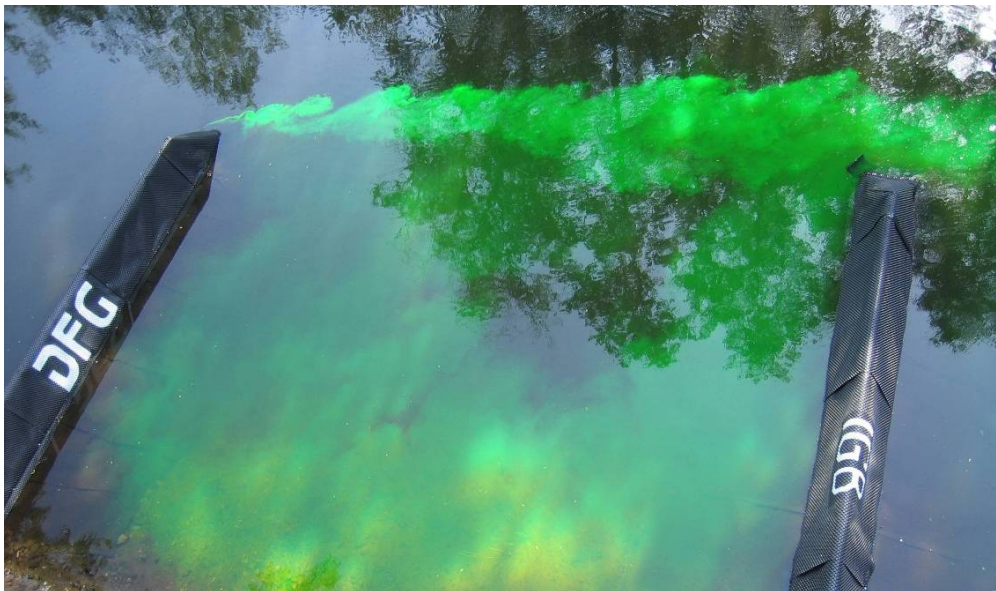


Figure 2.8: Mixing layer developing at the groyne tip (river Spree, 2007)

These so-called “detached mixing layers” (DML) develop from Kelvin-Helmholtz shear instabilities in the shear layer and are characterised periodic vortex shedding and formation of roller-type vortices. These vortices pair and grow until they are absorbed by larger structures in the main channel. These larger structures form the so-called “global mixing layer” (GML) between the main channel and the groyne fields. The GML is initiated at the first DML and maintained by the velocity gradient between the highest velocities in the main channel and the lowest velocities in the groyne field. Due to the shallow flow conditions, the structures in the GML are predominantly horizontal and two-dimensional. They can merge and develop into large coherent structures associated with the inverse energy cascade and are convected with the main flow. The horizontal extent of the structures is often much larger than the water depth because in shallow flows they are confined by the riverbed and the free surface (Figure 2.9). This was also proved for field conditions by ENGELHARDT et al. (2004) based on velocity measurements in a groyne field in river Elbe. The authors clearly identified low-frequency energy peaks with -3 slope in their auto-correlation spectra of the transverse velocity component – indicative for the large two-dimensional structures of the GML. Consequently, the momentum exchange between the main stream and the groyne field is influenced by the GML.

Coherent structures get advected into the groyne field, some of them to their full extent and some of them interacting with the subsequent groyne – causing the break-off of structures and redistribution of

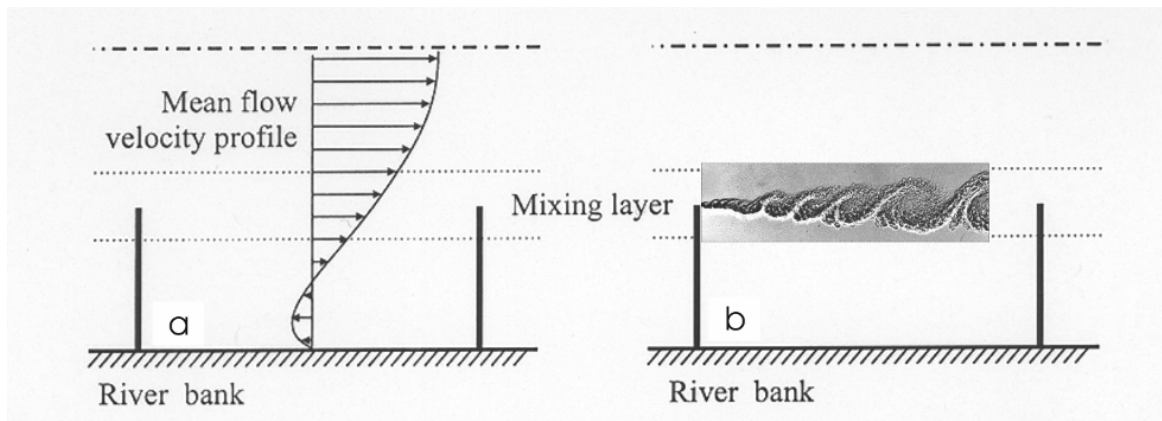


Figure 2.9: Mixing layer developing at the interface of the groyne field and the fast stream (a) and eddies that are shed at the groyne tips, merge and grow in size during their travel downstream (b).

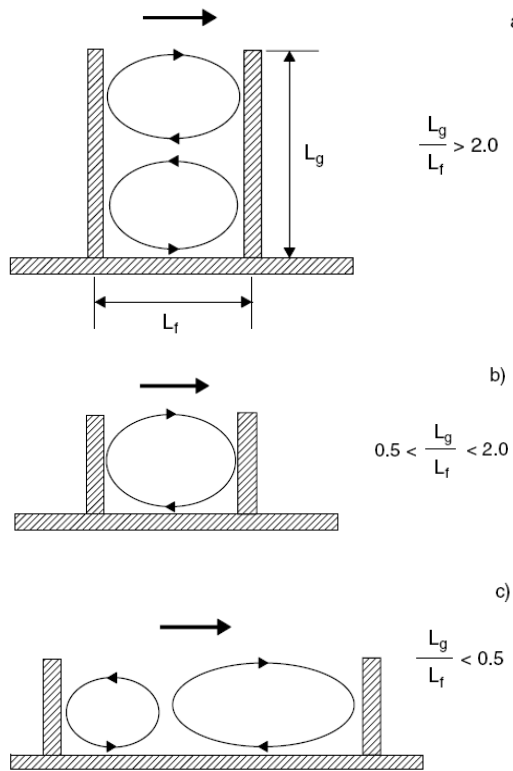
turbulent energy and stresses. The importance of small-scale three-dimensional turbulence on these structures has been identified for shallow mixing layers, but practically unknown in the complex case of groyne interaction. Nevertheless, UIJTTEWAAL et al. (2001) and WEITBRECHT (2004) concluded from their flume studies that they play only a minor role in the overall exchange processes between groyne field and main channel.

In general, most of what we know of the flow dynamics in groyne fields comes from experimental flume studies. For example, MUTO et al. (2002) applied large-scale particle image velocimetry (PIV) to investigate the instantaneous and mean surface flow in a groyne field located at the river Yodo in Japan. Solid particles were added at the groyne tip as floaters and their trajectories were recorded. In addition to the field study, a laboratory study with a down-scaled groyne field geometry was conducted. The effects of the aspect ratio and water depth on the velocity distributions were analysed and turbulence characteristics at the groyne field interface were clarified. The PIV data collected in the field study showed the flow was highly unsteady inside the recirculation zone. For example, at a certain time a large recirculation region was observed to develop within the groyne field and a small counter rotating zone was presenting the downstream corner. A few minutes later, the size of the large recirculation diminished significantly. The bulging into the main stream no longer existed, but, instead, the main flow entered into the embayment. It was deduced that a significant mass exchange between the channel and the embayment can occur through this process. The lab experiments did not exhibit these same unsteady characteristics. The authors concluded that variances between field and experimental studies are caused by the complex bathymetry of the natural river and by insufficiencies in the scaling, particularly due to the lower Reynolds numbers.

McCOY et al. (2008) conducted numerical simulations of a sequence of emerged groynes. They used Large Eddy Simulation (LES) which has become a state-of-the-art tool for the simulation of laboratory-scale flows. LES resolves the motion of the largest and most energy-containing structures while the small dissipative eddies are captured by a turbulence model. For their aspect ratio of 0.5, McCOY et al. (2008) found the typical one-gyre recirculation pattern inside the groyne field with two small secondary counter-rotating gyres in the corners. Their highest turbulent fluctuations were located within the shear layer in the interface of main channel and groyne fields, particularly around the head of the groynes where the strongest velocity gradients appear. An advantage of LES is the detailed insight into turbulence and the interaction of structures with the groynes. The authors found, that coherent structures from the GML were either convected in the main channel and past the groyne without interacting with the tip of the groyne (“total escape event”) or the structures interacted with the groyne tip. In the latter, the structure was broken-off – one part was advected into the embayment transporting mass and momentum from the main channel into the groyne field. The other part was either stretched around the groyne tip and dissipated or merged with other eddies shed from the DML before interacting with the subsequent groyne field. In some cases, structures were convected entirely inside the groyne field, along the stoss-side of the downstream groyne where they formed a jet-like inflow (“total clipping event”). The authors stated that structures that entered the groyne field lost their coherence progressively as they moved along the groyne due to the interaction with bed-shear generated vertical small-scale turbulence. However, these structures substantially increased the mixing at the boundary with the main recirculation region and were thus crucial for mass exchange between the main stream and the groyne field. McCOY et al. (2008) also demonstrated that the structures are dissipated before they reach the recirculation centre which is an area of long residence times.

2.2.3 Effect of aspect ratio

SUKHODOLOV et al. (2002) conducted flow velocity measurements in groyne fields at the river Elbe and confirmed lab results from UIJTTEWAAL (1999) in which the aspect ratio was identified to determine the number and location of gyres. For an aspect ratio $0.5 < L_g / L_f < 2.0$, a single primary gyre develops (Figure 2.10a).



Velocities in the centre of the gyre and in the corners of the groyne field are low but are increasing towards the gyre margins (UIJTTEWAAL et al. 2001). If the aspect ratio is < 0.5 , a secondary, smaller gyre starts to evolve (Figure 2.10b). This smaller gyre is disconnected from the main stream and driven by the primary gyre. It rotates much slower and in opposite direction (UIJTTEWAAL 2001; WEITBRECHT 2004). Several field studies demonstrated that under certain bathymetric changes, both gyres may rotate in the same direction. This is the case if banks protrude and cause a physical separation of the gyres. The secondary gyre is then driven by the main channel (SUKHODOLOV et al. 2002). For aspect ratios > 2.0 , e.g. in maritime harbours, a two gyre system establishes (Figure 2.10c).

Figure 2.10: Recirculation pattern depending on the aspect ratio: length of groyne L_g and length of groyne field L_f (taken from SUKHODOLOV et al. 2002).

2.2.4 Effect of groyne orientation

Flow patterns in groyne fields are also influenced by the inclination angle α between the groyne field and the main stream direction (Figure 2.11). Forward inclined groynes with $\alpha > 90^\circ$ increase the size

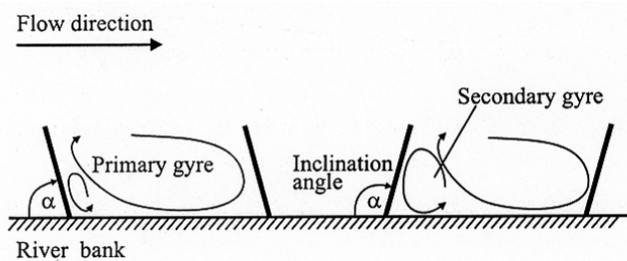


Figure 2.11: Groyne fields with different inclination angles (α) and their influence on the development of the two gyre system (taken from WEITBRECHT 2004).

of the secondary gyre in the upstream corner of the groyne field (WEITBRECHT 2004). The amount of deposition between groynes is largest in case of forward inclined groynes. Groynes of this kind are therefore best suited for bank protection and sedimentation purposes. Groynes that are perpendicular to the flow protect a smaller area.



Figure 2.12: A sequence of backward inclined groynes at the river Elbe near Havelberg, Germany (image: Google earth).

Backward inclined groynes with $\alpha < 90^\circ$ decrease the secondary gyre and the area with very low flow velocities covers a smaller part of the groyne field (WEITBRECHT 2004). Backward inclined groynes are not suitable for bank protection purposes, as they tend to attract the flow. The flow towards the root of the downstream groyne threatens the surrounding bank area, as well as the groyne itself. For the purpose of maintaining a deep navigable channel, on the other hand, perpendicular or backwards inclined groynes perform best (Figure 2.12) (KLINGELMAN et al. 1984).

2.2.5 Effect of the stage of submergence

Only a few studies were investigating the effect of different stages of submergence of groynes. One reason for this might be that submerged conditions were classically considered as insignificant, since the groynes were designed for emerged conditions during or below mean water levels. Another reason might be the complexity and three-dimensionality of the flow patterns around submerged groynes, which requires advanced measurement techniques which resolve the vertical flow structures. This can not be achieved by the common surface PIV and PTV methods which were applied in the laboratory until recently.

TOMINAGA et al. (2001) were the first to apply particle image velocimetry (PIV) measurements in the lab in several vertical and horizontal plains within an embayment between submerged and emerged groynes. The authors studied three-dimensional flow and vortex structures for groynes under different stages of submergence. They identified a vertical separation of the flow in front of the first groyne. The top-flow was overtopping the crest and caused a large vertical recirculation in the lee of the groyne which occupied the entire groyne field. The down-flow at the stoss-side was directed towards the bed and formed a small vertical roller with horizontal axis parallel to the groyne. Contours of Reynolds stresses clearly revealed the development of a DML originating at the upstream tip of the groyne. At this location, pronounced vortex shedding associated with the vertical and horizontal DML was observed. By decreasing the level of submergence, the authors found: (1) the centre of the vertical recirculation moves downstream, (2) velocities in the groyne field and in the main stream increase, (3)

the vertical roller near the bed at the stoss-side increases and (4) the deflection and intensity of the DML increases.

UIJTTEWAAL (2005) found in his surface PIV studies in the lab that the main feature of submerged conditions is to increase the intensity of three-dimensional effects and to make the flow more complex in general. He found for his idealised flume geometry but realistic setup as found in real rivers that the flow patterns in the groyne field shifted periodically from a gyre-like horizontal structure associated with emerged conditions to almost uniform flow parallel to the main stream. For low stages of submergence, structures from the GML were advected into the groyne field and then completely interrupted the established gyre-recirculation pattern. Compared to the emerged case, substantially higher velocities and turbulent intensities were present in the surface layer. Eddies were shed from the vertical mixing layer originating at the groyne crest due to the vertical flow separation in the lee of the groyne. Uijtewaal concluded that for an accurate simulation of the flow behind submerged groynes, a fully 3D LES model is required to represent the complex three-dimensionality of the large scale flow structures.

YOSSEF (2005) continued the work of UIJTTEWAAL and conducted further experiments with emerged and submerged groynes in the lab with a focus on morphological impacts of submerged and emerged conditions. Like UIJTTEWAAL, he observed uniform parallel flow alternating with a gyre-like recirculation pattern for relatively low stages of submergence ($\zeta = 1.2$). The velocity time series proved that low-frequency fluctuations were present for both emerged and submerged conditions, but the turbulence characteristics in the submerged case differed significantly from the emerged. With increasing stage of submergence, the vertical velocity gradient decreased and the vertical mixing layer shed from the crest weakened. Moreover, YOSSEF (2005) stated that the DML in the submerged cases extended further into the main channel and had a rather constant and larger width.

McCOY et al. (2007) conducted a LES investigation on exchange processes between two submerged groynes. The groynes were highly-idealised and far from geometrical similarity to groynes under natural conditions. Nevertheless, their results supported UIJTTEWAAL (2001) and YOSSEF (2005) in the point that the horizontal flow patterns from bottom to mid-depth were gyre-like and similar to emerged conditions. For high levels of submergence ($\zeta = 1.4$), the overtopping and accelerated flow remained parallel to the main stream flow direction whereas a clear gyre-like recirculation pattern was observed for water levels below crest height. The authors proved that the momentum exchange between the main flow and the groyne field was driven by coherent structures generated by the two mixing layer systems – the horizontal mixing layer (DML) also found for the emerged case and the vertical mixing layer due to the separation of the flow at the lee-side of the groyne. It should be noted, that only two groynes were simulated, thus no GML could establish in this case. The authors stated that the qualitative development of coherent structures and their interaction with the groyne field is

similar for the horizontal and vertical mixing layer. This is not surprising, as the height and width of the groynes was almost identical. The probability of coherent structures being either totally or partially entrained into the groyne field was higher for the vertical mixing layer. Consequently, more than 50% of particles entrained into the groyne field would be removed again due to interaction with vertical structures. In general, the particle or contaminant removal process was up to three times faster in the submerged case.

2.2.6 *Effect of groyne design*

UIJTTEWAAL (2005) investigated four different groyne shapes and studied the effect on flow dynamics and in particular on exchange processes through the mixing layer. Groyne type A was a standard groyne typical for large rivers; type B had a gentler head slope (1:6 compared to 1:3 for groyne A); type C was composed of vertical rods and permeable; and groyne type D was a combination of type B and C. Results for the emerged case for groynes A and B showed that a gentler head slope reduced the momentum transfer and the turbulent intensities at the groyne head. In case B the shear layer was prolonged and thus the velocity gradient was less steep – resulting in a weaker DML. For submerged conditions, turbulence intensities were reduced for both, type A and B. From this, the author concluded that type B causes less scour in the mixing layer region than type A. In case of permeable groynes, the horizontal gyre disappeared. The flow is seeping through the groyne, velocities are reduced and a uniform parallel flow established along the groyne fields. This prevents strong horizontal velocity gradients and the associated vortex shedding from the groyne tips. Uijttewaal concluded that if groyne type C is submerged, a high conveyance capacity will be maintained with high velocities near the bank. Groyne type D caused surprisingly high velocity fluctuations due to instabilities of the flow around the groyne tip which changed between a parallel flow through the groyne and a circulation around the groyne tip. Finally, the author pointed out that the bathymetry of real river reaches may have an important effect on these processes which has to be considered and investigated.

2.2.7 *The role of groynes for ecology*

Today many rivers are regulated or canalised for navigational purposes, water power supply, flood control, water utilisation, etc. In particular lowland rivers which formerly exhibited a natural meandering course are straightened and disturbed in their sediment transport – with huge negative impact on the biological function, water quality, ecosystem diversity and quality of life in general.

Straightening increased the slope of river and thus flow velocities, shear stresses and sediment transport capacity. In addition, river engineering constructs such as dams or weirs became physical barriers, cutting the river into several sub-sections and disturbing the longitudinal and transversal sediment, flow and ecological continuum. As a result, aquatic habitats degraded extremely. Floodplains were cut-off, large woody debris and riparian or bank vegetation were removed and the

river morphology lost its structural diversity. Consequently, there was a loss of habitat diversity which decreased the abundance and richness of aquatic and terrestrial plant and animals. In general, groynes diversify the flow and morphology and thus have good potential for synthesizing demands from ecology and economy. This is the case when changes in land use management are not feasible and widening or re-meandering of the river has to be prevented – limiting the rehabilitation efforts to in-stream measures like groynes only.

For example, SHIELDS et al. (1995) showed that a variable bathymetry composed of scour and deposition zones adjacent to groynes provided cover and shelter for fish from high velocities – thus providing a good habitat. The authors describe results of a restoration project in which spur extensions were added to existing groyne length to improve aquatic habitats by accelerating natural processes, promoting the recovery of channel equilibrium, vegetation and stream-flood plain interaction. The channel cross-section and geometry remained fairly unchanged, but the pool habitats increased by five times due to increased scour and deposition. The biological response included an order of magnitude increase in fish biomass, doubling the number of fish species found in the reach, and an increase in average fish length.

BISCHOFF & WOLTER (2001) examined if conditions at groyne heads in a canalised lowland river in Germany provide potential habitats for juvenile fish which prefer higher flow velocities (rheophilic species). They showed that fish younger than one year, which are big enough to leave the sheltered groyne field habitats, preferred shallow water depths combined with moderate to high current velocities. These conditions are only found at groyne heads during low water season. Fish between one and two years were restricted in the same way. Favourable conditions near the groyne head were provided by a minimised danger of predation due to the shallowness and a better availability of food by e.g. drifting benthic organisms. The authors pointed out that groyne heads with a smoother, longer slope extend these “areas of interest” for fish and would improve the habitat conditions.

In a further study, WOLTER et al. (2004) investigated the impact of navigation-induced currents on fish displacement. The authors showed, that the majority of recently hatched roach (*Rutilus rutilus*), and perch (*Perca fluviatilis*) were not able to resist the hydraulic forces induced by navigation along the banks of canalised rivers. The fish were either displaced from their preferred feeding grounds into less favourable habitats with poorer feeding conditions, or they were swept into deeper water where they were exposed to substantially higher predation. The authors emphasised the importance to improve fish recruitment by providing shallow embayments with low flow velocities for juvenile fish.

NAKANO & NAKAMURA (2006) conducted a study on the effects of different restoration strategies in a lowland river. They examined the effects of re-meandering and groynes on macroinvertebrate communities in a canalised river section. In general, shallow marginal habitats which are characterised by lower hydraulic stresses and a stable riverbed were preferable habitats for various

macroinvertebrate species. In this sense, groyne fields provide ideal conditions for colonisation. The authors also suggested that groynes may have a potential in enhancing habitat diversity by altering the flow conditions. They concluded that groyne structures are an alternative strategy for the recolonisation of macroinvertebrates - even if the reconstruction of meanders would be the most effective and desirable way for conservation of lotic macroinvertebrates in lowland rivers.

2.3 Problem identification

In order to plan and implement an optimal groyne design, it is crucial to study and reveal the involved exchange and transport processes. In the last few years, a number of experimental studies and numerical investigations have identified this need. Most of them were investigating the flow and turbulence patterns around a single groyne field embanked by two emerged groynes. Only a few studies were focusing on a sequence of groynes or on submerged conditions (UIJTTEWAAL et al. 2001; TOMINAGA et al. 2001; McCOY et al. 2007).

However, the flow around groynes is controlled by many complex phenomena associated with turbulence. One feature of turbulence are the spatially and temporally fluctuating velocity fields, another - in particular for groynes - the occurrence and interaction of multiple shear layers. Eddies are shed from these layers and initiate the formation of large coherent structures. These large-scale structures have a significant influence on the transverse exchange of mass and momentum, which is important for dispersion of nutrients, pollutants and sediment transport (VAN PROOIJEN & UIJTTEWAAL 2002). Therefore, the knowledge of essential mechanism of mixing layer development is of great practical and theoretical value for groyne field hydrodynamics. During submerged conditions, vertical and horizontal shear layer coexist and result in three-dimensional and highly complex flow structures (UIJTTEWAAL 2005). Many techniques applied in laboratory are restricted technically to two-dimensional analysis such as surface PIV and PTV - unable to capture the full three-dimensionality. Furthermore, morphological changes like scour and deposition are difficult to simulate in laboratory due to the limitations of scaling. For example, in a groyne field at river Elbe scouring was observed in the lee of the groynes and deep inside the groyne field. It was suggested that this phenomena occurs during floods when groynes are submerged (SUKHODOLOV et al. 2002). Unfortunately, previous lab experiments and numerical simulations could not give a satisfying answer to this as no such observations had been made before. Instead, the complexity and irregularity of conditions in the field were claimed. This points out the gap between highly-idealised, fully controllable and detailed lab studies and coarse but naturally complex field studies under rather uncontrollable conditions.

Most of the experiments on the flow in groyne fields were conducted in the laboratory. However, the applicability of laboratory results to natural streams is restricted as it is practically impossible to obtain large Reynolds numbers and at the same time keep scale with bathymetry, discharge, water levels,

composite bottom roughness or bedforms. Interaction of these factors contributes to the development or decay of turbulent flow structures like mixing layers and coherent structures. Laboratory studies help to understand individual processes and explain how the processes evolve in detail but they are not able to identify what actually happens in natural streams.

On the other side, field studies give only a snapshot of reality but they are often difficult to perform. They are expensive and time-consuming and locations of interest are often hard to access. Mixing layers at groyne fields are often located in proximity of intensive navigation where it is practically impossible to perform measurements (SUKHODOLOV et al. 2004). Standard groynes are usually emerged but can be submerged in cases of flood events when conditions are too rough to measure in situ. Thus, hardly any field measurements for submerged groynes exist, in particular not for a sequence of groynes. In cases where direct comparison was possible, e.g. between the mean flow patterns in groyne fields in lab and field (SUKHODOLOV et al. 2002; SUKHODOLOV et al. 2004), a certain correspondence was proved but turbulent features were still not covered in detail.

This gap gave the motivation to establish a “hydraulic lab in the field” at IGB, combining the advantaged of lab and field studies. This means that boundary conditions should be controllable to the highest possible extent (e.g. discharge, geometry) but taking into account the complexity imposed by the natural scale. Advantages of field-scale experiments are to perform measurements in the real state and scale of nature, considering effects of high Reynolds numbers, effects of composite roughness and bedforms or non-uniform surface slopes. Additionally, improvements of field equipment and apparatuses over the last two decades enable precise measurements. Field-scale experiments assist to understand the complexity of open channel turbulent flows. Scaling effects can be examined to help to improve and interpret laboratory studies and provide real-scale parameters for numerical modelling. Furthermore, field experiments naturally enable to include ecological aspects on a real-scale.

Thoughtful examination of experimental and field studies on turbulent flow structures in groyne fields revealed that experimental studies are conducted under idealised flow situations and their results are therefore not easily applicable to the inhomogeneous, hydraulically rough, three-dimensional flows in natural streams. On the other, there is a lack of field data commensurable in the amount and level of details to get a closer insight in the hydrodynamics in groyne fields. The “lab in the field” will account for both. In this thesis the results of this new approach of the “lab in the field” will be presented and the gap between experimental and field studies will be filled by the comparison of the obtained data set with existing literature.

2.4 Aim and objectives of the thesis

The main aim of this thesis is to present and analyse the results of the intensive field measurements and experiments on flow patterns in groyne fields during emerged and submerged conditions. Specifically, the following main issues will be addressed:

- Presentation of the mean velocity and turbulent kinetic energy distribution within the groyne field and for different horizontal levels across the water depth,
- Analysis of the evolution of coherent structures and their impact on exchange processes between main channel and groyne field,
- Comparison between the measured emerged and submerged results and discussion of similarities and differences,
- Presentation and discussion of the main findings of the study in the frame of previous investigations.

3 MATERIAL AND METHODS

The approach of the research campaign at IGB was to create a “hydraulic lab in the field” and thus, field experiments and measurements took the fundamental part of the project and of this thesis. To perform field experiments and measurements under controlled conditions, an appropriate river reach had to be found. An ideal section was the Spree near Berlin. An important factor for establishing the field laboratory at the place was the relatively steady discharge controlled by a weir located 20 kilometres upstream, making it possible to perform field works over a period of five weeks under relatively constant conditions. The river reach was already known from previous scientific studies at IGB taking advantage of the installed infrastructure such as two cabins for equipment and personnel, four gauging stations and an automated system for monitoring water level, turbidity, pH-value, oxygen concentration and temperature.

For the groyne field study, a sequence of seven groynes was constructed on the right bank of the river prior to the experiments. The measurements were conducted in May/June 2007 and comprised detailed point measurements of local flow velocities and turbulence characteristics using acoustic Doppler velocimeters (ADV), particle tracking (PTV) experiments with floating candles and dye tracer injections to visualise the flow and to provide additional information on the evolution of large quasi two-dimensional flow structures.

In the following, the experimental river reach, setup, equipment and techniques are described including details on data collection and processing. Finally, a short summary of the entire experimental program is given including tables with the most important boundary and experimental conditions.

3.1 Experimental river reach

3.1.1 Geographical location

Field experiments and measurements were conducted in the river Spree near Freienbrink, approximately 40 km south-east of the city of Berlin, Germany. The Spree is a typical lowland river, which originates in the Lusatian Hills on the German border to Czech Republic and merges with river Havel after a length of about 400 kilometres. The study reach was located in a 32 km long section of the Spree called “Müggelspree”, between the weir “Grosse Tränke” near Fürstenwalde and lake “Dämeritzsee” near Erkner, just outside of Berlin (Figure 3.1a).

In general, the river reach exhibits a meandering course and is characterised by abundant aquatic and riparian vegetation in the period from May to September. Many meanders are cut off and the straightened reach is stabilised by stone armoured banks. The experiments were performed in one of the cut-through, hence providing an almost straight channel of a length of around 400 meters. The

remaining oxbow is separated from the main channel by a pipe bridge clogged by debris preventing exchange of surface water (Figure 3.1b, 3.1c and 3.1d). The cross-section of the channel has a trapezoidal shape and the channel width varied between 20.9 and 21.3 m during the measurement campaign.

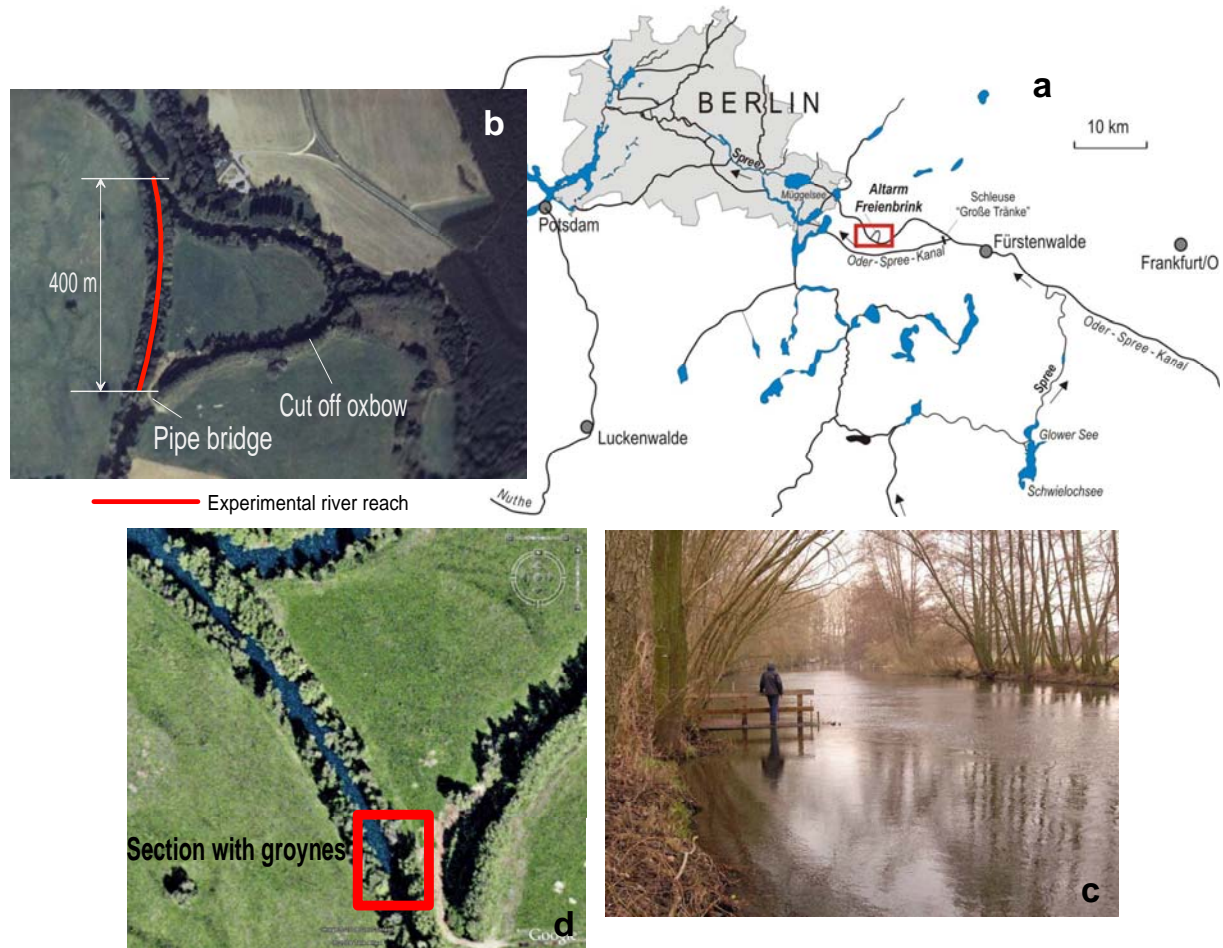


Figure 3.1: Map of the federal states of Berlin (a), airborne pictures of the river reach (taken from Google earth) (b) and (d) and a picture showing the location of the experimental river reach at the river Spree, 2007 (c).

3.1.2 Hydraulic regime

The weir “Grosse Tränke” is operated by the local waterways services and situated about 20 km upstream of the experimental reach and controls the discharge in the experimental river reach. During winter season, discharges of 15 to 20 m³/s are supplied whereas the discharge decreases to 3.5 to 5 m³/s during summer. Mean velocities range from 0.2 to 0.6 m/s and mean depths from 0.8 to 1.8 m.

Figure 3.2 shows the time-series of water level fluctuations during the experimental period. The graph contains three sources of information: a) data of a pressure logger installed in the downstream part of the section and converted into water depth, b) total discharge measured at “Grosse Tränke” and converted to water levels by means of a stage-discharge curve at Freienbrink (see Figure 3.3) and c) direct water level readings at the gauging poles in the experimental section. Discharge data provided by the weir “Grosse Tränke” was converted to discharge at Freienbrink by assuming a mean

retardance time of 18 hours which was estimated with a bulk velocity of 0.3 m/s along the 20 km stretch between both locations. Additionally, the discharge was measured twice by tracer tests with uranin dye injection before experiment 1 (7.71 m³/s) and during experiment 2 (6.35 m³/s) – see chapter 3.3.3 for details.

During experiment 1, the water level was relatively constant at around 1.14 m. Only during the last day the water level dropped rapidly by approximately 0.3 m before rising again prior to experiment 2, providing mean water depths of 0.94 m. The water level decreased again during the last days of experiment 2 before steadily dropping until the end of the measurement campaign. Nevertheless, the conditions were ideal during the ADV measurements between 19th and 23rd of May 2007 (experiment 1), and from 28th to 30th of May 2007 (experiment 2).

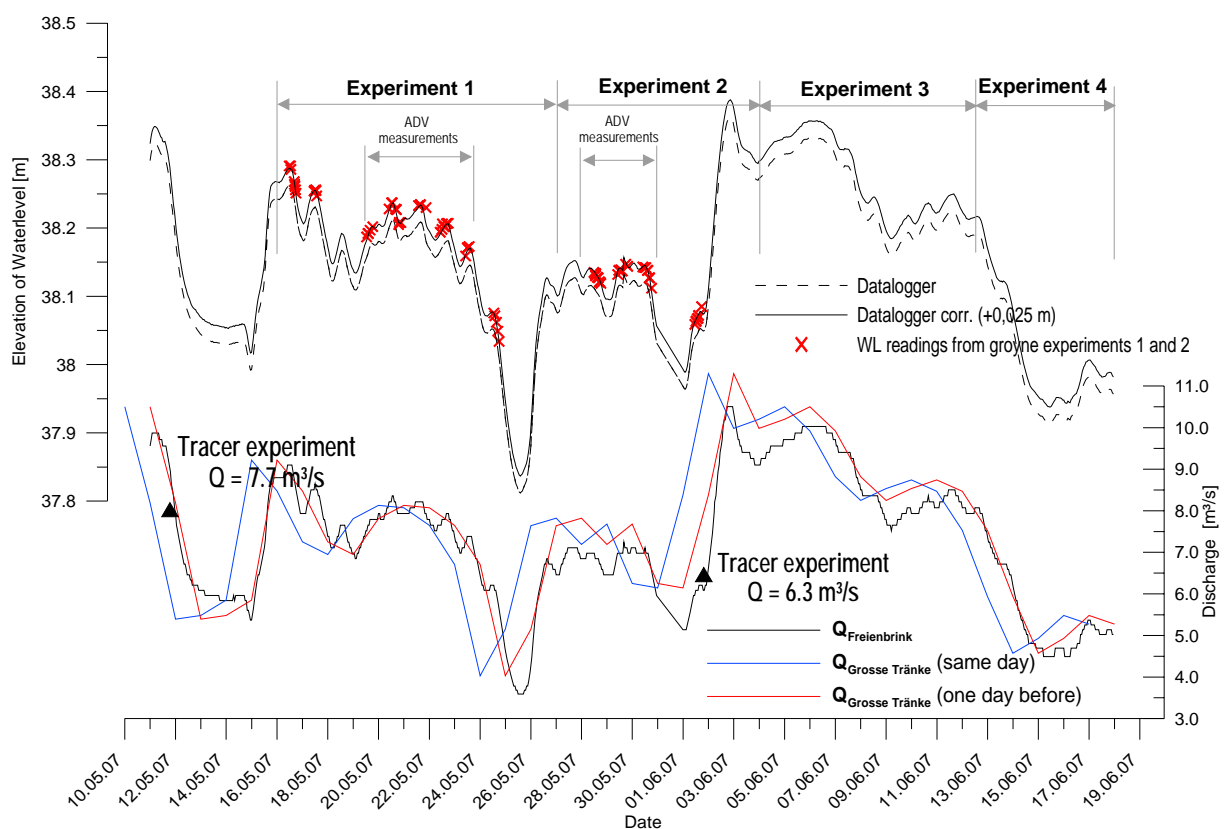


Figure 3.2: Elevation of the water level calculated from water level readings from pressure loggers of IGB (raw data and corrected data) compared with water level readings at gauging poles during experiment 1 and 2 (above); discharges according to mean cross section at the river Spree near Freienbrink and tracer experiments, 2007 (below).

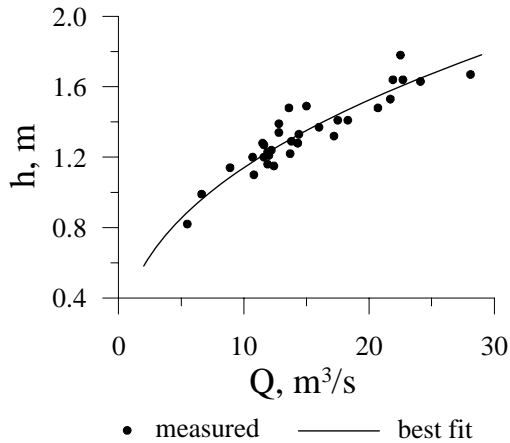


Figure 3.3: Stage-discharge relation at the experimental river reach at the river Spree, data from the last ten years.

Discharges were calculated on the basis of water level readings, a mean cross section and an existing stage-discharge relation that was obtained from previous investigations at the river reach (Figure 3.3). Discharge data, provided by the weir “Grosse Tränke” was taken the previous day (distance of 20 km and bulk velocity of 0.3 m/s results in a travel time of approximately 18 h) and compared to calculated discharges, as demonstrated in Figure 3.2. Additionally, the discharge was measured by means of uranin dye injection once shortly before experiment 1 and once during experiment 2.

Table 3.1: Hydraulic characteristics during experiment 1 and 2. Surface slope was calculated as the water level difference across the poles of the gauging stations (Fr=Froude, Re=Reynolds, g = gravitational constant, ν = kinematic viscosity of water).

	date	Discharge Q	Bulk velocity u_Q	River width B	Average depth h	Surface slope S	Shear velocity U.	Fr-number	Re-number
		[m ³ /s]	[m/s]	[m]	[m]	mean	$u_* = (ghS)^{1/2}$ [m/s]	$Fr = u_Q(gh)^{-1/2}$	$Re = u_Q h \nu^{-1}$
EXP 1	16.05. - 25.05.2007	7.7	0.3	21.5	1.14	1.01×10^{-4}	0,03	0.066	2.5×10^5
EXP 2	26.05. - 03.06.2007	6.5	0.3	20.7	0.94	8.06×10^{-5}	0,03	0.059	1.69×10^5

3.1.3 Morphology

The riverbed in the “Müggelspree” is naturally dynamic and subject to macrophyte growth whereas the banks are stable and protected by riprap.

The bed roughness of the reach is subjected to seasonal changes in morphology and vegetation, sediment transport and the related occurrence of bed forms (SUKHODOLOV et al. 1998) as well as aquatic vegetation growing on the river bed. Morphological structures are represented by alternate bars (30 – 50 m long, 20 – 40 cm high), oblique sand dunes (10 – 12 m long, 15 – 20 cm high), nearly two-dimensional sand waves (2 – 5 m long, 7 – 10 cm high), and by vegetation induced bed forms (20 – 25 m long, 4 – 6 m wide, 20 – 25 cm high).

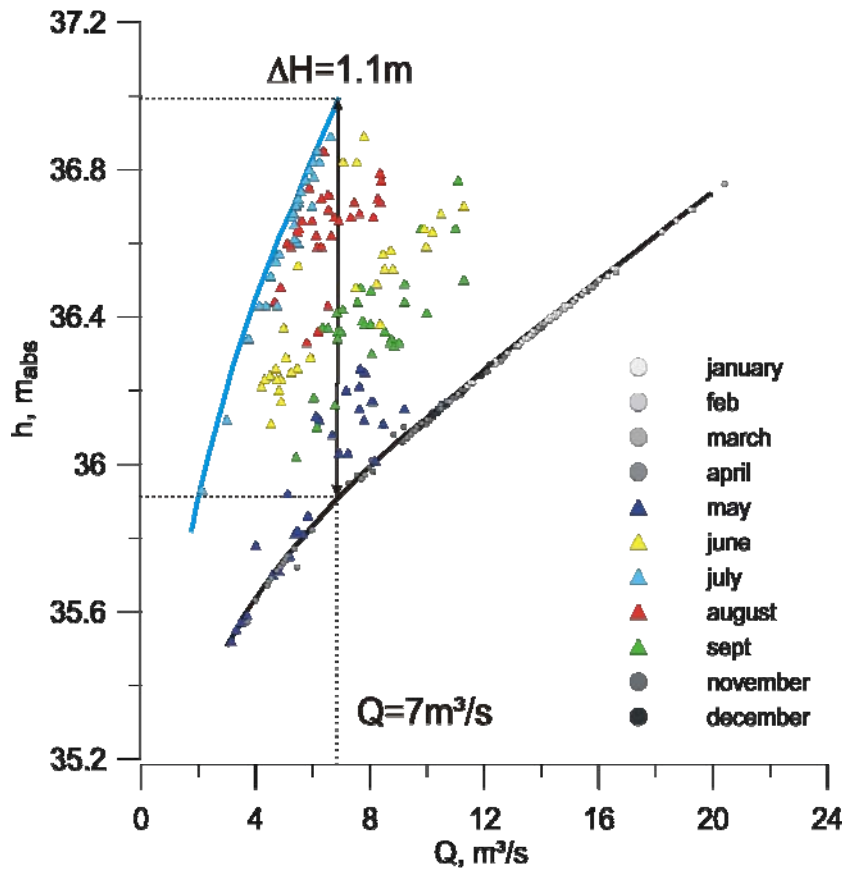


Figure 3.4: Stage – discharge curve of the weir “Grosse Tränke” at the river Spree, 2007 (no data from October)

Vegetation-induced bedforms are the result of interactions of the near-bed flow with the plant patches causing erosion and depositional areas. These bedforms develop over sand dunes that remained from previous higher water level periods and are superimposed by ripples. The crests of sand waves are directed perpendicular to the mean flow direction and develop only at discharges higher than 10 m³/s. At the end of the vegetative season, the sand waves are washed off and are mainly replaced

by vegetation-induced bedforms. Areas without vegetation and with smaller grain sizes provide conditions for ripple regimes during summer (SUKHODOLOV & SUKHODOLOVA 2007).

The bathymetry of the study reach was surveyed several times during the last decade. Figure 3.5 shows the conditions one year prior to the start of this study, and Figures 3.6a and 3.6b show data of bathymetric survey and characteristic grain sizes of riverbed sediments from a survey in 2005 (SUKHODOLOV & SUKHODOLOVA 2007).

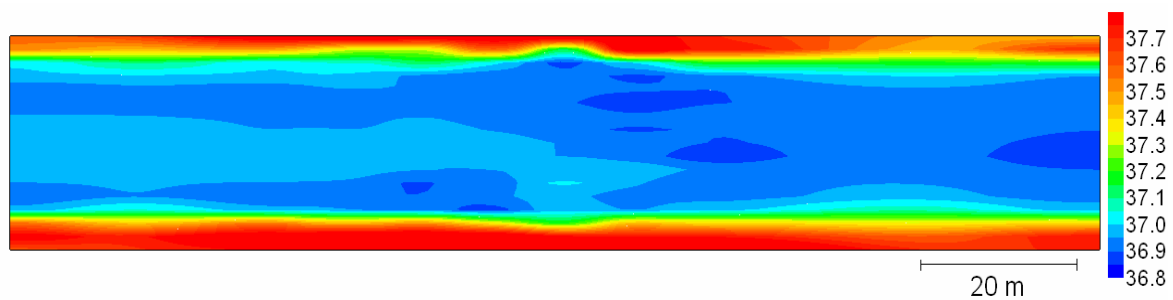


Figure 3.5: Riverbed elevation (meter above sea level) at the experimental reach (river Spree), in May 2007 before the experiments.

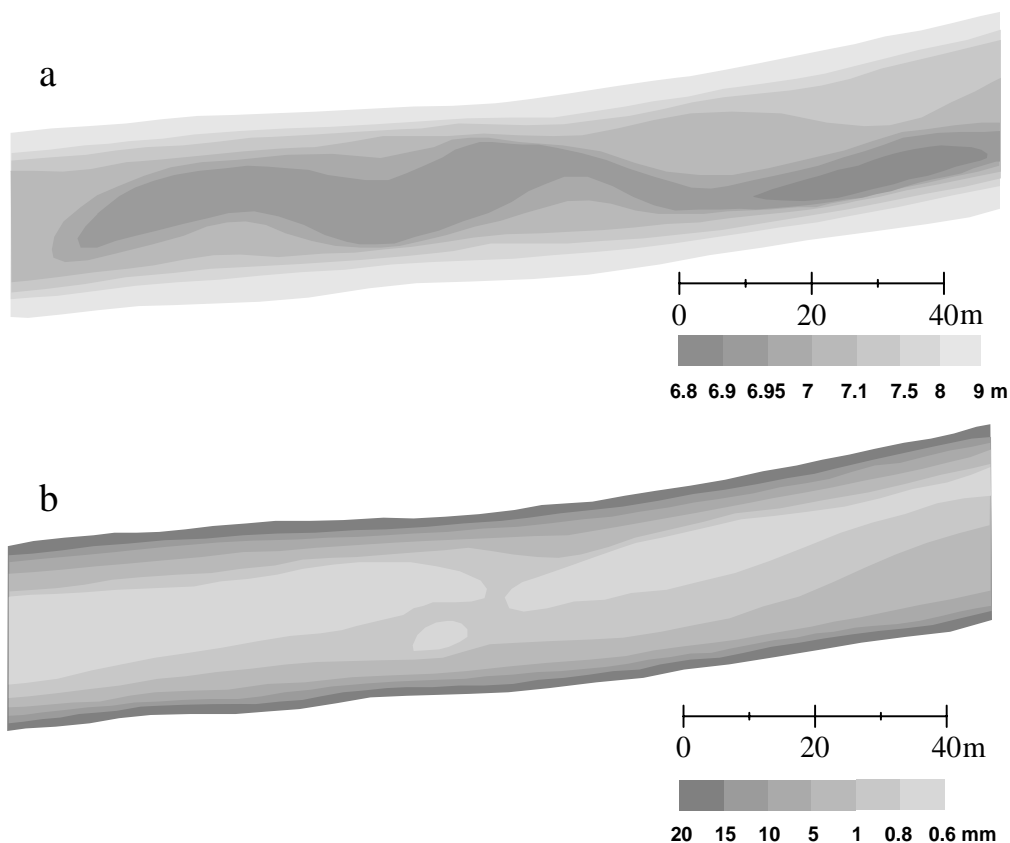


Figure 3.6: Riverbed elevation (meter) (a), and mean sediment particle diameter (d_{50}) (b) at the river reach (river Spree) in 2005 (SUKHODOLOV & SUKHODOLOVA 2007).

3.2 Groyne construction and experimental setup

Seven groynes, each having a length of 7 m and a distance of 9 m, were constructed along the right riverbank (Figure 3.7a). Groynes 1 to 3 were simple vertical walls; groynes 5 and 6 were fully shaped like standard river groynes with sloped sides, and groynes 4 and 7 were only shaped on one side for economical reasons (Figure 3.7a). Wooden frames of a height of 0.7 m were first constructed underwater to provide submerged conditions with $\xi = 1.6$ (see Figures 3.7b). Then sheet piles were rammed into the river bed to protect the groyne from being undercut by the flow. The frames were then blocked with wooden panels and finally covered with dimpled sheets (Figure 3.7c). For experiments with emergent condition, the groynes were heightened up to 1.2 m (Figure 3.7d) by additional constructs. The quantity of groynes was chosen in order to establish fully developed GML conditions in the last two groyne fields and to be able to remove groyne 6 to decrease the aspect ratio in the second phase of the experimental program. In total, four experiments were conducted: experiment 1 and 2 were performed at an aspect ratio of 0.75 for submerged and emerged conditions respectively, and experiment 3 and 4 (which have not been analysed in this thesis) at an aspect ratio of 0.35. Detailed ADV measurements were performed around and between groynes 5 and 6 (Figure 3.7a). Additional bathymetric surveys across the entire river width were conducted within a grid of 1

m x 1m and along groyne 1 to 7. An overview of the whole measurement campaign and employed techniques can be found in chapter 3.3.

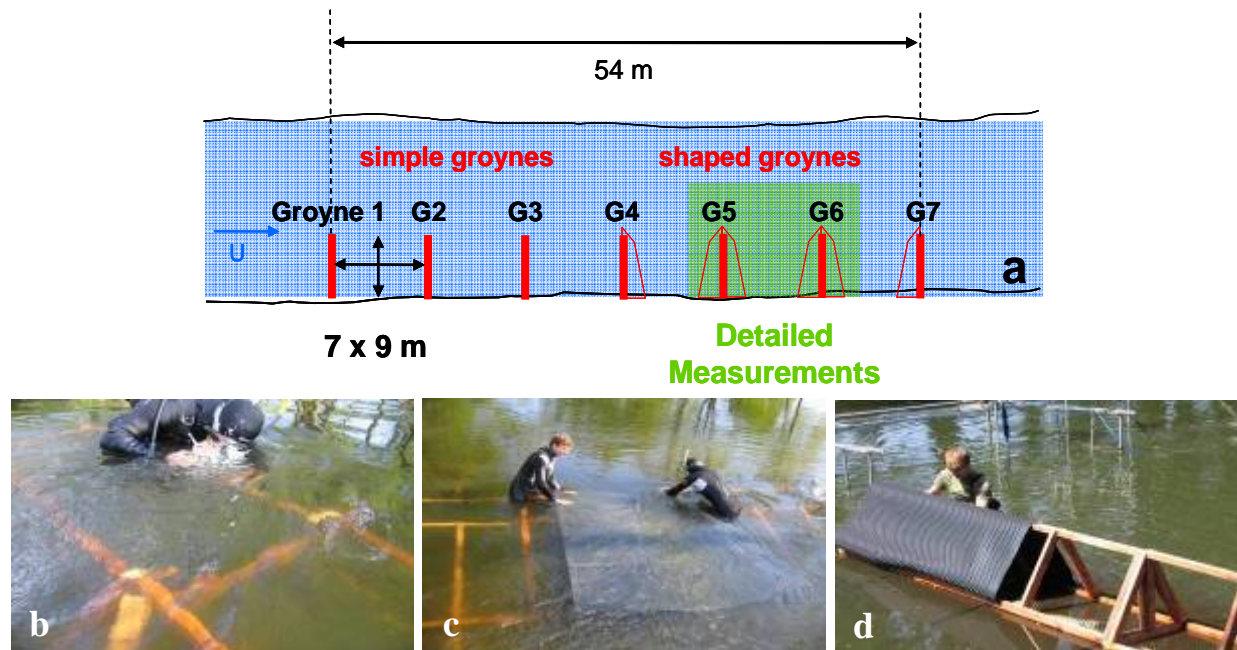


Figure 3.7: Experimental setup (a), and construction works (b) – (d) (river Spree, 2007).



Figure 3.8: River reach (river Spree) with installed groynes: submerged (a) and emerged conditions (b), 2007.

3.3 Field experiments and measurements

3.3.1 ADV point measurements – short-term

Experimental setup

Acoustic Doppler velocimeters (ADV) were used to measure flow velocities in groyne field 5 and 6.

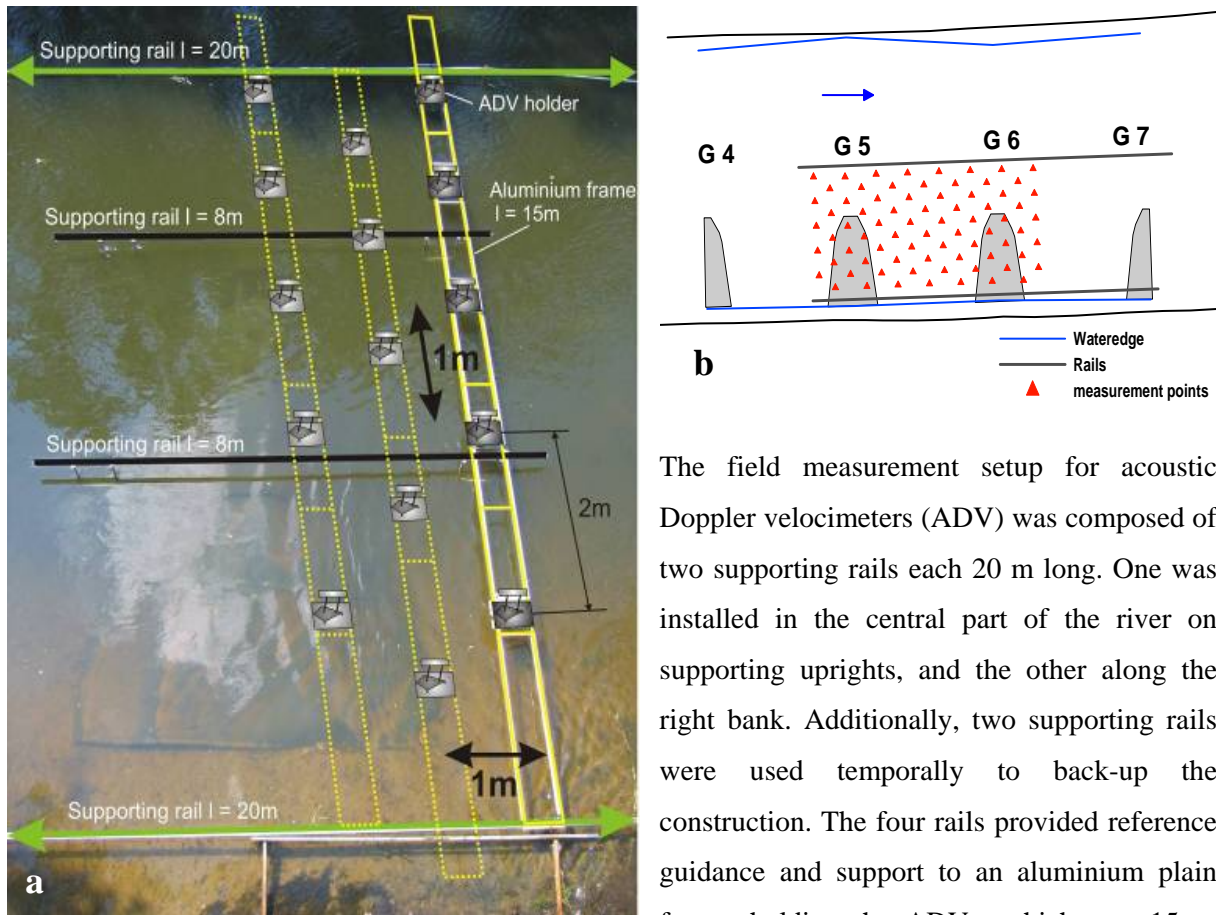


Figure 3.9: Experimental setup for ADV point measurements (a) and positioning of probes (b) at the river reach at the river Spree, 2007.

Five ADVs were fixed on holders onto the frame and spaced 2 m apart from each other. The aluminium frame was then traversed longitudinally with an increment of 1 m and staggered 1 m for every second longitudinal position (Figure 3.9). This method allowed an economic handling and an optimum coverage of the groyne field by ADV measurement points.

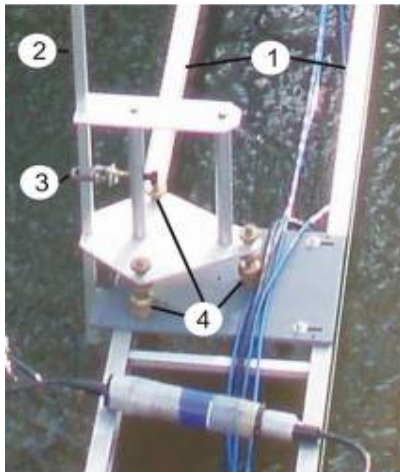


Figure 3.10: ADV mounting system employed for field measurements at the river Spree, 2007

The ADV holders were designed and custom-made at IGB (Fig 3.10). They can be firmly mounted on the plane aluminium frame (1). The ADV probe is fixed on a guiding rod (2) which can be vertically adjusted by a fixing screw (3). Three additional screws (4) are used to level the holders horizontally and to keep the guiding rod and the ADV probe upright. The system is stable and lightweight. It is hardly showing any vibrations and thus providing accurate ADV measurements. Furthermore it does not interfere with the flow near the sampling volume.

Measuring equipment

Flow velocities were sampled with two NorTek acoustic Doppler velocimeters (NDV, Oslo, Norway) and three NorTek Vectrino Velocimeters (Oslo, Norway). Vectrinos show further improvements to the NDV representing the second generation of ADVs. ADV devices are operating based on the Doppler shift effect and measure the 3D velocity of small particles such as zooplankton or suspended sediments transported with the flow. They are today widely used for single-point measurements in lab and field applications. Basic principles, description of the devices, principles of operation such as accuracy and measurement errors are discussed in the following sub-chapters.

Nortek Doppler Velocimeters (NDVs)

NDVs consist of three main modules: the measurement probe (Figure 3.11, 1), the signal conditioning module (Figure 3.11, 2) and the signal processing module (Figure 3.11, 3). The probe is fixed on a thin stem that is attached to a flexible 1-meter cable ending in the signal-conditioning module which is covered by a waterproof housing. The processing unit is connected to a portable computer from where the NDV unit is operated.



Figure 3.11: Nortek Doppler Velocimeter NDV employed for field measurements at the river Spree, 2007

The measurement probe comprises a separate transducer head and three receiver arms which are positioned in 120° increments along a circle around the transducer and are slanted 30° towards the axis

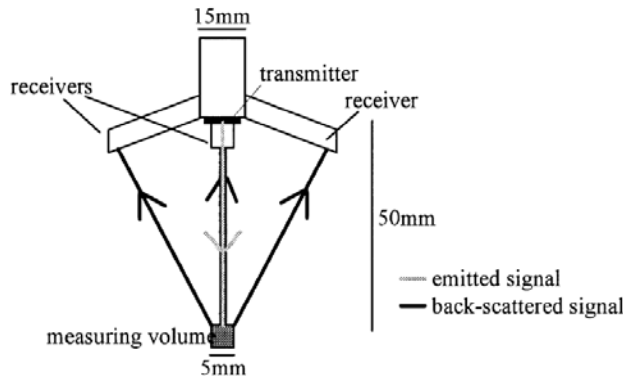


Figure 3.12: Sensor head of an Nortek Doppler Velocimeter

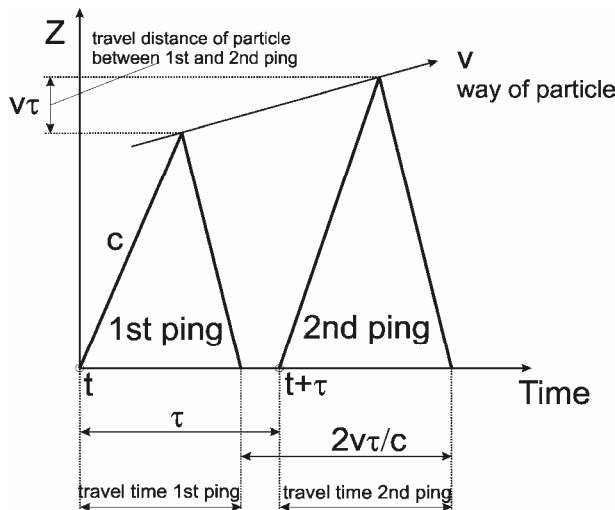


Figure 3.13: Schematic diagram of pulse-to-pulse coherent method

(from transmitter to particle in water and back) (Figure 3.13) between first and second ping is thus $\frac{2v\tau}{c}$. The offset in phase is $2\pi f \times \frac{2v\tau}{c}$ where c is the speed of sound in water and f is 10 MHz according to the NDVs operating frequency (LACY & SHERWOOD 2004). The instrument measures the phase shift and converts it into velocity data:

$$v = \frac{\Delta\Phi \times c}{4 \times \pi \times f \times \tau}$$

Measure velocity is an average of many ping pairs that increases accuracy. Acoustic Doppler velocimeters are able to record data at a sampling rate up to 25 Hz and are able to operate in changing flow conditions with velocities up to 2.5 m/s.

of the transducer. The NDVs used in this study were lab-types, having their focal point - the sampling volume - 5 cm below the probe head (Fig 3.12). The shape of the sampling volume is cylindrical. The vertical extent of the volume is defined by the length of the transmit pulse and the width of the receive window and can vary between 0.6 and 7.2 mm. This setup of the NDV probe is providing only little interference with the flow.

Acoustic Doppler Velocimetry is using a method called pulse-to-pulse coherent Doppler technique. The transmitter arm (Figure 3.12) emits pairs (first and second ping) of 10MHz pulses, one pulse shortly after the other, and each pulse is reflected by particles in the water and detected by the three receiver arms, the first at time t and the second at time $t + \tau$ where τ is the interval between the two pulses. If the flow velocity is assumed to be v , the reflecting particles travel a distance of $v\tau$ during the interval τ . The difference in travel time

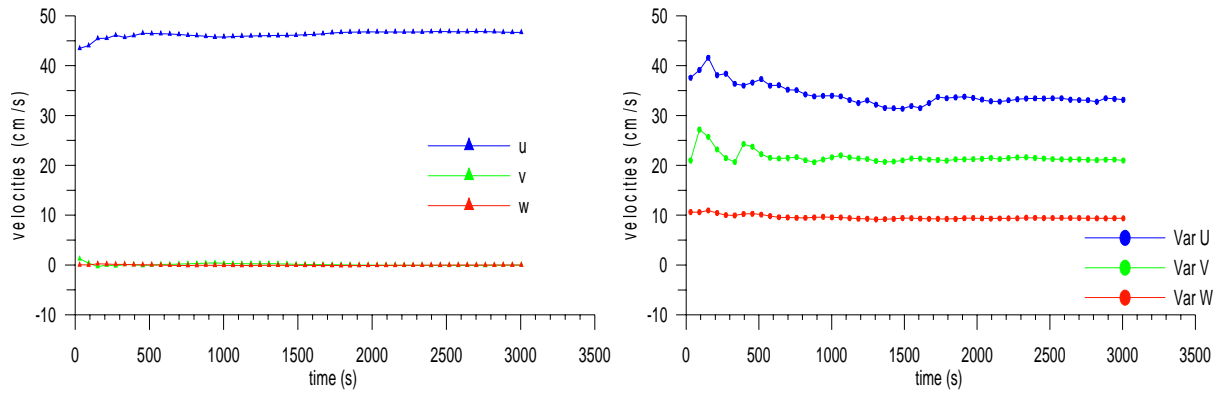
NorTek Vectrino Doppler Velocimeters

Figure 3.14: NorTek Vectrino Doppler Velocimeter employed for field measurements at the river Spree, 2007.

NorTek Vectrino Doppler Velocimeters (Figure 3.14) operate similar to NDVs but exhibit some improvements. Vectrinos are about the same size as the NDV, but their measure head has a smaller volume and thinner, rounder and more streamlined receiver arms. The transducer head samples a volume with an adjustable length of 3 – 15 mm and a diameter of 6 mm and which is positioned approximately 50 mm away from the transducer beam. The Vectrino measures four velocities: one streamwise component u , one transverse component v and two vertical components w_1 and w_2 . The additional receiver provides redundancy and allows for a better spectral estimate of the vertical velocity component (RUSELLO et al. 2006). Compared to the NDV, the Vectrino can measure all four velocities simultaneously without any breaks by applying parallel receivers. It shortens the interval time between the pulse pairs, thereby providing a higher maximum possible sampling rate of 200 Hz (RUSELLO et al. 2006).

Data collection

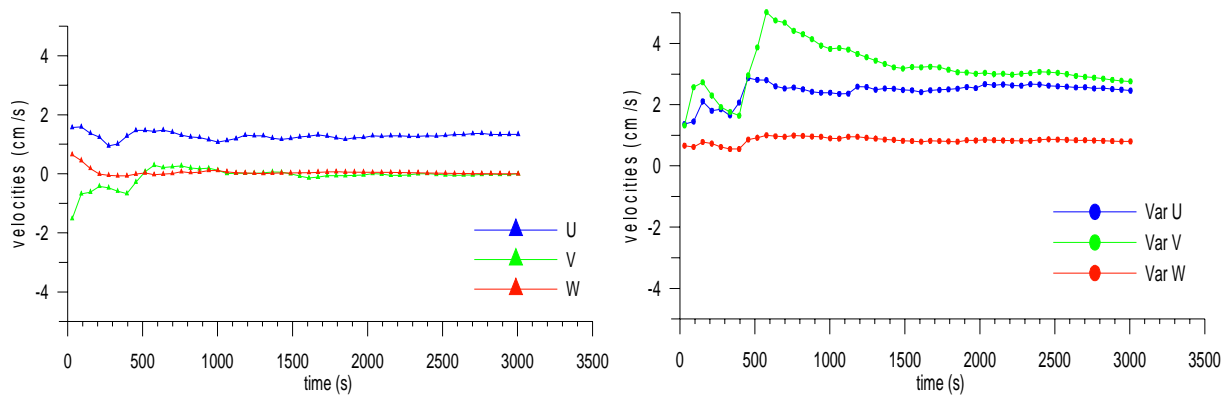
ADV measurements were performed in staggered verticals across groyne field 5, between groyne 5 and 6, and in the region adjacent to the main channel. Eight point measurements, uniformly distributed over the local river depth, were taken in each vertical. Increments between points varied from 5 to 15 cm depending on the local depth, the lowest measured points were approximately 3 cm above the river bed and the highest positions were seven centimetres below the water surface. The time series of three dimensional velocities were sampled at 25 Hz and at intervals of 240 seconds (4 minutes). The measurement intervals were chosen on a compromise between covering a dense enough grid and completing all measurements in reasonable time. At four locations, additional long-term measurements were taken and analysed towards stationary (see also chapter 3.2.2). Results of the stationary analysis at two locations in the GML and the groyne field are presented in Figure 3.15 and 3.16. In general, the measurement period of 240 seconds proved to be a good compromise to capture mean velocities and variations with acceptable inaccuracies. Note that the velocities and variances in the groyne field are an order of magnitude smaller than in the mixing layer.



Percentage error:

U	V	W	varU	varV	varZ
-1	241	-558	16	0	7

Figure 3.15: Stationary analysis for mean velocities (left) and variances (right) in the mixing layer – field experiments at the river Spree, 2007.



Percentage error:

U	V	W	varU	varV	varZ
-27	1516	-272	-29	-36	-26

Figure 3.16: Stationary analysis for mean velocities (right) and variances (left) in the groyne field (different velocity scale as compared to mixing layer) – field experiments at the river Spree, 2007.

NDVs and Vectrinos were operated by the PolySync software package (NorTek AS, Norway). PolySync is an option if one would like to control multiple velocimeters from a single computer or combine Vectrino and NDV units. It allows the user to setup data collection parameters like sampling rate, record length, recording file, and more. The program provides a real-time display of the velocity data, SNR, correlation, and others; it records the data into compact binary files on a hard disk, and monitors and displays status information and error warnings. Boundary profile measurements can be performed in addition to velocity measurements. This feature uses the acoustic signal strength to identify the distance to the boundary and plots it over time (NorTek, user manual). It can be used for measuring relatively fast morphodynamic processes like the movement of bedforms.

Data processing

Time series of ADV measurements were processed with the versatile commercial software package ExploreV 1.5 (Nortek AS, Norway). The software provides interactive graphical environment enabling fast and comprehensive data treatment (Fig 3.17).

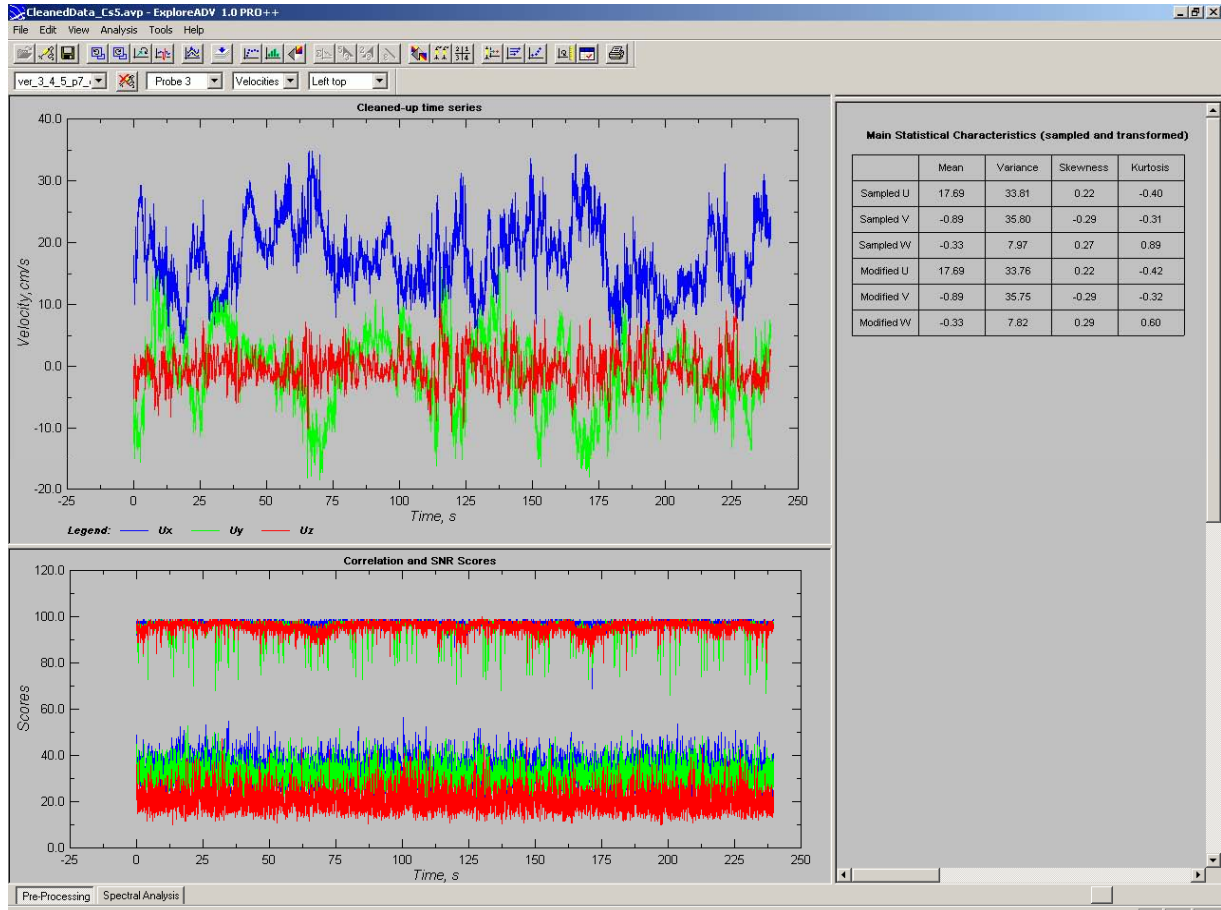


Figure 3.17: ExploreV with filtered time series, correlation and SNR scores and main statistical characteristics of measurement during submerged conditions in groynes field five (river Spree, 2007).

Sources of errors in ADV turbulence measurements can originate from either (1) random inaccuracies in measurement of Doppler-shift caused by turbulence and acoustic (Doppler) noise or from (2) non-random errors caused by limitation of the measurement technique (NYSTROM et al. 2002). Both types of errors can affect the accuracy of turbulence measurements.

Non-random errors like ambiguity errors result from phase shift measurements. The pulse-to-pulse coherent method cannot distinguish between phase shifts which are not in the range of $\pm \pi$ and thus maximum measurable velocity without aliasing has a phase change of $\pm \pi$. According to equation (3.1)

maximum measurable velocity is $v_{max} = \frac{c}{4f\tau}$. Five different velocity ranges can set v_{max} : ± 3 , ± 10 ,

± 30 , ± 100 , and ± 250 cm/s. The lower the range the longer is the interval between the transmitted pulses τ and the smaller is the overall number of transmitted pulse pairs. Shorter intervals allow for

measurements of more dynamic and higher velocities but cause more noise into the velocity signal (LANE et al. 1998). If the wrong range is set, spikes in the velocity records can occur.

Spikes can also be produced by boundary measurements when the signal that gets reflected from the boundary interferes with the signal returning from the sampling volume. This occurs when the time a signal needs for travelling from the sampling volume to the boundary and back equals the interval τ between ping pairs. This problem can be avoided by setting the right velocity range (LANE et al. 1998). Random Doppler-shift measurement errors caused by acoustic (Doppler) noise are the main reason for inaccuracies in turbulent measurements. Doppler noise can result from (1) suspended particles that remain in the sampling volume only for a limited time, (2) rapid changes in velocity structures because of small-scale turbulence, and (3) beam divergence of the probe (NIKORA & GORING 1998).

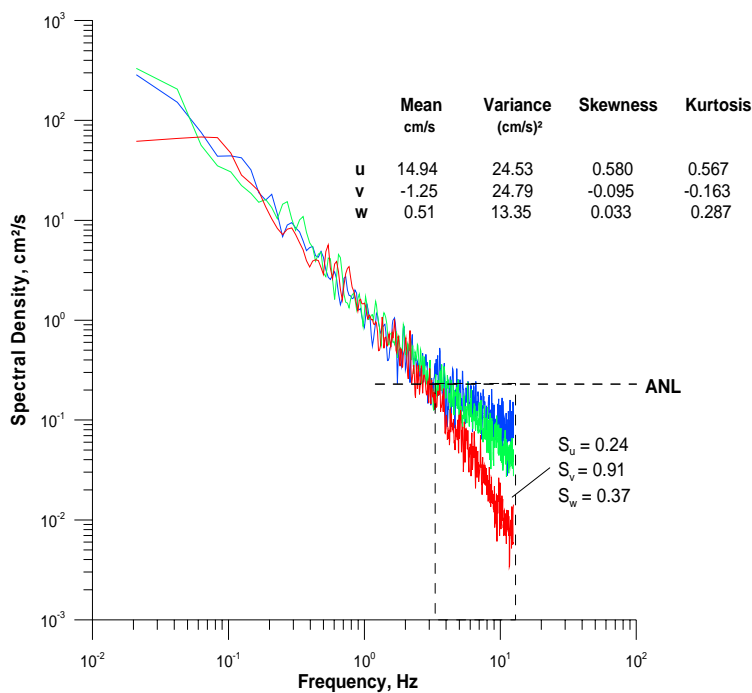


Figure 3.18: Power spectra for streamwise (blue), transverse (green), and vertical (red) components and statistics of the velocity distribution recorded during submerged conditions upstream near groyne 6 inside the groyne field (river Spree, 2007).

These factors can significantly affect the horizontal velocity components in the velocity spectra at higher frequencies. For the vertical component the noise is negligible small. A simple technique how to reduce Doppler noise in turbulent measurements is suggested in NIKORA & GORING (1998).

The value of noise can be estimated with spectral analysis by integrating the spectra with higher frequencies than the Acoustic Noise Level (ANL) over the frequency (S_u , S_v , S_w) and compare

to the total spectra of variance. However, measurements in the river Spree showed only small disturbance (max. 5% of total variance) by acoustic noise (Fig 3.18) and thus it was not necessary to correct the data set.

With ExploreV, measured time series were inspected visually to identify possible problems. ExploreV allows treating time series including bad samples by either linearly interpolating the bad sample between neighbouring values or by completely removing them. In case of interpolation the data can

still be used for spectral analysis which was the reason for choosing this option. Furthermore ExploreV provides the user with different methods to specify bad samples. One can set the Correlation Score threshold for velocities, the SNR threshold, and the velocity threshold. The latter is expressed as a multiple of the standard deviation of each velocity component. Spikes always generated velocity values more than 3 standard deviations from the mean (3σ). These spikes were removed and replaced using a 3σ filter in the time series option of ExploreV. Another option is the Spike Filtering method using an acceleration threshold value. This threshold is specified as a multiple of the gravity acceleration g . In this study the default value $g = 1$ was used. In all cases this post-processing procedure did not greatly affect the values of means, producing changes of only a few mm/s. Frequency distributions of the velocity data were also examined to identify outliers caused by interfering pieces of debris, leaves or fish in the sampling volume or by essential vibrations.

Spectral analysis

Spectra analysis was used to determine the inertial ranges and other subranges. After visual inspection of velocity records and filtering of erroneous samples data arrays were composed of each profile and the basic mean and turbulence statistics were exported as text files.

Presentation of contour and vector plots

Vector maps of mean velocity and contour maps of the turbulent kinetic energy in different horizontal and vertical plains were plotted. Turbulent kinetic energy contours were interpolated by hand and digitalised afterwards. Reynolds stresses $-u'w'$, $-u'v'$ and $-v'w'$ were measured with ADVs and are presented in two horizontal plains (see Appendix). Based on the stresses, an integral friction coefficient can be determined which is representing the loss of kinetic energy due to all sources of friction and turbulence. What makes this determination rather complicated is the coexistence of different flow classes (wall boundary layers, mixing layers, jet-like flows) and the changes in local mean flow direction due to the recirculation patterns. For example, the classical bottom friction factor definition only holds for simple boundary-layers flows without transverse stresses. In recirculating flows and evolving mixing layers – horizontal and vertical - profiles of Reynolds stresses are not linear over depth but affected by additional stresses along the water column. It was thus hard to extrapolate the profiles at some specific regions – especially in the emerged case. To overcome these problems, the friction factors here were determined from the sum of all stress components. The maximum stresses extrapolated to the bed then give a “pseudo shear-velocity”

$u_* = \left(\left(\overline{u'v'} \right)_{\max}^2 + \left(\overline{u'w'} \right)_{\max}^2 + \left(\overline{v'w'} \right)_{\max}^2 \right)^{1/4}$. Next, the bottom friction factor c_f was calculated by

$c_f = \left(\frac{u_*}{\bar{u}} \right)^2$ where the mean velocity was the local U in the submerged and the product $(UV)^{1/2}$ in the

emerged case.

3.3.2 ADV point measurements – long-term

Experimental setup

Long term measurements were performed in order to identify GML and DML coherent structures developing in the experimental river reach with groynes.

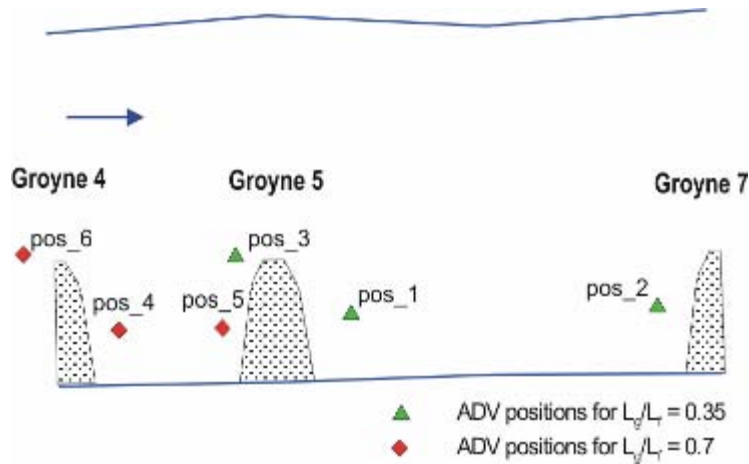


Figure 3.19: ADV positions for long term measurements of field measurements at the river Spree, 2007.

Four long term measurements with NDVs were performed at emerged conditions and after removal of groyne 6 (see also chapter 3.4). Two probes were placed inside the groyne field between groyne 5 and 7 (Figure 3.19: pos_1 and pos_2), one probe was installed inside the same groyne field (Figure 3.19: pos_1) and other probe was positioned approximately 1.5 m upstream to the tip of groyne 5 (Figure 3.19: pos_3).

Both probes were placed inside the groyne field between groyne 4 and 5 (Figure 3.19: pos_4 and pos_5) to allow measurements for the higher aspect ratio (experiment 3 and 4). The last constellation was one probe inside the groyne field between groyne 4 and 5 (pos_4), and the other probe 1.5 m upstream of the tip of groyne 4 (pos_6) (Figure 3.19) – representative for experiment 1. The probes were fixed upside-down on an aluminium rod which was rammed into the river bed. ADVs were kept at a level of approximately 20 cm below the water surface. Velocity measurements (50 minutes each) and boundary distance to water surface measurements to record water surface fluctuations were performed with this setup.

Data processing

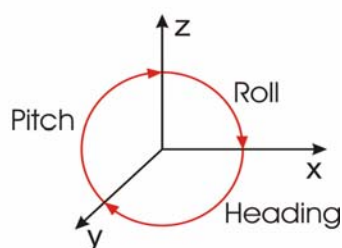


Figure 3.20: Change of NDV probe orientation

ADV data gained from long term measurements were processed as described in chapter 3.3.1.4. However, due the “upside down” setup of the ADVs, the orientation of the sampling volume of the probe had to be changed. It had to be rotated 180° in the vertical plane (due to the upside down position), also called pitching, and be aligned with the local streamline (also called heading) (Figure 3.20).

Autocorrelation is a mathematical tool for finding repeating patterns, such as the presence of a periodic signal, or identifying the missing fundamental frequency in a signal. It is used frequently in signal processing for analyzing time series of values. Informally, it is the similarity between

observations as a function of the time separation between them. More precisely, it is the cross-correlation of a signal with itself. Auto correlation function for velocity time series was calculated according to:

$$R_u(\tau) = \lim_{T \rightarrow \infty} \frac{\sigma_u^{-2}}{2T} \int_{-T}^T u(t + \tau) u(t) dt, \quad u = u', v', \text{ and } w'$$

where σ is the standard deviation, T is sampling period, t is the time, and τ is the time lag. $u = u', v',$ and w' are velocity vector components in streamwise, transverse, and vertical direction respectively.

In order to examine the turbulent flow, in particular coherent structures further, auto spectra of turbulence were constructed. They were obtained by applying Fourier transformations to autocorrelation functions

$$S_u(f) = 4\sigma_u^2 \int_0^{\infty} R_u(\tau) \cos 2\pi f \tau d\tau$$

where σ is the standard deviation, τ is the time lag, and f is the frequency. This transformation allows viewing and analysis of correlations in the frequency domain. The ordinates of the auto-spectra are the amounts of turbulent energy related to a certain eddy via its dominant frequency.

Cross-correlations between measured time series at position 4 and 5, and 4 and 6 were conducted. Cross-correlation is a standard method to measure the time shift between two time series. Cross-correlation function for a pair of synchronous records is defined as:

$$R_{1-2,u}(\Delta x, \tau) = \lim_{T \rightarrow \infty} \frac{\sigma_{1-2,u}^{-2}}{2T} \int_{-T}^T u_1(t + \tau) u_2(t) dt$$

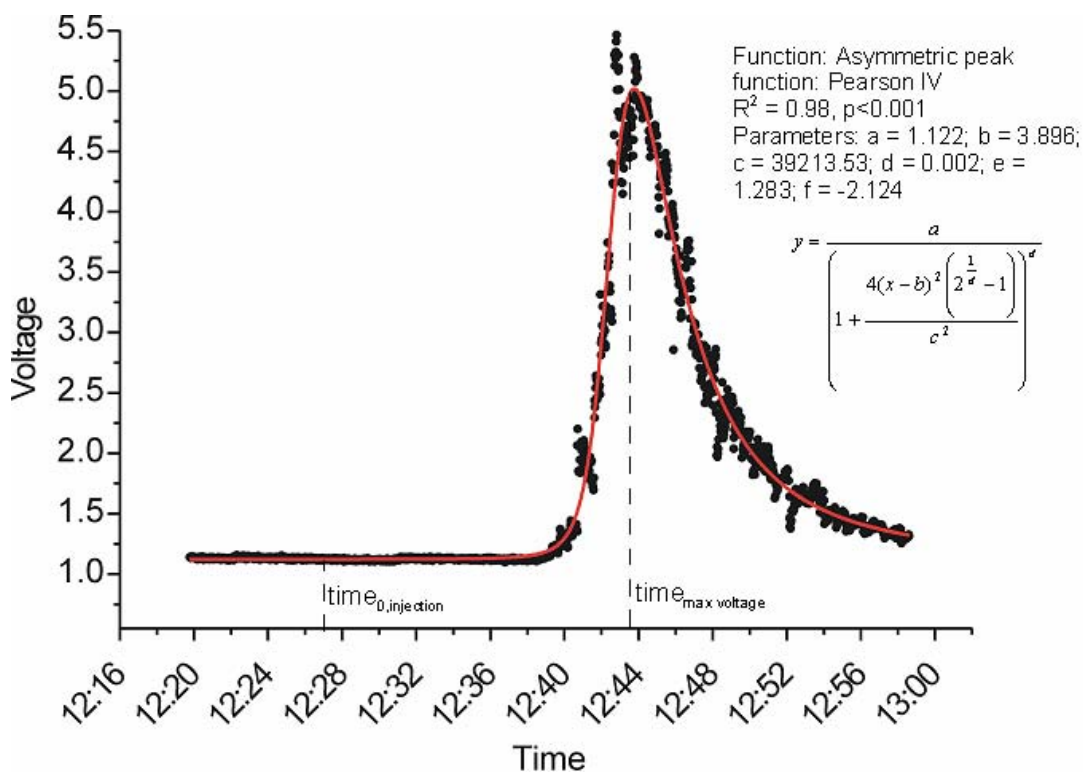
where u_1 and u_2 are the mean velocities in streamwise direction at two different measurement points, and Δx is longitudinal spatial lag.

3.3.3 Tracer studies



Figure 3.21: Dye injection for tracer studies: uranin dye injected as a line source across the river (river Spree, 2007).

For the discharge estimation, dye was injected as a line source across the channel (Figure 3.21) at gauging station 1 (see also 3.2.3) and the concentration was measured 297.8 m downstream at gauging station 4 by a fluorometer. Results of the distribution of uranin concentration over time and curves of best fit (Pearson IV) are shown in Figure 3.22. Knowing the time lag between injection and peak voltage at the measurement point and the distance between the place of injection and the fluorometer, the velocity was calculated.



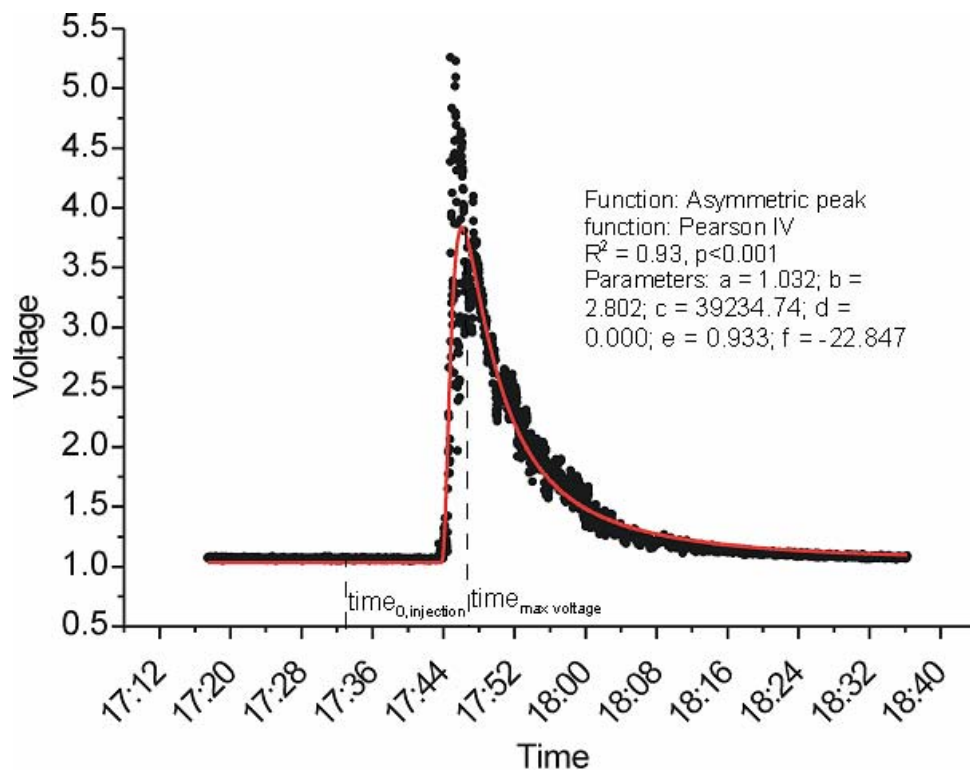


Figure 3.22: Distribution of uranin concentration over time for experiment 1 (above) and experiment 2 (below). Red lines represent the curves of best fit obtained by fitting voltage against time using an asymmetric peak function (Pearson IV).

3.3.4 Visualisation technique – Dye Injections

Dye injections with uranin were conducted to visualise the flow patterns in the groyne field. Approximately five grams of uranin powder were dissolved in 15 l of water (Fig 3.23a) and injected punctually at selected points e.g. at the tip of the groyne (Fig 3.23b and Fig 3.23c). The spreading of the tracer cloud was recorded by a camera (type Olympus C-5060) installed on a platform constructed in a nearby tree, 12 m above the water level.



Figure 3.23: Dye injection: Dissolving of uranin dye (a), fixing of the injection tube (b), and injection (c).

3.3.5 Particle tracking velocimetry (PTV)

PTV is a Lagrangian method to determine flow field characteristics and dynamics of coherent structures by capturing trajectories of particles moving with the flow. PTV has been developed in the laboratory and the present application to the field scale can be considered as unique and highly innovative. The main problems associated with PTV in the field are the type of and how many particles to use, how and where to place them into the current, how to accomplish good contrast between the particle and the background, and how and from where to record the particles. This has been intensively discussed in the master thesis on field application of PTV of CHRISTIAAN ERDBRINK (2007) who participated in the first experiment on shallow mixing layers at IGB in 2006. Experiences from the previous campaign were of great value for further improvements of the PTV method. As surface floaters, custom-made tea candles with reinforced wicks were added to the flow. A camera was mounted 12 m above the water level on a platform to record the motion of the floaters. The focus of the camera was covering groyne field 5 where the detailed ADV-measurements were conducted too (Figure 3.7a). Like last year, the experiments were conducted during late evening after sunset to achieve optimum contrast between floaters and water surface.

One significant improvement was the installation of the rails which were used as reference points for the images. This was accomplished by placing tea candles at locations with known coordinates on the rails and to record them before releasing the floaters. In the submerged case (experiment 1) the candles were added to the flow from a bridge upstream, installed on top of groyne 1. Around 250 candles were released by four persons in a time interval of 20 minutes. Two more persons helped operating the camera and collecting the floaters by kayak downstream of the groyne section. The release points of candles during the emerged conditions (experiment 2) were more widely spread. Most candles released from the bridge were entrained into the first groyne field and thus, out of reach of the camera angle. For this reason, floaters were also added at the upstream groyne tip and in the fast stream close to the groynes where an operating platform was anchored.

A significant limitation was the influence of wind during experiment 4, when candles were pushed towards the right bank by the upcoming wind. Minor problems were that spilled wax made candles stick to each other, in particular for emerged conditions when drifters slowly recirculated in the groyne field. The storage capacity of the camera was large enough to record 20 minutes which was a sufficient period to catch most of the released candles.

3.3.6 Water level readings

Alongside the right bank of the experimental river reach, four locations for water level readings had been installed, each including three to five gauging poles rammed into the river bed at different levels (Figure 3.24). The poles are simple dowels with a nail on top and their positions and elevations are known from total station surveys. Water level readings were taken several times a day by measuring the distance between water level and the top of the poles and later converted into absolute water levels (Figure 3.2).



Figure 3.24: Experimental river reach with gauging stations (GS) 1 to 4 at the experimental river reach (river Spree, 2007).

3.3.7 Topographical survey

Measurements of river depth were performed with hydrometrical wading rods. Along both banks of the river, starting 3.5 m upstream of groyne 5 and ending 7 m downstream of groyne 7, marking poles were placed one meter apart from each other and georeferenced by a total station survey. A steel cable with meter-markings was then stretched between these poles across the river and water depth readings were performed with a wading rod at each mark, resulting in a grid of 1 x 1 m (Figure 3.25). Knowing the measured offset of the poles to the marks on the cable and the water level readings at the gauging poles, the absolute coordinates of the bathymetry were calculated.

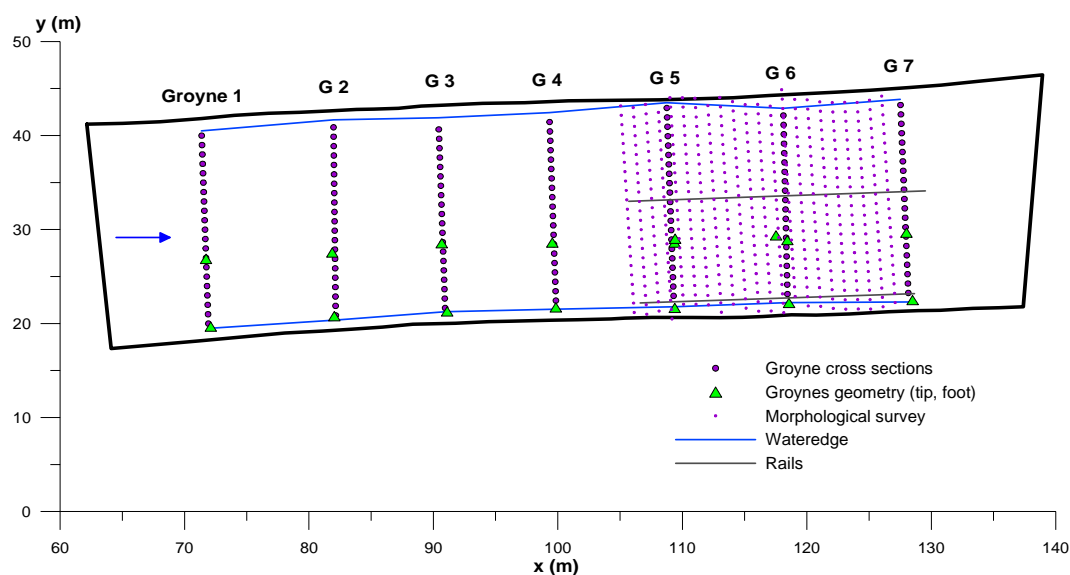
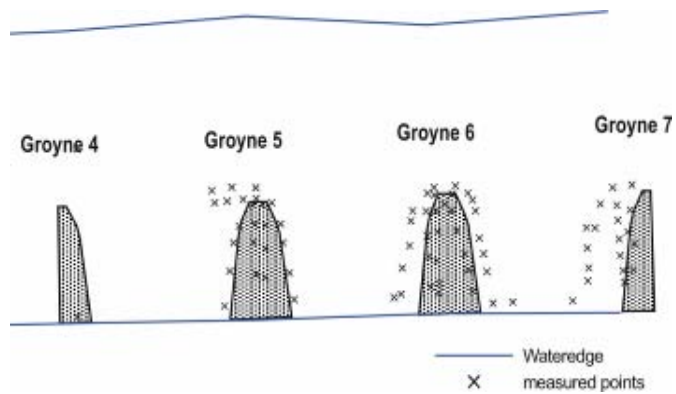


Figure 3.25: Topographical survey of river reach with groynes – measurement points at the experimental river reach (river Spree, 2007).

All groyne cross sections and additional profiles further up- and downstream were measured accordingly to allow extrapolation of data. Information about bathymetry of the river bed could also be collected at every vertical of ADV measurements where water depths were taken as well. Handwritten data was later converted to digital form for further analysis and representation in graphical format.



Furthermore, a geodetic survey with the total station was accomplished during experiment 1. Geographical coordinates and elevations above the sea level were measured using ELTA R55 (Carl Zeiss Geodetic Systems, Germany). The aim of the survey was to get additional coordinates of the groynes as well as the levels of scour

Figure 3.26: Points measured by total station for geographical coordinates of groynes and groyne fields at the experimental river reach – river Spree, 2007..

and deposition (Figure 3.26).

3.4 Experimental program - overview

	EXP1	EXP2	EXP3	EXP4	Outcomes	Comments
date	16.05 - 25.05	26.05 - 03.06	04.06 - 11.06	12.06 - 17.06		
helping hands	W. Brevis N. Rütger A. Reiprich	B. Vowinkel A. Reiprich	W. Uijtewaal C. Erdbrink C. Wirtz A. Reiprich	A. Reiprich		
setup	$\zeta = L_g / L_r$ 0.7 1.6	0.7 emerged	0.4 emerged	0.4 not verified		L_g = groyne length; L_r = distance between groynes h = water depth; H_g = groyne height
ADV short	600	480			mean and turbulent flow characteristics	
ADV long		x	x		coherent structures, correlations	
boundary distance	x				sand dunes movement	Drop of water level by 40cm
WL fluctuation		x	x		seiche in groyne field	Data could also be used for experiment 2
PTV	x	x	x	x	vizualisation of large scale structures	
Dye Injection	x	x	x	x	vizualisation of flow field	
Tracer	x	x			discharge	
Morph. Survey	x	x	x	x	bathymetry	Data not further analysed in this study
Total Station	x				bathymetry, positioning	Data not further analysed in this study
WL Readings	x	x	x	x	water level gauging	
Comments		1 Verimo defect		PTV not useable		

4 EXPERIMENTAL RESULTS AND ANALYSIS

This chapter presents the results of the field measurements, including the mean flow field and statistical turbulence quantities such as turbulent kinetic energy and Reynolds stresses. The bottom friction and shear velocities are derived from these data and summarised in tabular form for direct comparison. Furthermore, special regard is given to the analysis of coherent structures and exchange processes based on long-term measurements of velocity and water level fluctuations. The results in each subchapter will start with the analysis of emerged conditions and be followed by submerged conditions. All data are in a Cartesian coordinate system with streamwise coordinate x , transverse coordinate y from main channel towards right bank and vertical coordinate z relative to the river bed. The corresponding mean velocities are denoted U , V , W and the turbulent intensities are denoted u' , v' , w' .

4.1 Mean velocity patterns

Emerged case

Plan-view vector maps of mean velocities revealed a clear recirculation pattern (Figure 4.1a-c). One large gyre established which occupied the entire groyne field. The lowest velocities were about 1 cm/s near the riverbed and 3 cm/s near the surface in the central part of the gyre. From this point on, velocities increased towards the gyre margins where maximum values of approximately 6 cm/s near the bed and 8 cm/s near the surface were measured. The gyre was well defined in all vertical plains and the magnitudes of velocities did not change substantially over the depth thus highlighting its two-dimensional character. In the neighbouring groyne fields, redundant measurements were taken which gave a good proof of stable and fully developed flow conditions in the measurement section and on the accuracy of measurements. In the topmost horizontal layer (Figure 4.1c), the presence of a secondary gyre in the corner of the groyne field was indicated by three vectors which counter-rotate against the primary gyre.

The longitudinal cross sections in Figures 4.2a-c emphasise the two-dimensional recirculation pattern in the groyne field. Figure 4.2a presents a section near the groyne tip where velocity vectors are pointing in streamwise direction in contrast to the section near the bank where the local flow is directed towards upstream and against the main channel flow (Figure 4.2c). At some locations close to the bed, vectors are not uniformly oriented over the water depth. One reason may be that these locations were close to the margins of the dimpled sheet coverage and thus affected by local seepage through the groynes. In general, this effect is negligible when comparing the mean flow pattern.

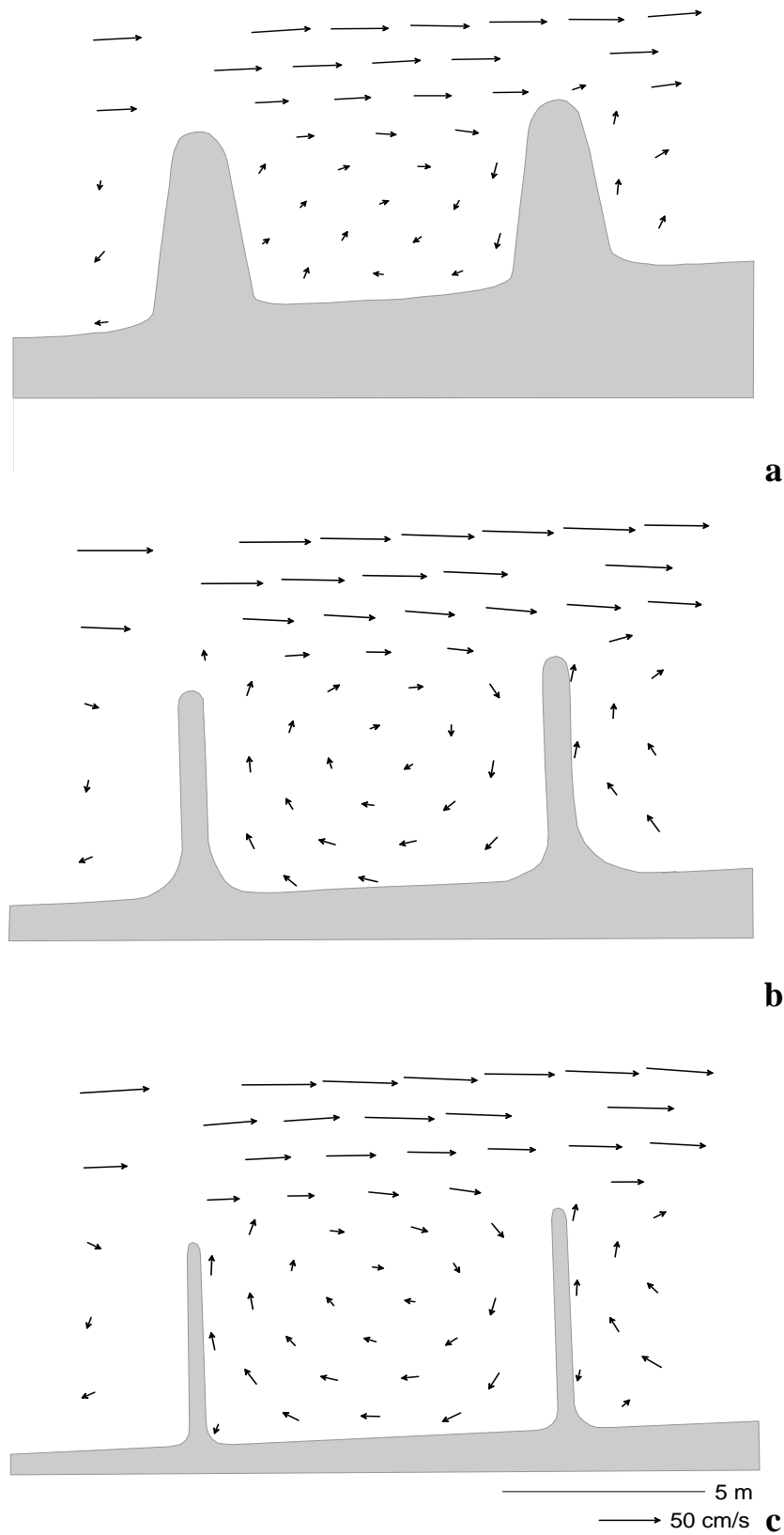


Figure 4.1: Vector plots of mean velocity for emerged conditions: near the bed (a), at groyne crest level (b), and near the surface (c) – field measurements at the river Spree, 2007.

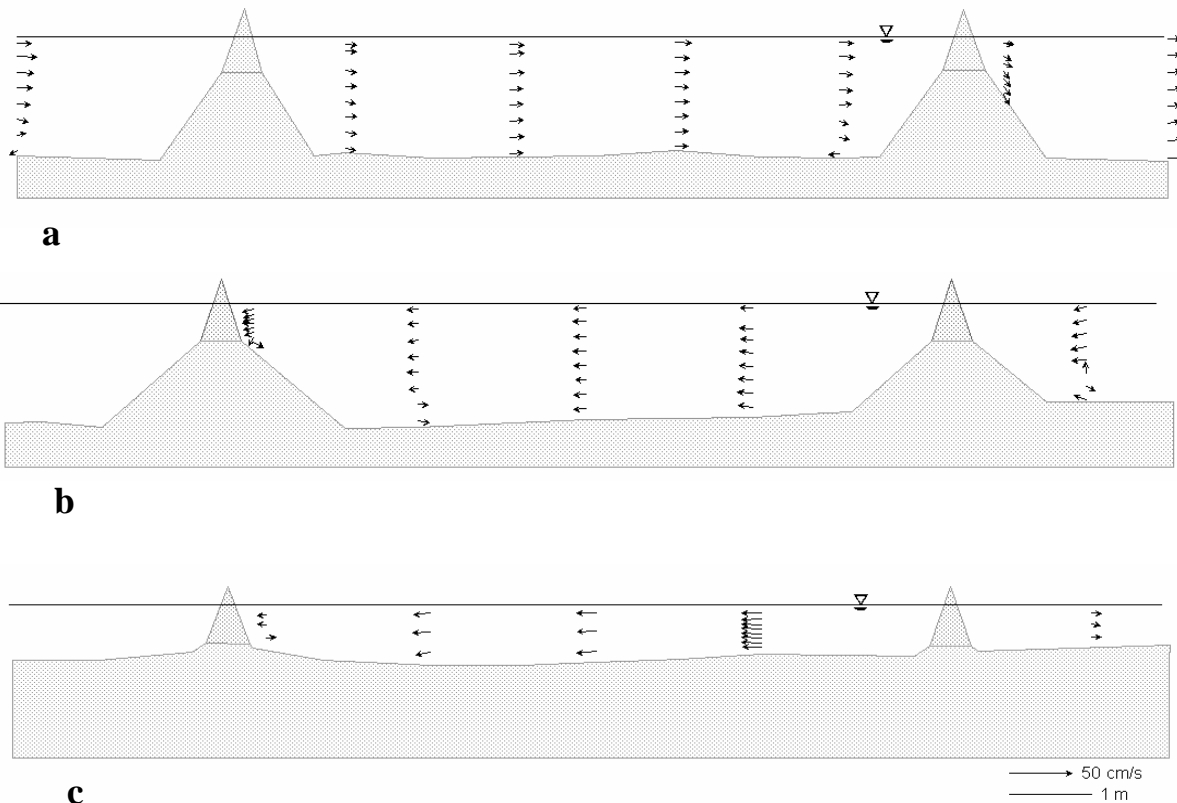
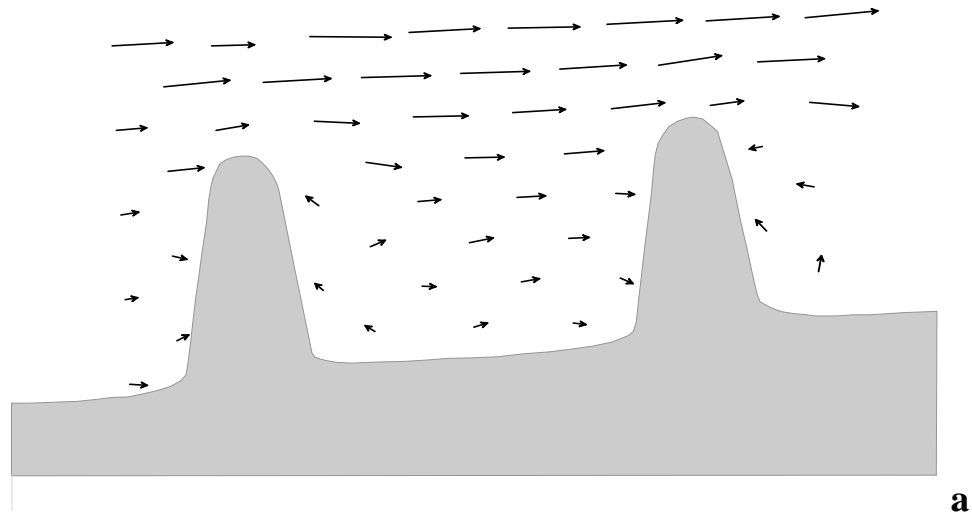


Figure 4.2: Vector plots of mean velocity for emerged conditions in longitudinal sections: a vertical plane 1.3 m inside the groyne field and away from the groyne tip (a), 2 m from the bank inside the groyne field (b), and near the bank (c) – field measurements at the river Spree, 2007.

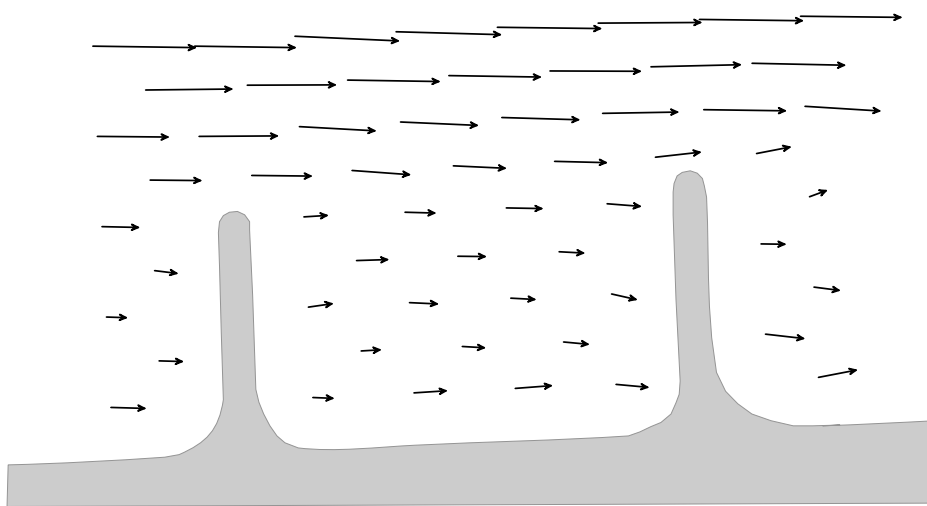
Submerged case

Figures 4.3a-c present plan-view vector maps in three horizontal planes. In all planes, the gyre pattern completely disappeared and the flow is oriented parallel to the main stream flow direction except at some points in the lee of the groynes and close to the bed which are affected by a vertical recirculation cell. This cell is clearly visible in the vertical velocity profiles in Figures 4.4a-c. The reason for the recirculation is flow separation at the groyne crest. The flow overtopping the groyne is accelerated due to an increased pressure gradient between the stoss and the lee-side of the groyne. Furthermore, the local pressure gradient which has its maximum above the groyne tip pushes the flow towards the banks (see Figure 4.5a) where accelerated velocities were measured. The reattachment of the streamlines is located at a distance of approximately 3 m downstream - around 4.5 times the groyne height (Figure 4.4a). The space in between is occupied by the large recirculation cell. Due to the bathymetry and cross-sectional shape of the groynes, the cell is not ideally two-dimensional like a cylindrical roller but decays towards the bank. Close to the bank the side slopes of the groyne are mild and prevent the overtopping flow from separation. In Figure 4.4c only the lowest vector in the lee is oriented counter-streamwise which points out that the cell has practically disappeared. Taking into account the horizontal DML at the groyne tip, the flow structure

becomes even more complex. The superposition of both DMLs causes the recirculation cell to rotate not only in vertical plane but also in a horizontal – causing spiralling flow paths behind the groynes (see Figure 4.5b).



a



5 m
50 cm/s

b

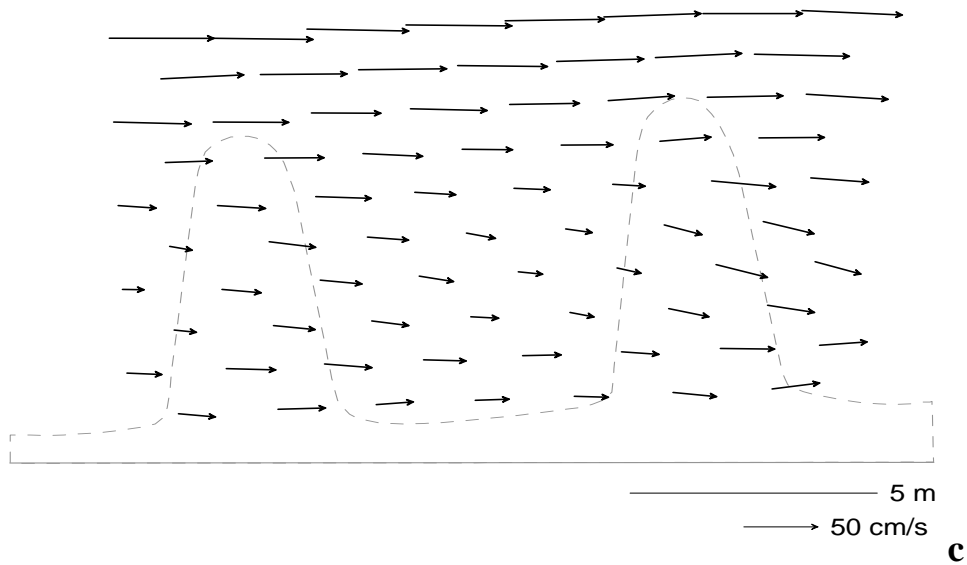


Figure 4.3: Vector plots of mean velocity for submerged conditions: near the bed (a), at the groyne crest (b), and near the flow surface (c) in submerged condition – field measurements at the river Spree, 2007.

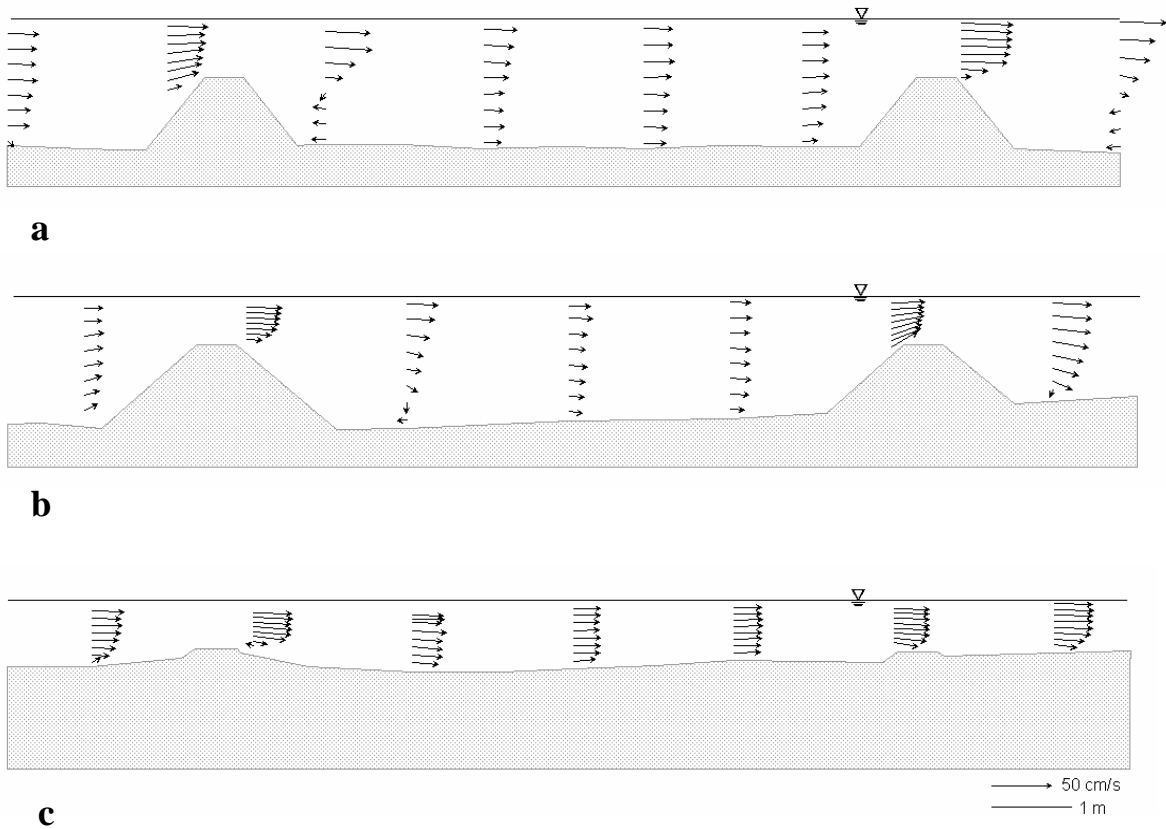


Figure 4.4: Vector plots of mean velocity for submerged conditions in longitudinal sections: a vertical plane 1.3 m inside the groyne field and away from the groyne tip (a), 2 m from the bank inside the groyne field (b), and near the bank (c) – field measurements at the river Spree, 2007.

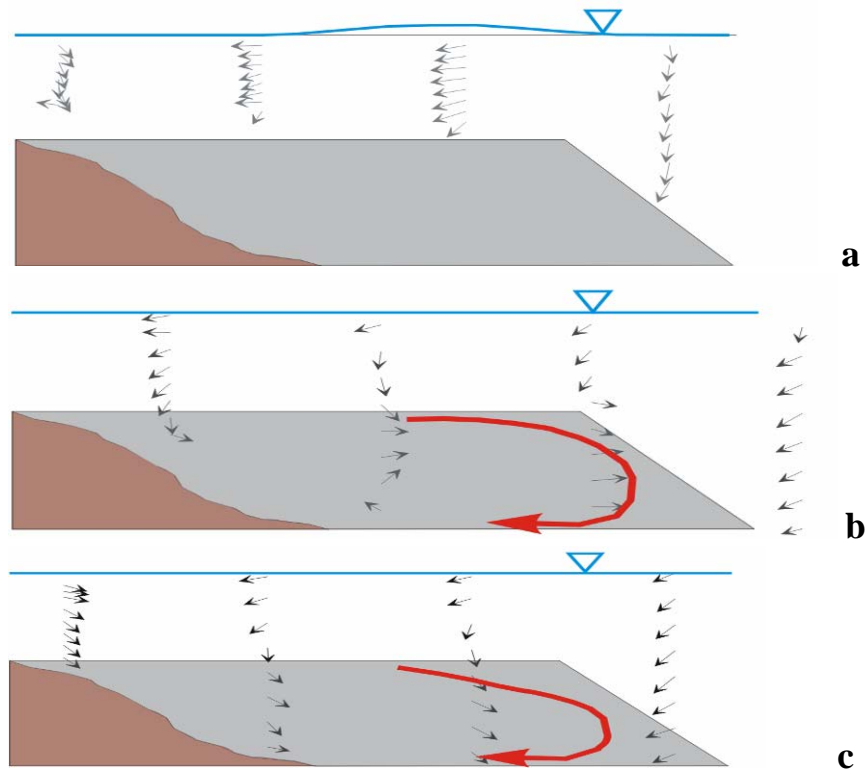


Figure 4.5: Mean velocity vector distributions in transverse sections through the groyne field during submerged condition, view towards upstream (water surface elevation is only schematic): on top of the groyne (a), in the lee-side of the groyne (b), and approximately 1.5 m downstream of the groyne (c) – field measurements at the river Spree, 2007.

4.2 Turbulent kinetic energy (TKE)

Emerged case

Contour plots of TKE for emerged conditions reveal the highly turbulent GML which occupies a width of approximately 3 m measured from the groyne tips. In addition, distinctive local strips of increased TKE are located between the main stream and the groyne field which corresponds to the location of the DML. The peak values are around $50 \text{ cm}^2/\text{s}^2$ close to the water surface and up to $65 \text{ cm}^2/\text{s}^2$ near the bed where the effect of bed shear superimposes (Figure 4.6a and b). The absolute magnitudes differ slightly between groyne tip 5 and 6, which may be related to minor constructional inaccuracies (e.g. orientation and length of the groynes). Another local increase of TKE occurs at the stoss-side of the downstream groyne which is associated with turbulent fluid advected by the gyre from the GML into the groyne field. In the centre of the groyne field, TKE has its minimum due to the low flow velocities which also points out, that this region is not affected by intrusions of large coherent structures from the GML (Figure 4.6a and b). The

longitudinal cross sections in Figure 4.7.a and b are located outside of the GML and DML and thus only reveal the locally increased TKE which indicates fluid advected from the GML in the main stream. In all verticals, TKE is distributed relatively constant over the water depth – well in agreement with the velocities and confirming the two-dimensionality of the flow in emerged conditions.

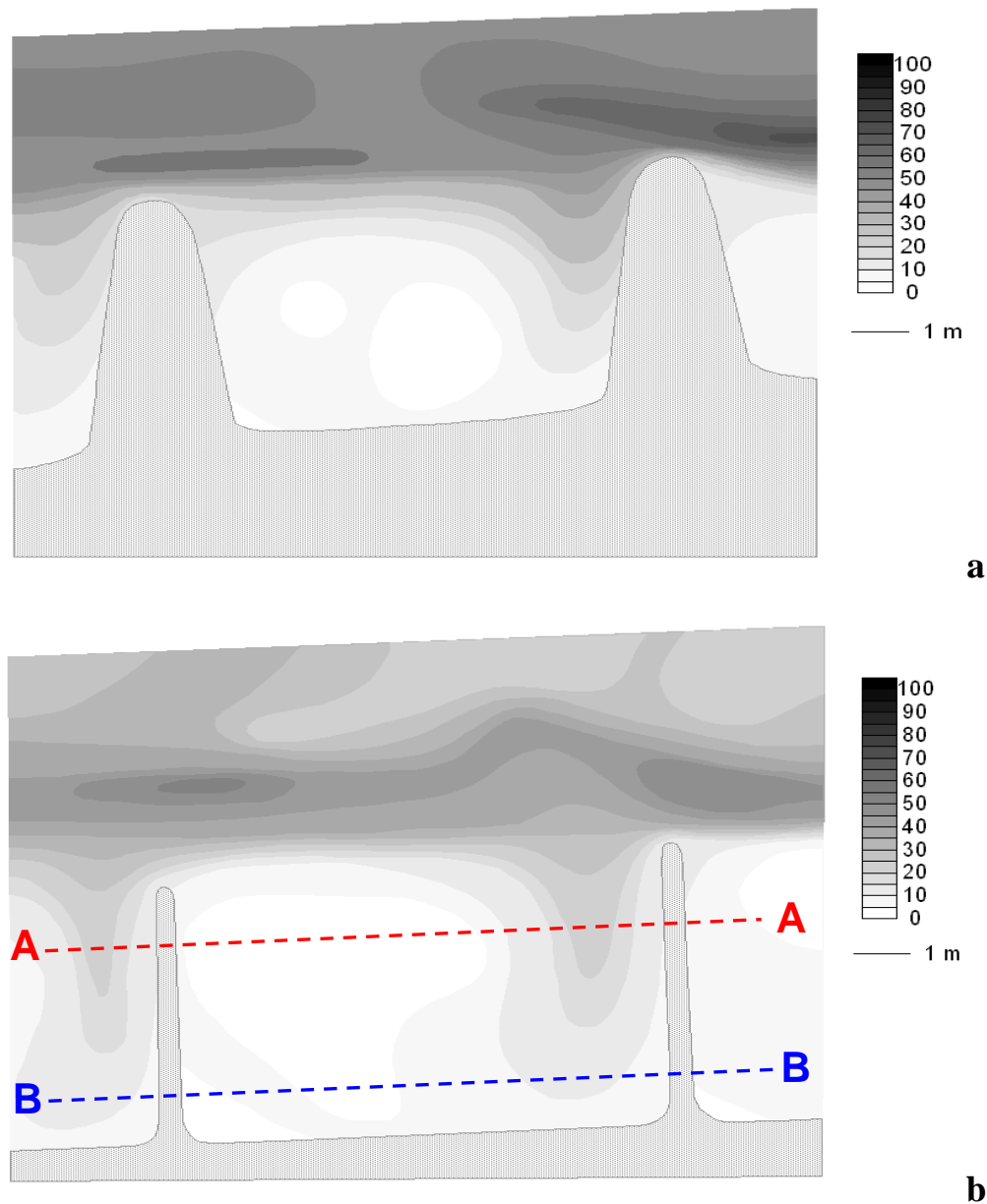


Figure 4.6: Turbulent kinetic energy distribution (cm²/s²) near the riverbed (a) and near the flow surface (b) in the groyne field during emerged condition – field measurements at the river Spree, 2007.

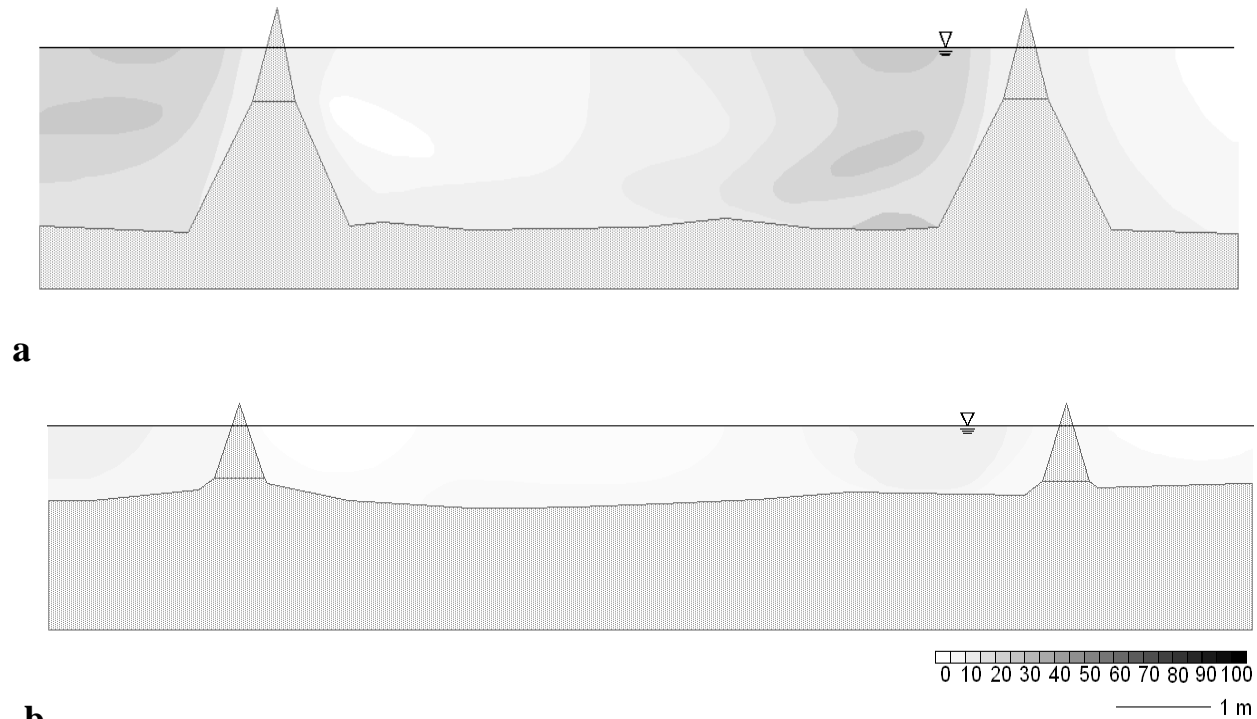


Figure 4.7: Turbulent kinetic energy distribution (cm^2/s^2) in longitudinal sections through the groyne field during emerged conditions: cross section A - A (a) and B -B (b) – field measurements at the river Spree, 2007.

Submerged case

The level of TKE is only comparable to emerged conditions in the region of the GML (Figure 4.8). All other sections have higher TKE magnitudes for submerged conditions due to the higher velocities in the groyne field. The most significant differences are the location and magnitude of the absolute maximum of TKE in the lee of the groynes. This is the region where the horizontal and vertical DMLs merge. Due to the acceleration of the flow overtopping the groyne, the vertical DML is even stronger which shows in the increased TKE close to the bed and around the reattachment point. Absolute values are up to $100 \text{ cm}^2/\text{s}^2$ and thus significantly higher than TKE due to the horizontal DML in the emerged case. Furthermore, the occurrence of such high TKE peaks inside the groyne field gives evidence for field observations right after flood events when damages and scour occurred not at the groyne heads but in their central parts.

The longitudinal cross section near the groyne tip captures clearly the high TKE due to the vertical DML. This shear layer evolves from the separation of streamlines from the groyne crest and grows vertically until it reaches the bed and the surface after around one third of the groyne field length (Figure 4.9a). The level of TKE steadily decreases towards the bank as the vertical DML weakens and wall boundary layer effects dominate (Figure 4.9b).

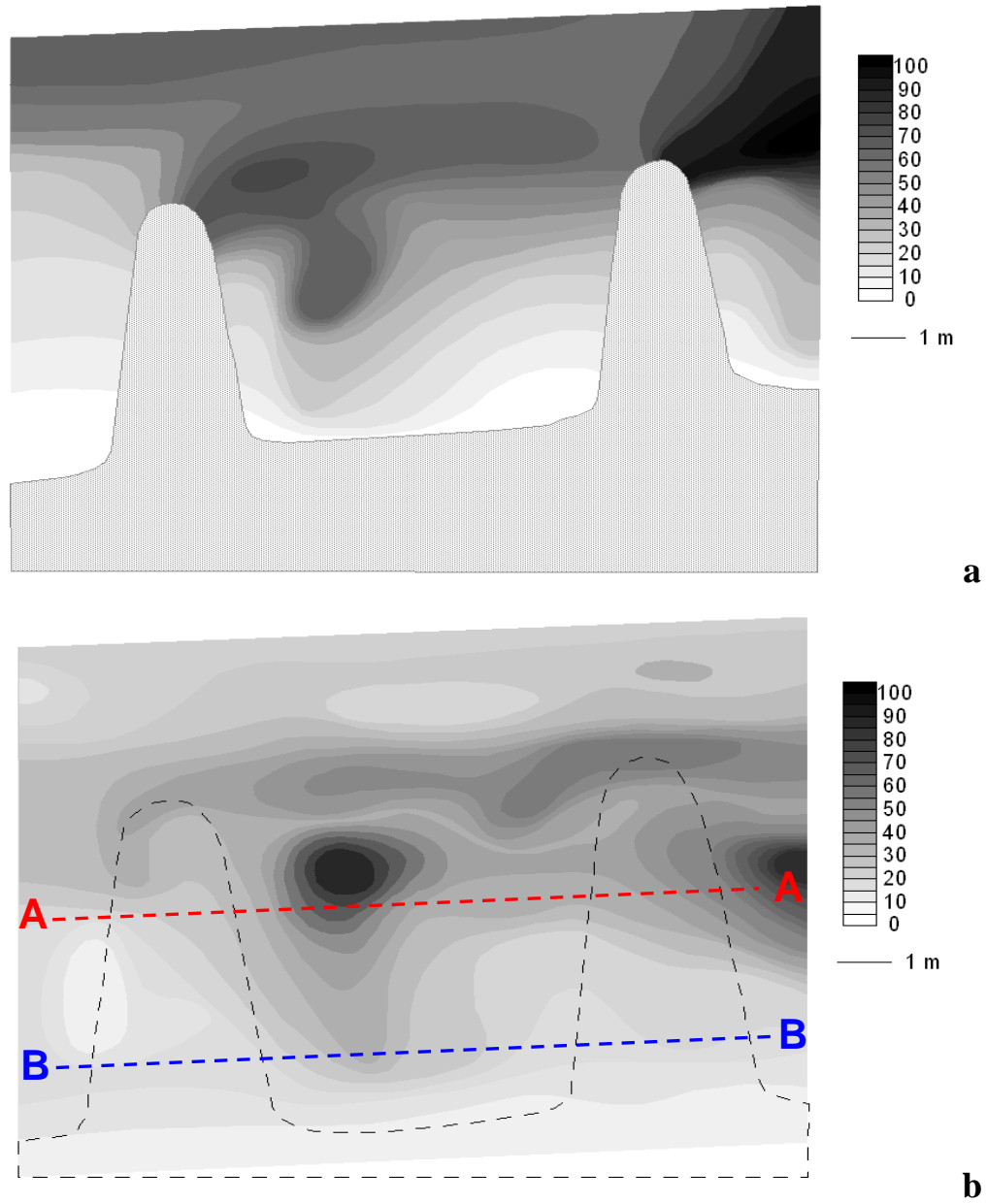
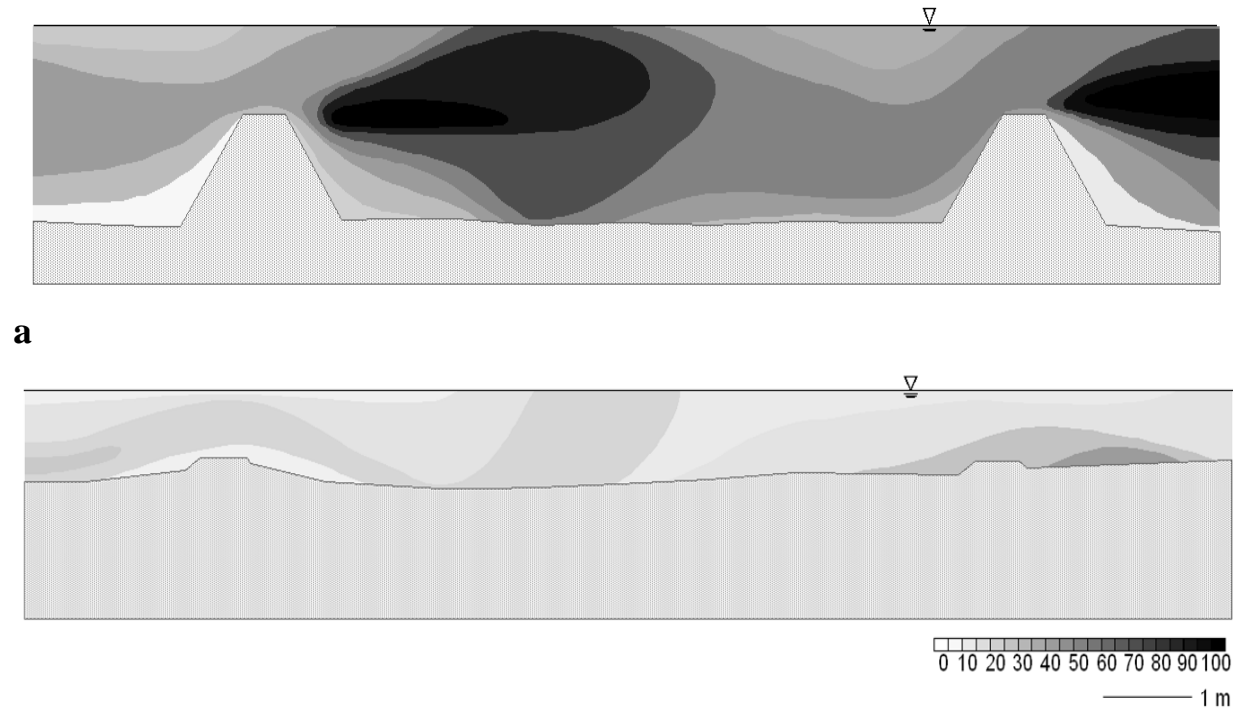


Figure 4.8: Turbulent kinetic energy distribution near the riverbed (a) and near the flow surface (b) in the groyne field during submerged condition – field measurements at the river Spree, 2007.



a

b

Figure 4.9: Turbulent kinetic energy distribution in longitudinal sections through the groyne field during submerged conditions: cross section A - A (a) and B -B (b) – field measurements at the river Spree, 2007.

4.3 Stresses, bottom friction and shear velocity

A detailed analysis of all three Reynolds-stress components was out of scope for the thesis. Instead, only some trends are presented in tabular form in Table 4.1 for emerged and Table 4.2 for submerged conditions. To directly compare the data, the groyne field was virtually separated into regions where different hydrodynamic mechanisms prevail. These regions are: DML and GML, the groyne field centre, lee-side and stoss-side of the groyne and banks. Shear velocities and bottom friction coefficients were determined using the methods introduced in Chapter 3.4. Exceedingly high values of bottom shear which occur in the lee and stoss-region of the groynes indicate the superposition of different hydrodynamic mechanisms such as horizontal with vertical DML or with bed shear stress – which principally is not valid. As there is no alternative to determine integral roughness parameters for such a complex flow, the values were kept in the Tables. Subsequent analyses will be performed with the data in chapter 5 – using some parameters of the GML where the method of bottom friction determination is reasonably accurate.

Table 4.1: Reynolds stresses $u'w'$ and $u'v'$, mean velocities u , bottom friction velocity u_* and bottom friction factor c_f , and turbulent kinetic energy TKE at different places around the groynes for submerged conditions. Values affected by uncertainty are marked with (*).

Exp 1 - submerged	$u'w'$ cm ² /s ²		$u'v'$ cm ² /s ²		u cm/s		u_* cm/s	c_f -	TKE cm ² /s ²	
	$z/h=0.15$	$z/h=0.90$	$z/h=0.15$	$z/h=0.90$	$z/h=0.15$	$z/h=0.90$			$z/h=0.15$	$z/h=0.90$
Global mixing layer	9.39	0.61	-2.61 - 11.14	10.73	38.90	57.49	3.88	0.01	61.14	23.85
Detached mixing layer	10.52	2.91	12.49	19.59	23.63	37.57	4.15	0.03(*)	72.89	42.89
Centre of groyne field	1.37	1.67	2.44	-6.82 - 23.14	6.96	15.06	3.24	0.15	22.91	28.98
Lee-side of groyne	3.22	4.39	-3.49	11.01	-2.74	27.04	7.40(*)	1.16(*)	30.38	35.89
Stoss-side of groyne	-0.46 - 1.67	0.64	-3.76 - 1.28	-14.45 - 10.62	3.85	11.03	1.82	0.08	10.70	23.63
Bank (inside groyne field)	-	0.33	-	2.95	-	16.92	1.38	0.01	-	11.51

Table 4.2: Reynolds stresses $u'w'$ and $u'v'$, mean velocities u , bottom friction velocity u_* and bottom friction factor c_f , and turbulent kinetic energy TKE at different places around the groynes for emerged conditions. Values affected by uncertainty are marked with (*).

Exp 2 - emerged	$u'w'$ cm ² /s ²		$u'v'$ cm ² /s ²		u cm/s		u_* cm/s	c_f -	TKE cm ² /s ²	
	$z/h=0.15$	$z/h=0.90$	$z/h=0.15$	$z/h=0.90$	$z/h=0.15$	$z/h=0.90$			$z/h=0.15$	$z/h=0.90$
Global mixing layer	8.62	-0.81 - 2.51	4.89	6.05	36.91	48.53	3.76	0.01	45.74	22.94
Detached mixing layer	9.21	1.13	11.60	15.56	21.56	34.32	3.70	0.03	53.65	36.76
Centre of groyne field	-0.07 - 0.23	±0.11	-0.18 - 0.96	-0.11 - 2.66	-1.62 - 3.99	-3.5 - 6.93	0.78	0.26	2.81	2.92
Lee-side of groyne	±0.61	-0.34 - 0.25	-1.42 - 0.73	-1.48 - 0.93	1.72	-9.76 - 3.77	1.14(*)	0.10(*)	4.17	3.00
Stoss-side of groyne	-0.66 - 0.49	-0.27 - 0.58	-1.38 - 2.63	-2.59	-2.51	±5.28	1.35(*)	0.14(*)	8.74	9.73
Bank (inside groyne field)	-	±0.04	-	-0.33	-	-6.30	0.64	0.01	-	2.65

4.4 Coherent Structures and Exchange Processes

Coherent structures were identified in previous studies to have a significant influence on groyne field exchange processes. It was therefore the aim of the study, to analyse long-term fluctuations of velocity and water surface elevation to get a clearer picture on how and if these processes are recognisable on a field scale. The mean flow and statistical turbulence characteristics (TKE, stresses) presented in the previous subchapters give only a rough idea but are not able to catch these features quantitatively, like the characteristic size and frequency of structures. Therefore, the analysis in this chapter uses spectral analysis of time-series of velocity and water surface fluctuations to identify peaks and slopes which are indicating the dominant frequencies and scales of coherent structures.

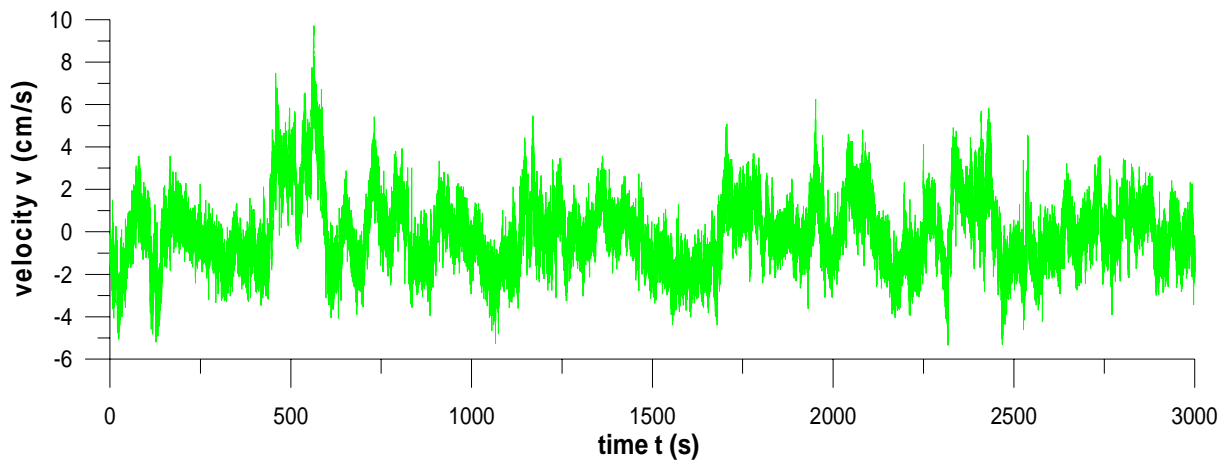


Figure 4.10: Flow velocity record for transverse velocities in the mixing layer at position 6 – field measurements at the river Spree, 2007.

Emerged case

Time series and autocorrelated power density spectra (auto-spectra)

Such a velocity time series for spectral analysis is presented in Figure 4.10 for a point located in the GML slightly upstream of the groyne tip at position 6 (see Figure 4.11a). The relatively low velocity range (± 5 cm/s) is typical for the transverse component v . The total measurement time was around 3000 seconds and within this period, clear low-frequency and high-frequency fluctuations can be recognised. For auto-correlation analysis, spectra were calculated at two positions (at positions 3 and 6, which are at the same location relative to the groyne tip) and averaged afterwards for better identification of frequency peaks. The averaged spectrum is presented in Figure 4.11b and clearly reveals three different slopes: the $-5/3$ slope of the Kolmogorov's inertial subrange indicating the dissipative energy cascade, the -1 slope associated with large-scale vertical structures generated by the bed shear and finally the -3 slope (Figure 4.11b). The latter is associated with quasi-two-dimensional horizontal structures and inverse energy cascade due to pairing and merging of smaller structures. The peak of these large-scale structures is around 0.02 Hz (with a period of $T = 1/f = 50$ s). In the higher frequency band, another important

frequency can be identified which marks the transition between the -1 and the -5/3 slopes. This frequency around $f = 0.3$ Hz identifies the beginning of the inertial subrange which can be roughly estimated by dividing the mean flow velocity by the water depth as characteristic velocity and length scales which gives $f = U/h = 0.3$ m/s / 1m = 0.3 Hz. At frequencies higher than around 3 Hz, the acoustic noise level increases and distorts the signal until the maximum sampling frequency of 25 Hz is reached.

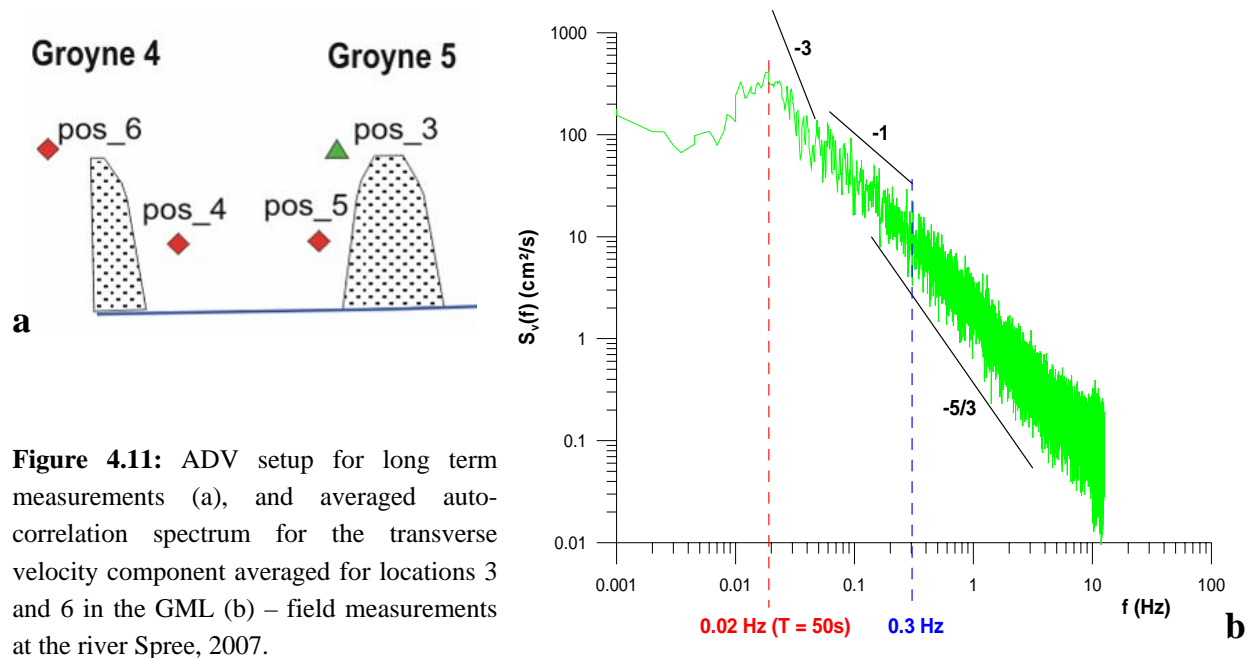


Figure 4.11: ADV setup for long term measurements (a), and averaged auto-correlation spectrum for the transverse velocity component averaged for locations 3 and 6 in the GML (b) – field measurements at the river Spree, 2007.

The same spectral analysis can be performed on time series of the water surface elevation fluctuations which were measured with upside-down operating ADVs (see methods 3.3.2). In laboratory, these fluctuations are typically too small or too high-frequent to be recognised. In the field, the time series in Figure 4.12 clearly show the fluctuations for two positions inside the groyne field (position 4 in the upstream and position 5 in the downstream end of the groyne field). Both series were measured synchronously for approximately 50 minutes and appear to be well in phase from a first look. The auto-correlation analysis at each points results in the Figure 4.13. The spectra has an absolute maximum at a frequency of around 0.0125 Hz but another local peak can be identified at 0.02 Hz – at the same frequency as the GML velocity fluctuations. From this can be concluded, that structures from the GML enter the groyne field and cause surface elevations related to the boiling and upwelling motions of the structures before breaking apart. An explanation for the shift of the peak towards lower frequencies can be given under the assumption that some structures interact with the groyne (hitting events) while others enter the groyne field before hitting. As a result, some structures would not reach the points inside groyne field anymore and therefore, the frequency of events would increase.

Cross correlations

Furthermore, it is interesting to investigate, how the two positions are interacting and to identify what hydrodynamic principle causes the water surface fluctuations. Cross-correlation analysis of the two time series can yield valid information for this and reveal the correlation and phase lag between the two points.

The cross-correlation functions between position 4 and 5 (within the groyne field) and position 4 and 6 (GML-groyne field upstream) are shown in Figure 4.14. The time shift between the y-axis and the maximum of the curve is the lag time which is around 1 second in the present case and thus too short to see in the figure using a scale of +/- 400 seconds. Anyhow, the lag time was determined by zooming in close to the y-axis. This time indicates how long structures need to propagate from one point to another. Knowing the time lag, the convective speed U_c of the structures can be determined by dividing the distance between the points by the lag time. For cross-correlation of positions 4 and 5 which clearly show a correlation functions, the convective speed is around 4 m/s ($\Delta x = 4$ m, $\tau_{max} = 1$ s). The cross-correlation further depicts that the phase has a period of approximately 80 s (distance from one local maximum to the next). Positions 4 and 6 show no correlation at all, the function practically disappears and no lag time could be identified (Figure 4.14). This means, the position inside the groyne field in the lee of the groyne has no correlation of water level fluctuations with the upstream GML. This is not surprising as the two positions are more or less hydraulically separated by the gyre system and the horizontal DML.

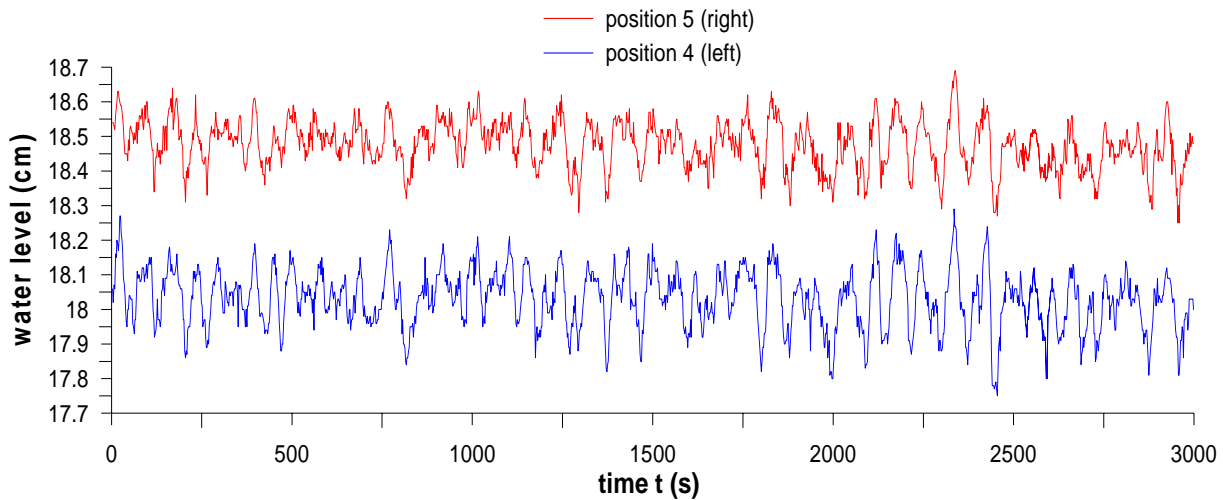


Figure 4.12: Time series of water level fluctuations in the groyne field at positions pos_4 and pos_5 – field measurements at the river Spree, 2007.

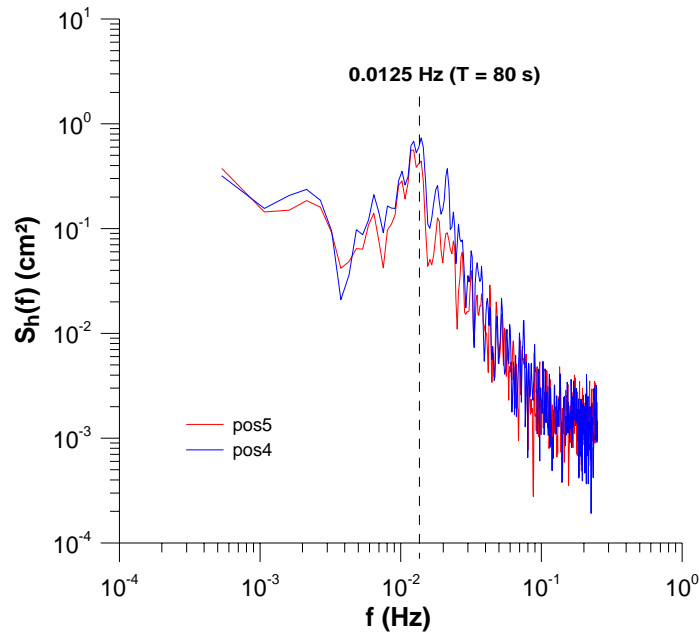


Figure 4.13: Auto-spectra for water level fluctuations in the groyne field at positions pos_4 and pos_5 – field measurements at the river Spree, 2007

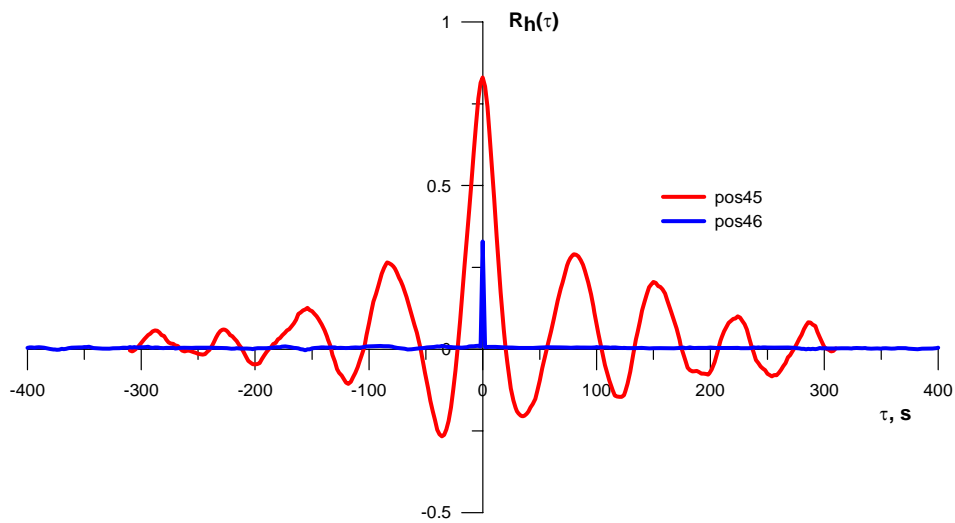


Figure 4.14: Cross-correlation function for the water level fluctuations measured synchronously at positions 4 and 5 and 4 and 6 respectively – field measurements at the river Spree, 2007.

Submerged case

Time series and autocorrelated power density spectra (auto-spectra)

For submerged conditions, unfortunately no long-term ADV measurements were conducted due to time constraints in the measurement campaign. Instead, auto-spectra of the short-term ADV measurements (250 s) were analysed to obtain at least some information on coherent structures. In order to gain interpretable results, spectral densities were standardised with mean velocity, streamwise turbulent intensity and depth for each measurement point according to ENGELHARDT et al. (2004):

$$S_i^*(f) = S_i(f) \frac{U}{u'2h}$$

where U is the local mean velocity, u' is the turbulent intensity, and h is the local water depth. Furthermore, the individual standardised spectra in each vertical averaged over their frequencies. Results of the standardised auto-spectra are shown in Figures 4.15b-d together with a map marking their location in the groyne field (Figure 4.15a).

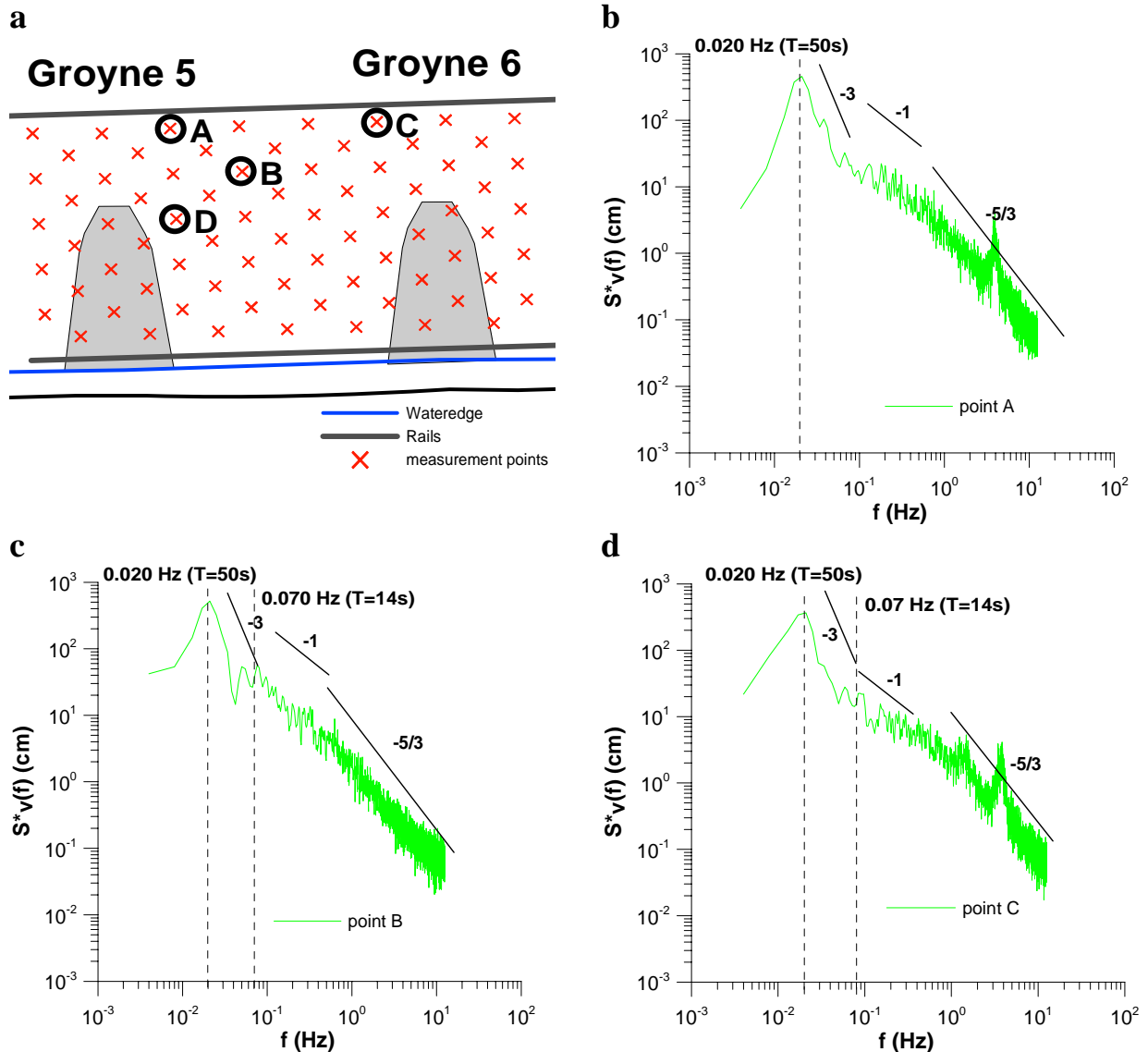


Figure 4.15: Overview of measured time series used for auto-spectra for submerged conditions (a), and auto-spectra (standardised spectral densities) in the mixing layer during submerged conditions: at point A (b), at point B (c), and at point C (d) – field measurements at the river Spree, 2007.

The spectra are very similar to spectra for the emerged case (see Figure 4.11b for comparison). The three slopes can be clearly identified and the peak frequency 0.02 Hz ($T = 50 \text{ s}$) associated with the GML structures is apparent in all spectra (Figure 4.15). In the auto-spectra at point B and C (Figure 4.15c and

d), another local maximum at a higher frequency of around 0.07 Hz ($T = 14$ s) is recognisable. This peak is associated with smaller structures evolving from the horizontal DML at the groyne tip. This is supported by the differences in the three points: point B has the clearest imprint of the DML structures, while it is less pronounced at points C and point D which are already quite far in the GML when DML structures merge with the GML structures and steadily lose their coherency. The unexpected peak in the $-5/3$ inertial subrange at auto-spectra at point A and C probably evolve out of vibrations of the ADV probe during the measurements due to high velocities in that area.

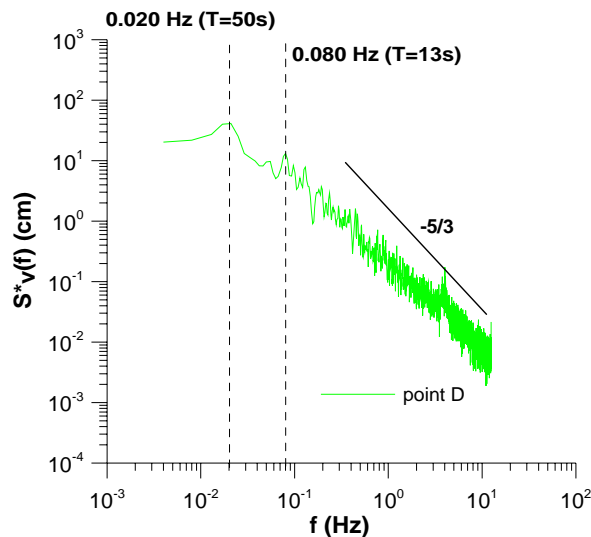


Figure 4.16: Auto-spectra (standardised spectral densities) in the groyne field during submerged conditions at point D – field measurements at the river Spree, 2007.

despite the significantly different mean velocity field, the coherent structures in both cases are comparable and the frequency peak associated with GML structures is an omnipresent feature mainly dependant on the horizontal mean velocity gradient between main channel and groyne field.

An additional auto-spectra was calculated for a location inside the groyne field. Figure 4.16 is from measurements at point D (see the map in Figure 4.15a) in the lee of the upstream groyne – close to the groyne tip and within the vertical recirculation cell. In comparison to the GML locations in Figures 4.15, the peak associated with the GML structures is less pronounced but still recognisable. At higher frequencies of around 0.08 Hz a local maximum is present which again refers to structures of the DMLs. For a more detailed analysis, longer time-series would have been advantageous. Nevertheless, the spectra presented here clearly give evidence that both the GML and the horizontal DML are also present in the submerged case. This means that

5 DISCUSSION

This chapter brings together the results of the field experiments with previous studies and the state-of-the-art presented in Chapter 2.2. The aim is to directly compare field, laboratory and numerical experiments and to derive a general perspective on flow hydrodynamics in groyne fields and their governing parameters. Some of the comparison will be based on qualitative analysis using additional material like photographs while for others parameters will be compared on a quantified basis. Furthermore, theory on shallow mixing layers will be applied to support some of the hypotheses and assumptions on DML and GML growth. The structure of this chapter is identical to the previous chapter on results and analysis (Chapter 4) and will start with a comparison of mean velocity patterns, followed by TKE and finally coherent structures –each first for emerged and afterwards for submerged conditions.

5.1 Mean velocity patterns

Emerged Conditions

During emerged conditions, the mean flow in the groyne field is characterised by a single, quasi-two-dimensional and horizontal gyre as shown in Chapter 4. Pictures taken from dye injection tests illustrate

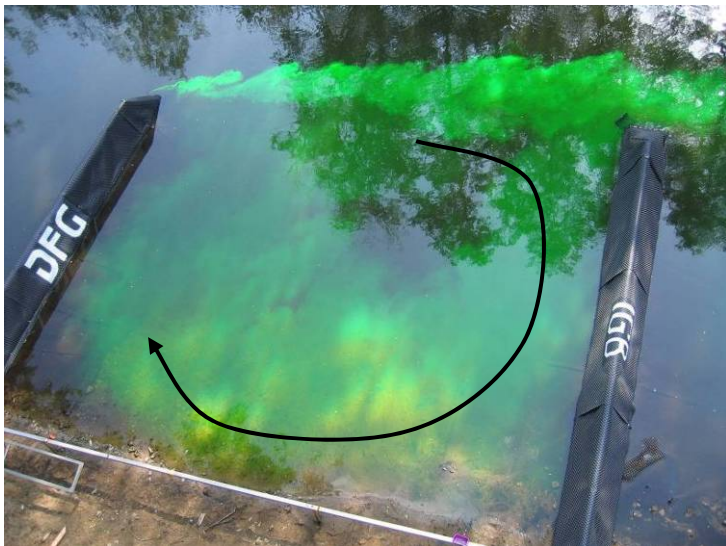


Figure 5.1: Uranin dye visualisation of the emerged flow pattern; injection point at tip of groyne 5 – field measurements at the river Spree, 2007.

this pattern (Figure 5.1).

As additional source of information, streaklines were determined from the PTV experiments with floating candles (Figure 5.2). The PTV camera frames cover groyne field 5 (on the left side of the pictures) and 6 (on the right side) and the transitional parts towards the main channel. Streaklines within groyne field 5 indicate that the path of the floaters follows the large single gyre. The picture is still perspective and thus the concentric gyre looks rather elliptic. Although PTV data is not “cleaned” from particles

which were stuck close to the banks, there is further indication for a small secondary counter-rotating gyre at the upstream corner – which was already mentioned in the mean velocity results in Chapter 4.2. It can be recognised that the interaction with the DML is decisive for the probability of a particle entering or missing the groyne field and that particles in the outer GML practically never enter the groyne field and

are subject to strong translatory motions (similar to the results of shallow mixing layer PTV, see ERDBRINK 2007).

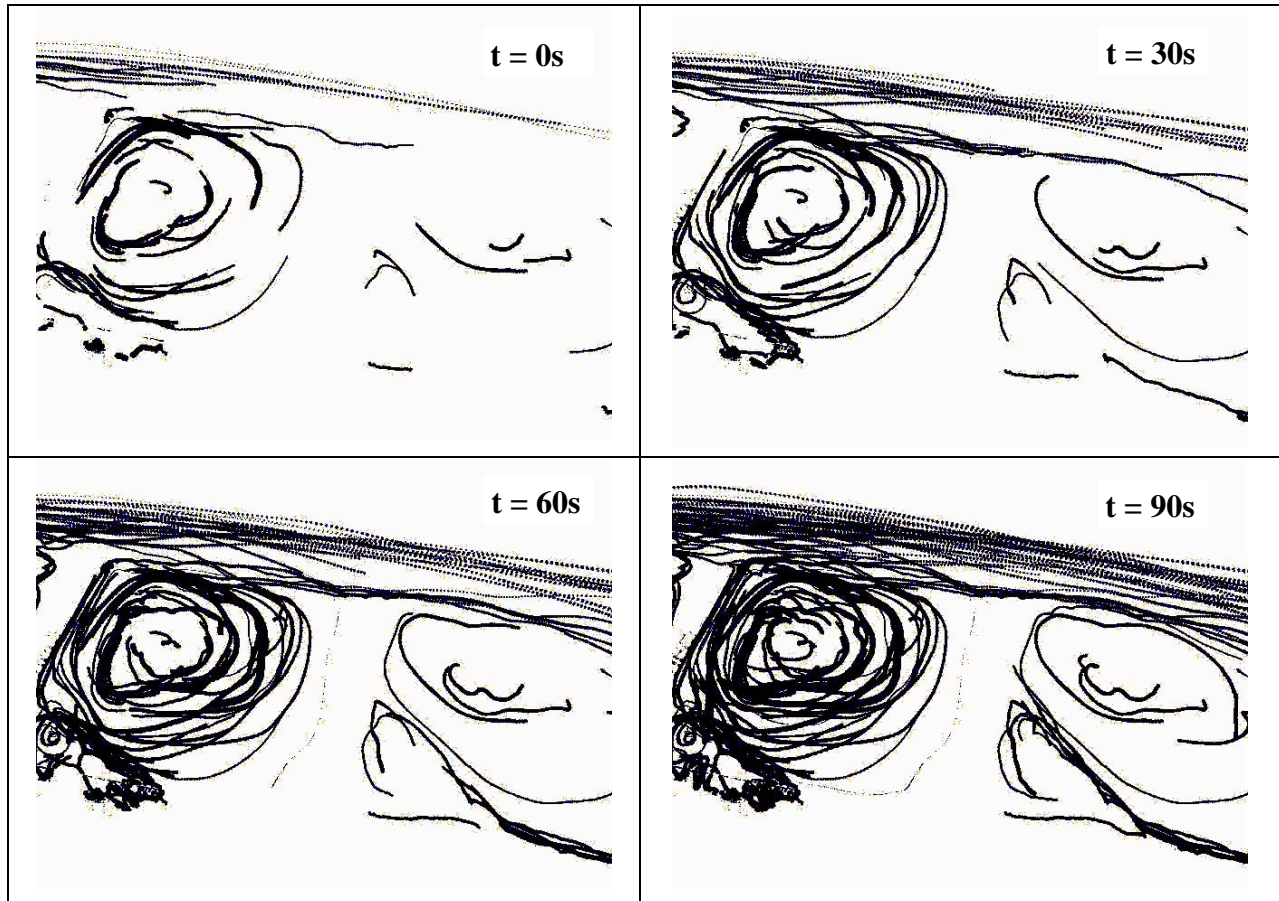


Figure 5.2: PTV streaklines for emerged conditions (provided by W. BREVIS); recorded area covers groynes field 5 (to the left) and 6 (to the right), and part of the main stream (top) – field measurements at the river Spree, 2007. The flow is from left to right.

This pattern is well consistent with previous laboratory, numerical and field studies conducted at similar aspect ratios (KIMURA & HOSODA 1997; FUJITA et al. 1998; SUKHODOLOV et al. 2002; ENGELHARDT et al. 2004; MCCOY et al. 2008; WEITBRECHT et al. 2008). Figure 5.3 shows comparative vector maps of the mean velocity. In all cases, the primary gyre in the centre is characterised by very low velocities which increase towards its margins. The gyre is circular – pointing out that the groyne field is at a sufficient distance downstream where the GML is already stable. The small counter-rotating secondary gyre at the upstream corner was also present in the other studies – even if sometimes not very distinct due to the low velocities. Figure 5.3a is from a surface PIV study in the laboratory by UIJTTEWAAL et al. (2001). Making use of additional dye visualisations, UIJTTEWAAL et al. concluded that the flow in the field is predominantly two-dimensional. This assumption was quantified in this study by measuring and analysing vertical velocity profiles. In large rivers like Elbe, flow patterns are also influenced by the groyne orientation (ENGELHARDT et al. 2004). Backward inclined groynes develop a

single but slightly deformed gyre (Figure 5.3b) where velocities at the lee of the upstream groyne exceed the ones at stoss-side of the downstream groyne but principally the primary gyre system is still the dominant mechanism. The same was found by FUJITA et al. (1998), where groynes were built perpendicular to the bank but the flow was bended, which consequently resulted in similar flow patterns as for backward inclined groynes.

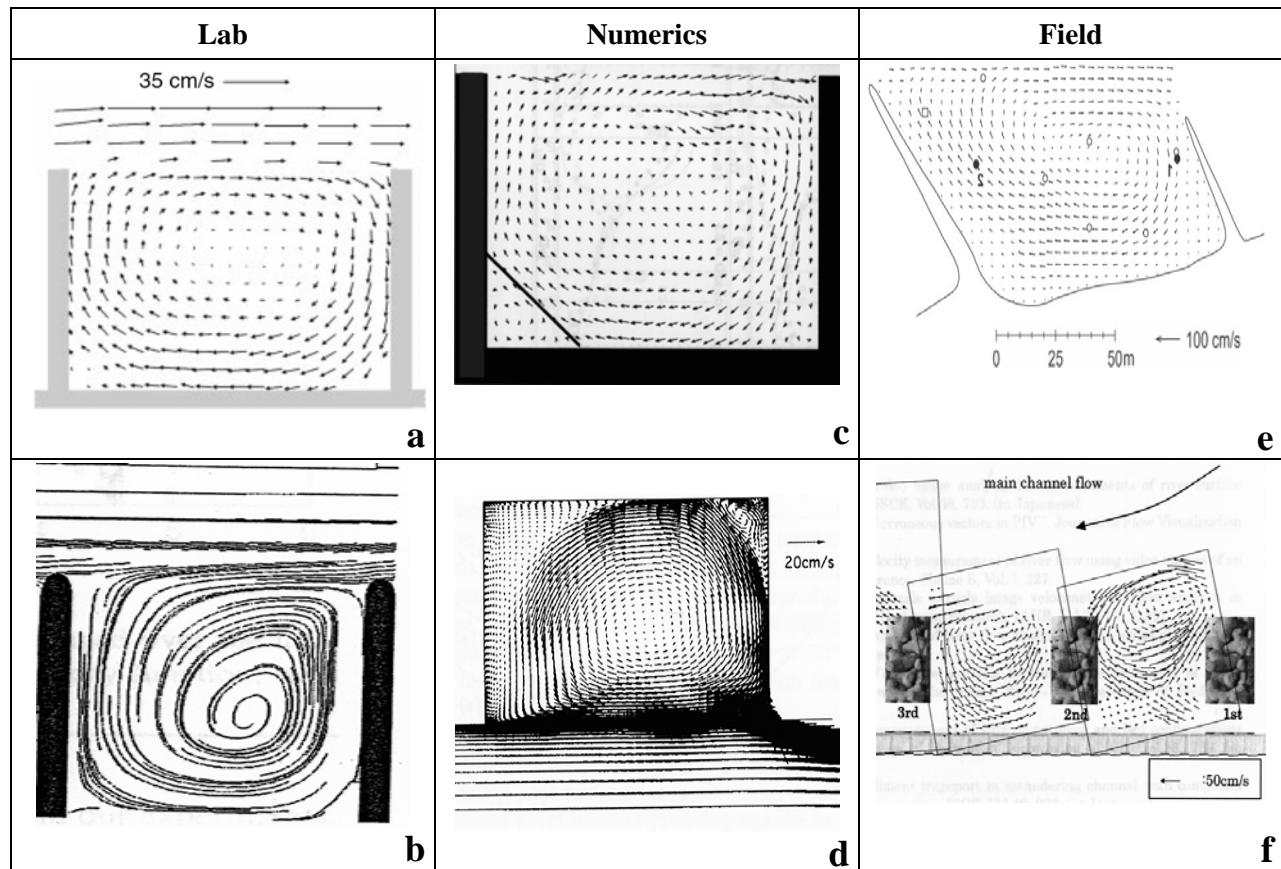


Figure 5.3: Mean flow patterns in groyne fields under emerged conditions: Lab: SUKHODOLOV et al. 2002 (a), WEITBRECHT et al. 2008 (b); Numerics: MCCOY et al. 2008 (c), KIMURA & HOSODA 1997 (d); and Field: ENGELHARDT et al. 2004 (e), and FUJITA et al. 1998 (f) – field measurements at the river Spree, 2007. Flow from left to right unless otherwise shown.

Submerged Conditions

During submerged conditions, the distinct horizontal recirculation pattern like in the emerged case disappears. The groyne field is still a region of reduced velocities compared with the main channel, but close to the banks increased velocities occur (see Chapter 4.1). The sequence of photographs in Figure 5.5 supports the results of the measurements with ADVs. Particles approach the groyne in-line and perpendicular to the main flow direction (Figure 5.4a). In the next pictures, the particles closer to the bank and the main channel are accelerated, while particles in the centre overtopping the recirculation cell are decelerated (Figs.5.4b-d).

Comparable data for submerged groynes is scarce, because most studies used surface PIV or PTV measurements without getting any information of the layers underneath. Anyhow, the velocity distribution in the topmost horizontal layer in the present study can be compared with surface velocities. In general, it is well in agreement with previous laboratory studies by UIJTTEWAAL (2005) – see Figure 5.5b. The flow over the groyne fields is relatively parallel to the main stream and the flow is accelerated over the crest of the groynes showing the highest velocities downstream of the crest.

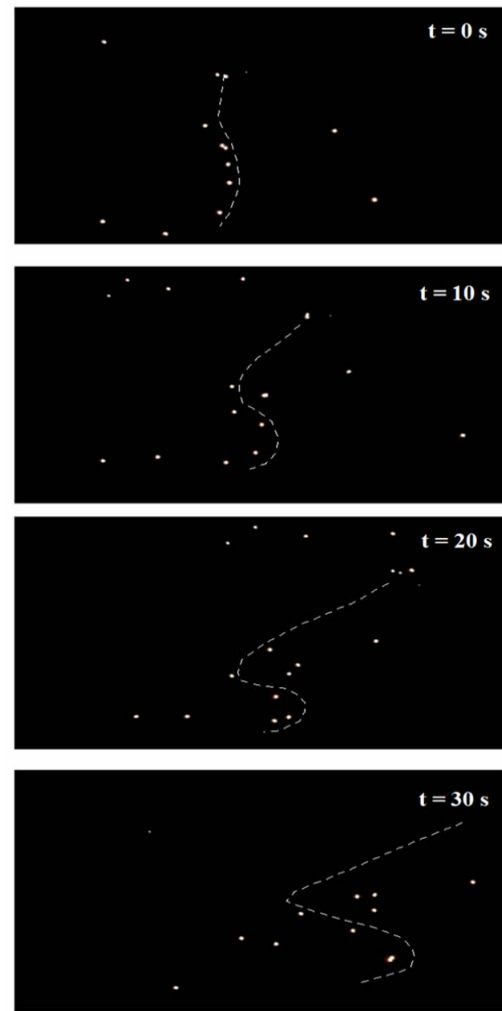


Figure 5.4: Example of a PTV record from groyne field 5 during submerged conditions – field measurements at the river Spree, 2007 (SUKHODOLOV et al. 2008).

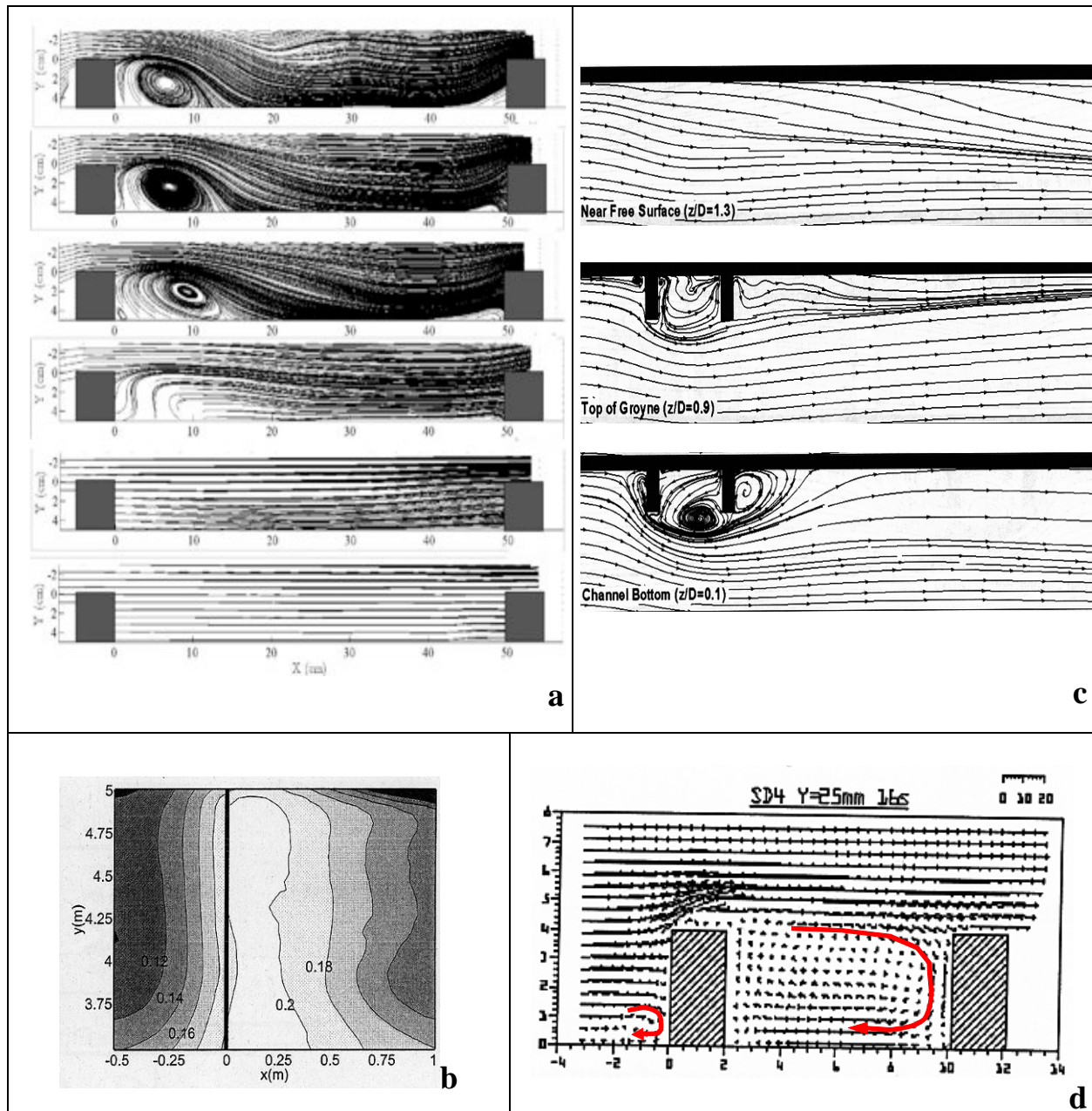


Figure 5.5: Mean flow patterns in groyne fields under submerged conditions: Lab: BREVIS et al. (2008) (from top: position 1, near the wall, to position 6 in the main stream, longitudinal cross-sections) (a), UIJTTEWAAL (2005) (m/s; solid line represents the groyne crest) (b), TOMINAGA et al. (2001) (longitudinal cross-section) (d); Numerics: McCOY et al. (2007) (from top: position 1, near the surface, to position 2 at the groyne crest, and position 3 close to the channel bottom) (c). Flow from left to right.

Lab experiments are conducted in rectangular flumes often with vertical walls which represent a simplified and idealised version of the bathymetry of real rivers. Besides, also model-groynes are often shaped in a simplified way without sloped sides. Consequently the upwelling of the water level and subsequent constant acceleration of the flow takes place along the total groyne crest. This is further influencing the transverse extension of the recirculation cell which is now present until reaching the flume walls (Figure 5.5).

McCOY et al. (2007) conducted LES simulations and the flow is accelerated over the crest of the groynes showing the highest velocities downstream of the crest – at the vertical separation zone. The study revealed that mean velocity pattern near the bottom are similar as for the emerged case. A gyre, half in size as the horizontal recirculation gyre for emerged condition, is developing in the groyne field. The gyre is present from the bed upwards to the crest of the groyne. This pattern was not present in this study which can be explained by the untypical groyne geometry in the LES study (Figure 5.6). Although the stage of submergence ζ was similar to the IGB field study, other ratios like length ratio (L_g / L_f) or the height ratio (H_g / L_f) are differing significantly (Tab. 5.2).

Table 5.2: Different aspect ratios in a LES study by MCCOY et al. (2007) and this study

	McCOY	This study
Submergence stage ζ h / H_g	1.4	1.6
Length ratio L_g / L_f	0.4	0.7
Height ratio H_g / L_f	0.7	0.1

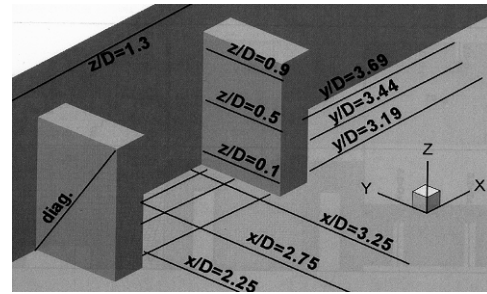


Figure 5.6: Channel flow with two submerged groynes used in a LES simulation (MCCOY et al. 2007).

YOSSEF (2005) studied the effect of three different stages of submergence ($\zeta = 1.4, 1.7$ and 2.0) in laboratory experiments. He found that at the low stage of submergence, a gyre establishes - analogous to emerged flow conditions. When the submergence is increased, this gyre is suppressed and the flow in the groyne field is uniformly directed parallel to the main channel flow direction (Figure 5.5c). The transition between these two patterns was identified at a stage of submergence of about 1.6 – similar to the present field study where no gyre established.

TOMINAGA et al. (2001) used PIV in vertical and longitudinal cross sections for submerged conditions in a relatively small flume in the laboratory. The authors identified two recirculating zones: a small vertical separation at the stoss-side of the groyne and the large recirculation in the lee (Figure 5.5d). The small recirculation can be attributed to the idealised rectangular groyne shape in the lab study. In the present IGB field study, the longitudinal groyne cross sections were mildly sloped and prevented the stoss-side separation. At the lee-side, the spacing between subsequent groynes was very narrow (groyne height H_g / groyne field length $L_f = 0.4$ as compared to this study $H_g / L_f = 0.07$) causing a pronounced vertical separation which occupies the entire groyne field (Figure 5.5d). This flow pattern resembles “skimming flow” conditions which were described by MORRIS (1955) for vertical wall boundary layers with large roughness elements (see Figure 5.7). In this case, the spacing between the roughness elements

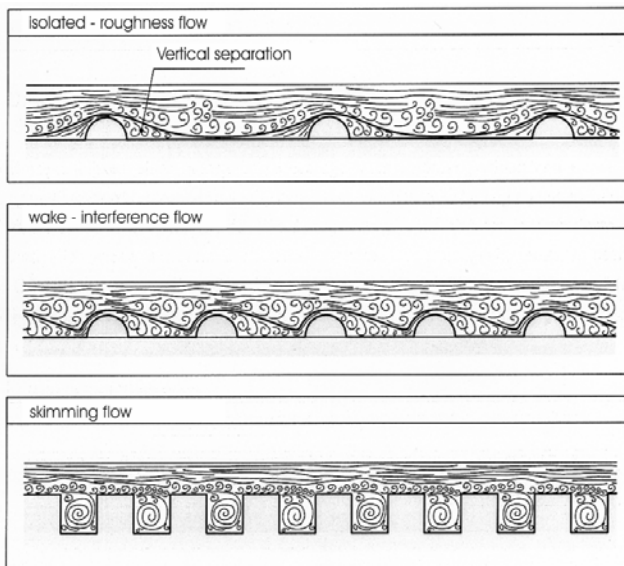


Figure 5.7: Flow patterns over rough surfaces, vertical plain; after MORRIS (1955).

is shorter than the reattachment length of the separation, resulting in a complete overlap with gyre-like vertical structures between the elements.

This laboratory setup –similar to the numerical grid of McCOY et al (2008) - is rather unrealistic for standard groynes in rivers which show characteristics of isolated roughness flows in Figure 5.7. Nevertheless, it points out that flow patterns associated with submergence or emergence are driven by the geometry of groynes (height/length and width) and not by the mere occurrence of overtopping flow.

5.2 Turbulent kinetic energy (TKE) patterns

Emerged Conditions

The distribution of TKE reflects production of turbulence by the horizontal and vertical velocity gradients in the shear layers and advection of fluid with high or low TKE by the mean flow (see Chapter 4.2).

In the field study of ENGELHARDT et al. (2004), the measurements were limited within the groyne field and zones of the DML and GML were only covered marginally (see Figure 5.8a). Inside the groyne field, the distribution of TKE is quite similar to the present study. Fluid with high TKE from the main stream enters the groyne field at the downstream end causing a jet-like intrusion of higher turbulent intensity. In the centre, TKE has a local minimum due to the low velocities and the physical separation of the centre by the DML and the gyre. This supports the assumption in Chapter 4.2 that large structures from the GML do not reach the central parts of the groyne field and are limited to the stoss-side of the downstream groyne where they are quickly dissipated while being advected by the gyre.

The same jet-like intrusion of TKE is represented in the LES study of McCOY et al. (2008) (Figure 5.8b). The level of TKE in the jet is approximately as high as in the DML – which is different from the IGB field study. Moreover, the DML is structured into two longitudinal strips separated with a local minimum in between. This gives evidence, that around the location of the DML two separate mechanisms occur. One is the vortex shedding in the DML (the longitudinal strip closer to the groyne field) while the other strip evolves from GML structures which are interacting with the groyne tip. Part of the structures enters the groyne field via the jet-like intrusion while the other part is advected past the groyne and into the main channel causing the increased TKE. This might be due to the idealised shape of the groynes which cause

stronger velocity gradients and provide sharp edges which provide fixed points where the flow separates. Consequently, the evolving DML is stronger than in field conditions with a more complex groyne geometry. Another interesting observation from the TKE plot of McCOY et al. (2008) is the growth of the GML. Evolving from the DML of the first groyne, it grows steadily until reaching the subsequent groyne where a scale-jump occurs. The mixing layer width at this location increases suddenly. The same effect occurs at the third groyne – further downstream the GML is more or less stable and of constant width.

TKE patterns from laboratory studies (UIJTTEWAAL 2005; YOSSEF 2005) are supportive to the IGB field study and show the maximum TKE in the area of the DML (Figure 5.8b-d). The jet-like intrusion of structures from the GML is also apparent in both studies. Furthermore, local maxima of TKE were measured around the stoss-side of the groyne inside the groyne field which is related to the interaction of structures from the GML with the groyne. In UIJTTEWAAL's case, the groyne is mildly sloped and causes an upwelling and boils when structures collide. This is associated with a redistribution of vertical to horizontal turbulence and increases the turbulent intensities in the horizontal plane which the PIV was restricted to.

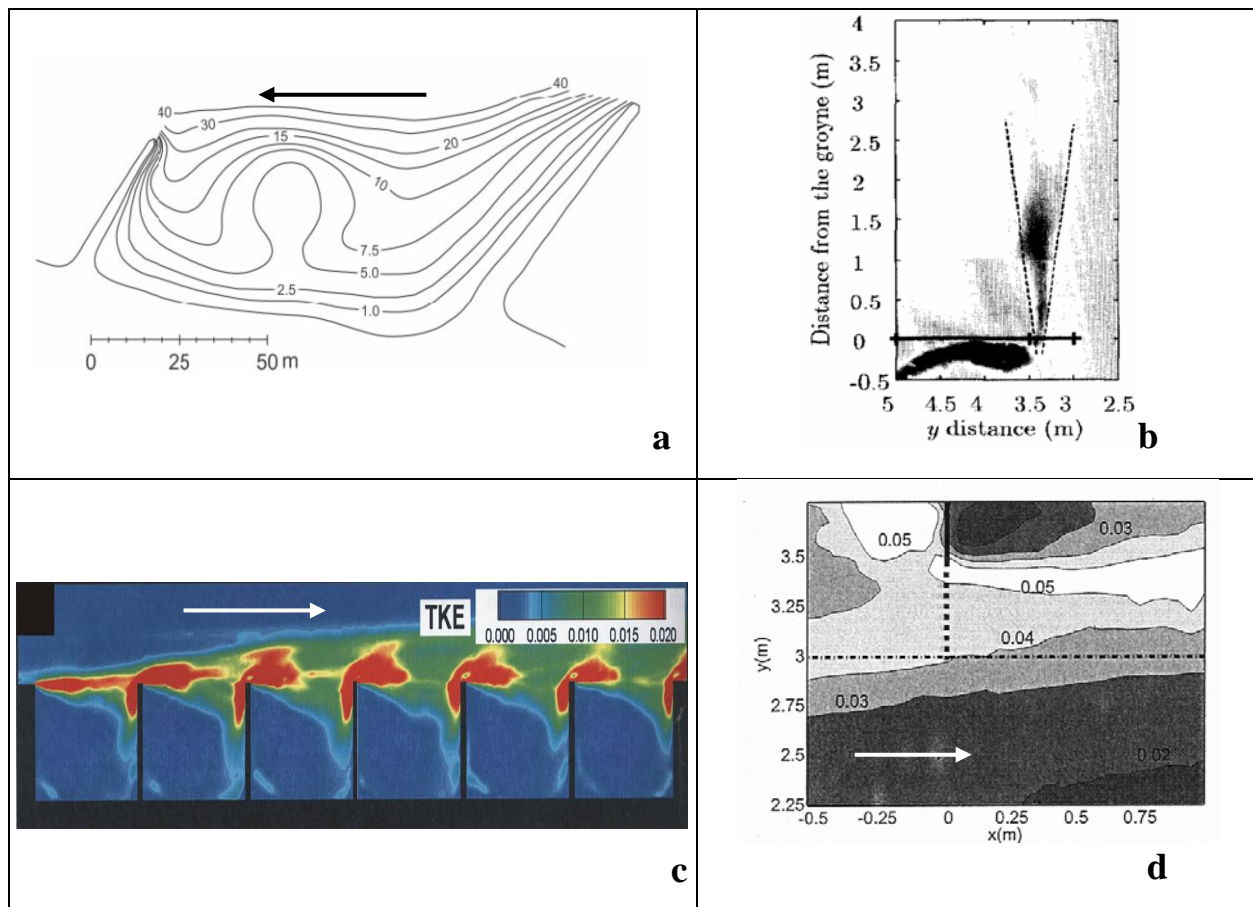


Figure 5.8: Distribution of TKE (cm^2s^{-2}) in a groyne field during emerged conditions: Field: ENGELHARDT et al. 2004 (a); Numerics: McCOY et al. 2008 (b); Lab: YOSSEF 2005 (solid line represents the crest of the groyne) (c), and UIJTTEWAAL 2005 (the lines mark the crest of the groyne and the groyne field – main stream interface) (m/s) (d).

Submerged Conditions

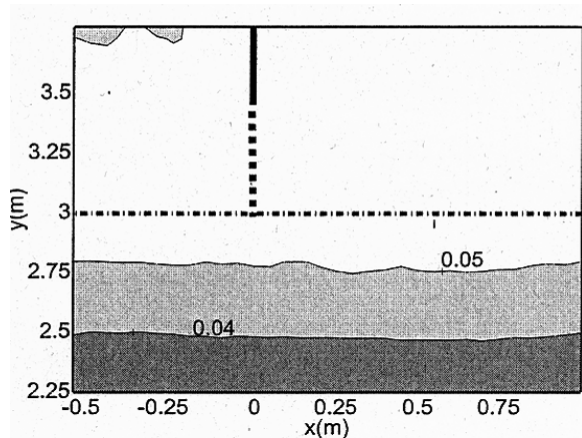


Figure 5.9: Distribution of the TKE over a groyne field (taken from UIJTTEWAAL 2005), (m/s), dotted lines indicate the submerged part of the groyne and the dash-dotted line points out the most shallow part of the groyne field. Flow from left to right.

In submerged conditions, vertical and horizontal DML evolve which make the flow highly three-dimensional. The use of surface PIV or PTV techniques in the lab is thus limited in detail and significance of the involved processes. The only directly comparable study by UIJTTEWAAL (2005) reveals increased TKE in the whole groyne field (Figure 5.9). Furthermore the contour lines are relatively parallel to the bank indicating a stable width of the GML. The distinct areas of increased TKE at the area of the DML and at the lee-side of the groyne are absent due to employed methods and techniques.

5.3 Coherent structures and exchange processes

Auto-spectra for emerged conditions

In this chapter, auto-spectra of laboratory measurements of YOSSEF (2005), field experiments of ENGELHARDT et al. (2004) and LES simulations of McCOY et al. (2008) will be compared with the ones measured during the IGB field study (see Chapter 4.3). They are presented in Figure 5.10 and each includes only the transverse velocity component. Only the LES study of McCOY et al. (2008) lacks a clear low-frequency peak with a -3 slope. All other spectra give clear evidence of these two-dimensional horizontal structures. It was proved for the own study in Chapter 4.3 that the peak is related to structures from the GML. In YOSSEF's case, two spectra are presented: position A is right behind the groyne, B is in front of the subsequent groyne (see Figure 5.10a). The spectrum of transverse velocity in point A (solid line in figure 5.23a) has one peak at the low-frequency range whereas at point B two peaks are found in the spectrum. YOSSEF (2005) states that the peak at higher frequencies is caused by DML structures and the lower frequency peak by large structures from the GML which would be consistent with the field data of Spree. To validate these assumptions, the scale and frequency of DML and GML structures was predicted by application of CHU & BABARUTSI's (1988) scaling laws and the Strouhal-number proposed by SUKHODOLOV & SUKHODOLOVA (2007) – analogous to Chapter 4.5. The data and results for this procedure are presented in Table 5.1.

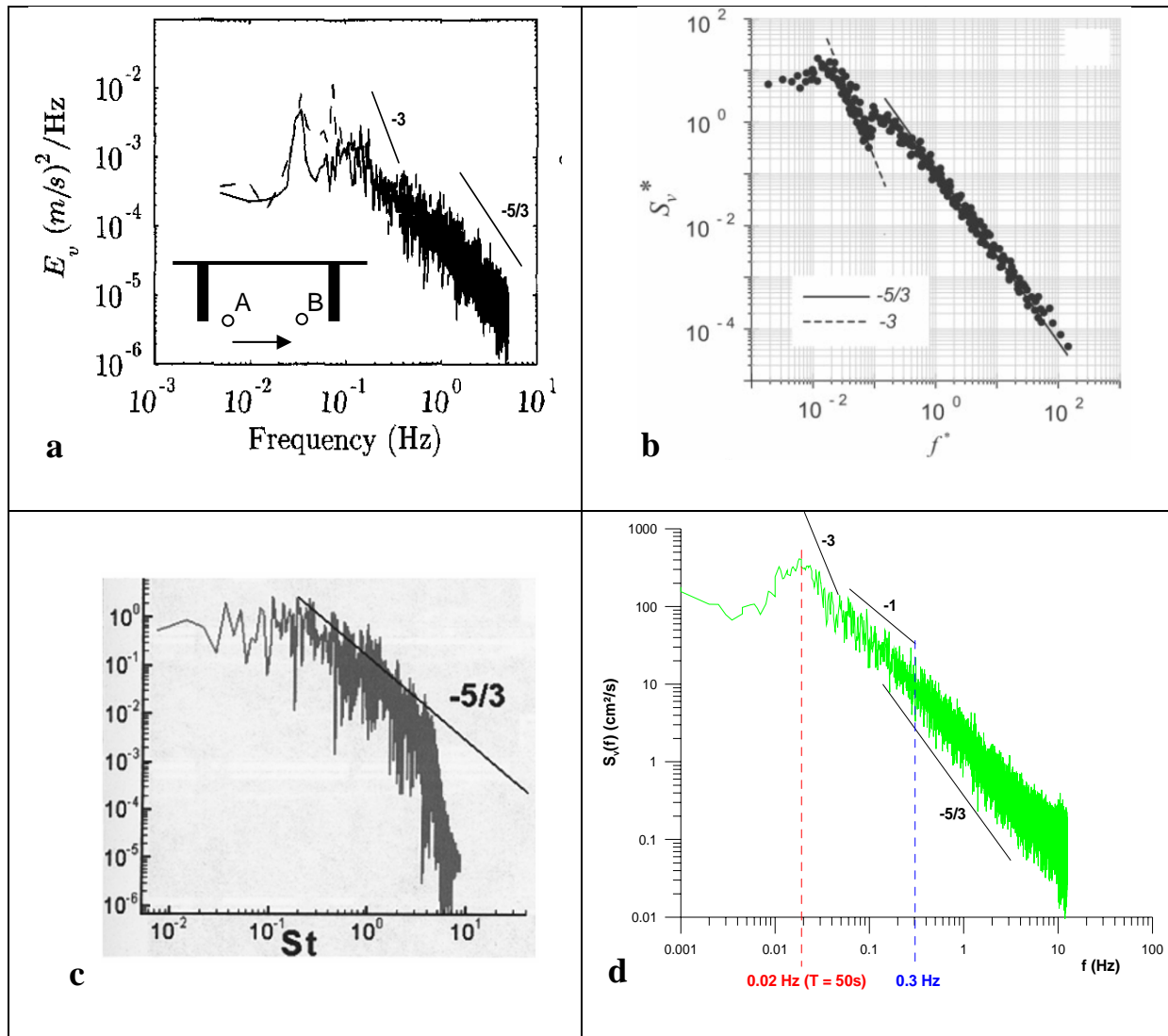


Figure 5.10: Auto-spectra for transverse velocities in the GML: Lab: YOSSEF 2005, solid line: measurement point in the GML, dashed line: measurement point a bit upstream of the downstream groyne tip (a); Field: ENGELHARDT et al. 2004 (b); Numeric MCCOY et al. 2008 (c); this study – field measurements at the river Spree, 2007 (d).

The frequencies calculated in this study (Table 5.1) correspond well with the frequencies measured by YOSSEF. At point A (close to the tip of the upstream groyne) large structures ($f = 0.04$ Hz) from the GML and vortices shed from the DML ($f = 0.36$ Hz) are recognisable (Figure 5.10a). At point B, the low-frequency peak (large structures in GML) is still present in a similar way as in point A. Furthermore, the DML-associated peak is lower at B ($f = 0.08$ Hz) pointing out that structures are still growing on their passage through the groyne field (Figure 5.10a). It can be concluded that in the lab study by YOSSEF (2005) the DML is not merging with the GML but remains stable along the groyne field - main channel interface. In the IGB field study, similar effects were observed but the stability and associated peaks in the

auto-spectra of the DML were less pronounced – in particular in comparison with the dominant peaks of the GML.

A likely reason for the differences between both studies is scaling effects. Compared to field conditions, lab experiments are generally conducted at higher velocities to obtain higher Reynolds numbers. Exaggerated velocities increase the vorticity of eddies shedding from the groyne which are consequently advected relatively further (YOSSEF 2005). Another aspect to consider is the geometry of the flume, in particular of the groyne fields. At the interface of groyne field and main channel there is a change in bottom elevation – similar to a compound channel. It is known that at high ratios of main channel depth to bank depth different momentum exchange processes occur, e.g. the horizontal exchange by mixing layer structures decreases and secondary currents become more important. Anyhow the comparison of auto-spectra reveals the importance of the GML which is establishing in all studies despite scale or differences in geometry and can be predicted with good accuracy based on theoretical considerations.

Tab. 5.1: Characteristic GML and DML parameters taken from YOSSEF (2005) and predicted frequencies and scales of coherent structures

	Δu (m/s)	$u_{c,0}$ (m/s)	$\bar{\delta}$ (m)	$\bar{\delta}^*$	x (m)	x^*	λ_0	c_f	h (m)	f (Hz)	T (s)
GML											
point A	0,30	0,15	0,750	-	-	-	-	0,006	-	0,04	27,52
DML											
point A	0,25	0,25	0,100	0,008	0,90	0,07	0,5	0,006	0,15	0,36	2,77
point B	0,25	0,25	0,313	0,025	3,60	0,29	0,5	0,006	0,15	0,08	12,18

GML and groyne field: wave or vortex interaction?

Low-frequency fluctuations in water levels and velocity are a typical phenomenon associated with groyne field hydrodynamics (KIMURA & HOSODA 1997; WIRTZ 2004). It is interesting to analyse if these fluctuations arise from standing waves oscillating in the groyne field or by coherent structures. The longest natural period for a standing wave in a basin at first overtone (see Figure

5.26) is defined as: $T = 1/f = \frac{\lambda}{c}$

where λ is the wave length and equals two times the length of the basin or, in this case, the groyne field length, c is the wave speed ($=\sqrt{gh}$), h the mean water depth in the groyne field during experiment 2 (estimated with 0.7 m), and g is the gravitational constant. The resulting resonance equals 7 s or a frequency of 0.14 Hz. This frequency is already in the noise level of the ADV spectra, and can not be the driving force of the horizontal recirculation in the groyne field. If the standing wave oscillation could be a

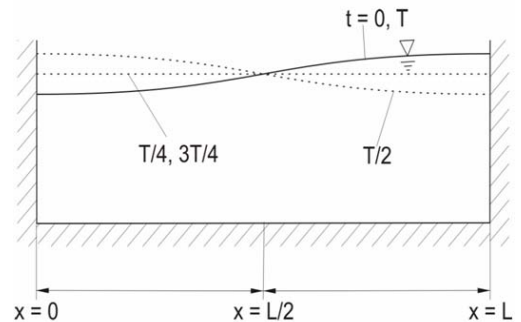
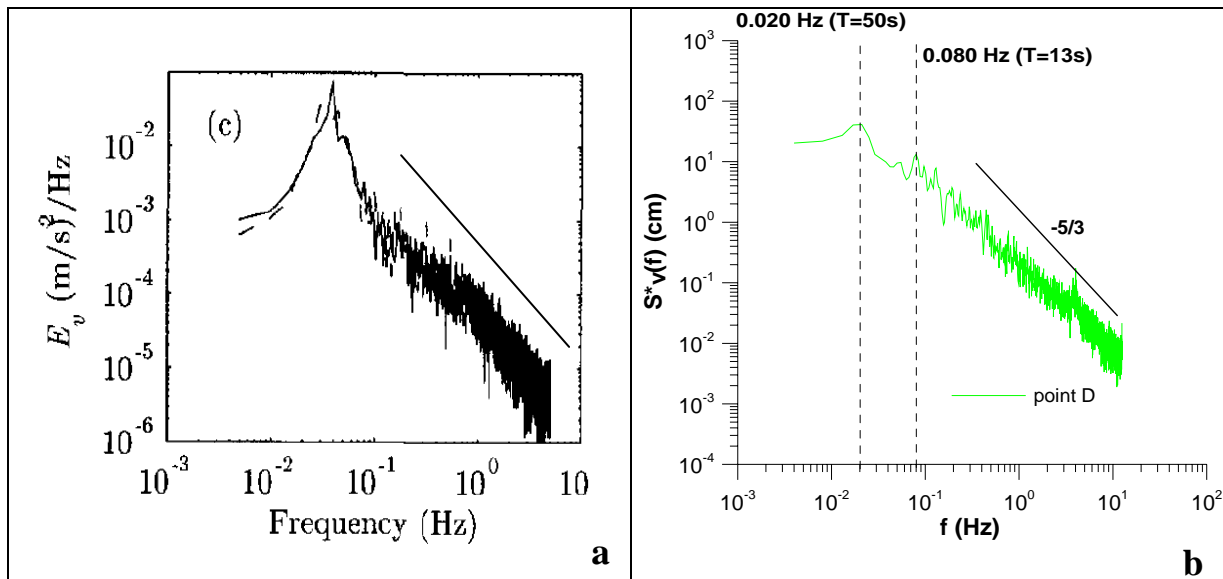


Figure 5.11: Standing wave with one overtone

base resonance on which the GML feeds, is an interesting question for further research but would exceed the frame of this thesis.

Auto-spectra for submerged conditions

Generally, for submerged conditions not many studies were dealing with the development and the advection of large coherent structures and associated exchange processes. Only YOSSEF (2005) presented auto-spectra from lab experiments with submerged groynes. These spectra are compared with the IGB field data from two locations in the vertical recirculation zone and inside the groyne field in Figure 5.29 a-d. In the recirculation zone (Figs. 5.12a, c) both spectra have low-frequency peaks associated with the GML. In addition, the field experiments revealed distinct local peaks of higher frequency which are related to the interaction between horizontal and vertical DMLs (see Chapter 4.3). These peaks are not recognisable in YOSSEF's study. At the second point in the middle of the groyne field (Figs. 5.12c-d), the GML associated peak has decreased but is still recognisable, while the DML peaks have vanished completely. This indicated that the contribution of the horizontal DML is stronger than the vertical DML and disappears inside the groyne field.



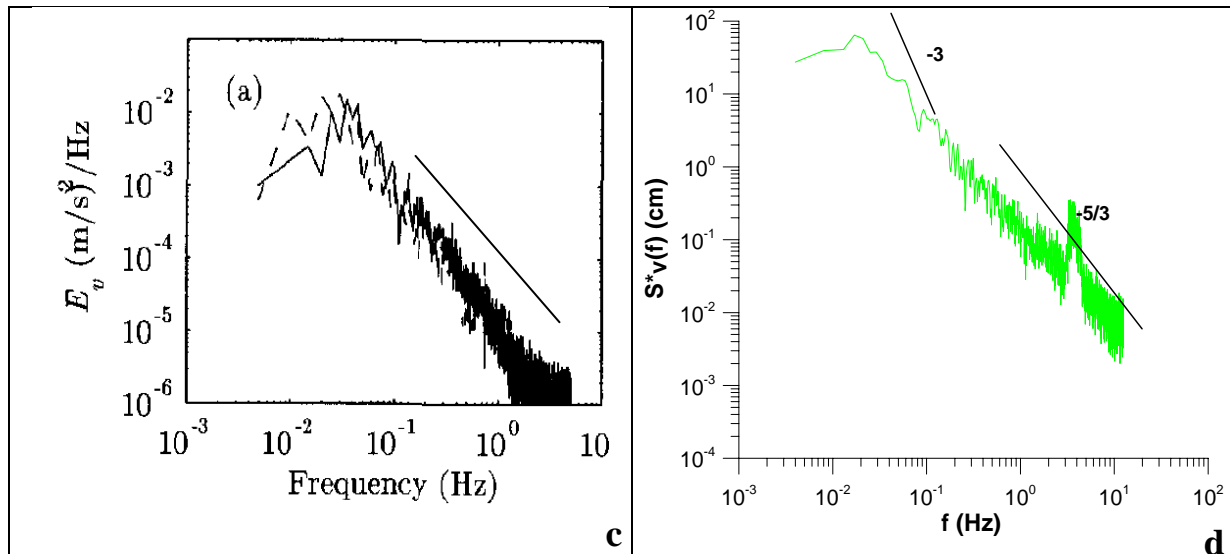


Figure 5.12: Auto-spectra for transverse velocities during submerged conditions: at the lee-side of the groyne: lab experiments (YOSSEF 2005) (a), and this study (standardised spectral density) (b); in the downstream half of the groyne field: lab experiments (YOSSEF 2005) (c), and this study - field measurements at the river Spree, 2007 (standardised spectral density) (d).

6 SUMMARY AND CONCLUSIONS

In this thesis the effects of a sequence of groynes on the mean and turbulent flow patterns and the exchange processes between the groyne field and the main channel were investigated. The study is based on a field campaign conducted at a straight river reach of the river Spree near Berlin. Seven groynes were constructed on the right bank following the design principles of groynes in large rivers like Elbe. In the thesis, data of emerged and submerged conditions for the same sequence of groynes were presented. The methodology of the field experiments involved (1) detailed point measurements of velocity and turbulence characteristics with acoustic Doppler velocimeters (ADV); (2) high-frequency fluctuations of water surface elevation; (3) long-term ADV measurements to obtain an insight into coherent structures and exchange processes between the main channel and the groyne field; and (4) visualisation of coherent structures and the entire flow field by particle tracking velocimetry (PTV) and qualitative dye tracer studies providing additional information on mean velocity patterns. Work on the thesis at IGB involved participation in the field-experiments and data-collection phase, post-processing of raw data and production of scientific graphs and plots. Furthermore, outcomes of the work were presented at an international conference (EGU Vienna, 2008) in the last phase of the thesis. The following subchapters will highlight the findings of the study and point out in which way research may contribute to an improved design of groynes - taking into account modern aspects.

Mean velocity patterns

For a length ratio of 0.7 the flow inside the emerged groyne field is characterised by a large horizontal and practically two-dimensional recirculation gyre which is well consistent with laboratory, numerical and large-scale field studies conducted at similar aspect ratios. In submerged conditions, the flow inside the groyne field is more uniform and almost parallel to the flow direction in the main stream. Passing along the groyne field, the flow was accelerated while overtopping the groyne and decelerated again downstream in the groyne field. Further areas of accelerated flow are found close to the banks, driven by the water level rise due to the stagnation upstream of the groyne head which caused a deflection of streamlines towards the bank. In the lee-side of the groynes, a vertical recirculation cell forms and reaches its maximum vertical extent close to the groyne tip. The downstream vertical reattachment point is located around 4.5 times the groyne height. Due to the bathymetry and cross-sectional shape of the groynes, the recirculation cell is not ideally two-dimensional but decays towards the bank. Comparison with literature in the submerged case revealed the lack of data and knowledge which has been significantly improved with the present study – including vertical profiles of velocity and turbulence which were unavailable from previous studies in this detail and accuracy.

Turbulence and coherent structures

The findings of this thesis reveal that the flow in groyne fields is significantly influenced by the development and interaction of mixing layers with the main flow. For simplicity the terms detached mixing layer (DML – for structures evolving locally from groyne tips and crests) and global mixing layer (GML – a superposition of local DMLs into a larger and wider mixing layer between main channel and groyne field) have been chosen. It was a surprising finding, that in both cases – submerged and emerged conditions – a GML evolves and is apparent as frequency peak in most spectra even if only short-time measurements were analysed. The GML is initiating from the DML at the first groyne tip and was further sustained by the “global” velocity gradient between the main stream and the groyne fields. Even if the mean velocity patterns differ substantially for the emerged and submerged cases, the coherent structures advected in the GML were characterised by identical peak frequencies. Furthermore, the structures are interacting with the flow inside the groyne field and are a source for instationary flow effects. During emerged conditions the coherent structures are interacting with the downstream groyne tip and are subsequently advected inside the groyne field causing fluctuations in water surface elevation. DMLs evolve at each groyne tip and are followed by peaks of turbulent kinetic energy which was similar in both cases again. DMLs are significantly affecting the local flow and the bed shear stress around the groyne tips but their influence vanishes inside the groyne fields. Structures in the DMLs lose their coherency with growing distance from the groyne tip and are amalgamated in the structures of the GML. During submerged conditions these effects are less pronounced but still recognisable. But the main difference results from the coexistence of a vertical DML shed from the groyne crest and a horizontal DML like in the emerged case. This forms a complex three-dimensional “recirculation bubble” in the lee-side of the groyne tip.

Implications for morphodynamic processes

The exchange of mass and momentum which is driven by large structures in the GML also affects the transport of sediments. The findings of this thesis indicate that during low water conditions, when groynes are usually emerged, fine sediments are likely to follow the path of the recirculation gyre. The entrainment of coherent structures and main stream sediments into the groyne field is primarily located at the downstream third of the groyne field length. From this point on towards the recirculation centre and the upstream groyne field corner, flow velocities and turbulence intensities drop and lead to deposition. Groyne fields in this way act as sediment storage zones and may cause sediment deficits in the main stream. This may enhance riverbed erosion due to the higher main stream sediment transport capacity and the decreased sediment supply. In submerged stages, sediments inside the groyne field are likely to be eroded as the sediment transport rate is proportional to the velocity. However, it has to be considered that

in case of high submergence (and assuming the same discharges), the flow in the main channel gets less accelerated when compared to emerged conditions resulting in an increased sediment supply in the main channel which could result in an increased sediment transport towards the groyne field.

The question for the optimal groyne design, regardless the purpose they are constructed for (navigability, bank protection, renaturalisation etc.) has drawn much attention recently. Groynes as river-structuring elements have become more important as nowadays the majority of rivers is canalised and the demand of ecological diversity has become more important. Many groynes were built or repaired without being aware of their effect on the flow patterns and the exchange processes between groyne field and main channel – in particular when flow conditions change from emerged to submerged due to increased flooding. This thesis has demonstrated that it is possible to perform field research in natural rivers on a high-level of detail and accuracy. The findings obtained from the “lab in the field” will be used for comparison between lab and field studies and as input data for numerical simulations in order to generalise the findings and to gain more universal insights into turbulent flow structures in groyne fields. This will include the analysis of “alternative groyne design” based on the new insights. This includes groynes constructed from living materials which are developed, tested and improved at IBLB/BOKU. Their specific characteristics like surface roughness, permeability, shape irregularity and wide spacing introduce new parameters into groyne design which partially can already be answered based on the findings of this thesis.

7 LITERATURE

- Alvarez, J.A.M. (1989) Design of groins and spur dikes. *Proceedings of the National Conference on Hydraulic Engineering* 296-301. New Orleans, USA
- Bijker, W.E. (2007) Dikes and dams, thick with politics. *Isis* 98, 109-123.
- Bischoff, A. & Wolter, C. (2001) Groyne-heads as potential summer habitats for juvenile rheophilic fishes in the Lower Oder, Germany. *Limnologica* 31, 17-26.
- Brevis, W., Nino, Y., Weitbrecht, V., & Jirka, G.H. (2008) On flow dynamics and coherent structures in submerged groyne fields. *Proceedings of the International Conference on Fluvial Hydraulics*. Izmir, Turkey
- Chu, V.H. & Babarutsi, S. (1988) Confinement and Bed-Friction Effects in Shallow Turbulent Mixing Layers. *Journal of Hydraulic Engineering-Asce* 114, 1257-1274.
- Engelhardt, C., Kruger, A., Sukhodolov, A. & Nicklisch, A. (2004) A study of phytoplankton spatial distributions, flow structure and characteristics of mixing in a river reach with groynes. *Journal of Plankton Research* 26, 1351-1366.
- Erdbrink, C. (2007) *Particle tracking in shallow mixing layer - A fluid dynamics laboratory in the field*. Msc thesis, Delft University of Technology. 1-151.
- Fujita, I., Hara, M., Moimoto, T., & Nakashima, T. (1998) Visualization and PIV measurement of river flow. *International Conference on Optical Technology and Image Processing in Fluid, Thermal and Combustion Flow*. on CD
- Hentschel, B. & Anlauf, A. (2002) *New insights in the physical and ecological processes in groyne fields* (eds A. van Mazijk & V. Weitbrecht), pp. 121-133. TU-Delft, Delft.
- Kimura, I. & Hosoda, T. (1997) Fundamental properties of flows in open channels with dead zone. *Journal of Hydraulic Engineering-Asce* 123, 98-107.
- Klingelman, P.C., Kehse, S.M. & Owusu, Y.A. (1984) Streambank erosion protection and channel scour manipulation using rockfill dikes and gabions. *Oregon State University, Water Research Institute, Corvallis, Oregon, USA*.
- Köhler, J., Pusch, M. & Gelbrecht, J. (2002) Die Spree - Zustand, Probleme, Entwicklungsmöglichkeiten. *Limnologie aktuell* 10, 1-384.
- Lacy, J.R. & Sherwood, C.R. (2004) Accuracy of a pulse-coherent acoustic Doppler profiler in a wave-dominated flow. *Journal of Atmospheric and Oceanic Technology* 21, 1448-1461.

- Lane, S.N., Biron, P.M., Bradbrook, K.F., Butler, J.B., Chandler, J.H., Crowell, M.D., McLelland, S.J., Richards, K.S. & Roy, A.G. (1998) Three-dimensional measurement of river channel flow processes using acoustic Doppler velocimetry. *Earth Surface Processes and Landforms* 23, 1247-1267.
- Lange, G. & Lecher, K. (1989) *Gewässerregelung, Gewässerpflege, Naturnaher Ausbau und Unterhaltung von Fließgewässern*, Paul Parey, Hamburg.
- Mccooy, A., Constantinescu, G. & Weber, L. (2007) A numerical investigation of coherent structures and mass exchange processes in channel flow with two lateral submerged groynes. *Water Resources Research* 43, 1-27.
- Mccooy, A., Weber, L.J. & Constantinescu, G. (2008) Numerical investigation of flow hydrodynamics in a channel with a series of groynes. *Journal of Hydraulic Engineering-Asce* 134, 157-172.
- Morris, H.M. (1955) Flow in rough conduits. *ASCE Transactions* 120, 373-410.
- Muto, Y., Baba, Y. & Aya, S. (2002) Velocity measurements in open channel flow with rectangular embayments formed by spur dykes. *Annals of Disaster Prevention Research Institute, Kyoto University* 45B-2, 449-457.
- Nakano, D. & Nakamura, F. (2006) Responses of macroinvertebrate communities to river restoration in a channelized segment of the Shibetsu River, Northern Japan. *River Research and Applications* 22, 681-689.
- Nikora, V.I. & Goring, D.G. (1998) ADV measurements of turbulence: Can we improve their interpretation? *Journal of Hydraulic Engineering-Asce* 124, 630-634.
- Nystrom, E.A., Oberg, K.A., & Rehmann, C.R. (2002) Measurement of turbulence with acoustic Doppler current profilers - Sources of error and laboratory results. *Proceedings of the Conference on Hydraulic Measurements & Experimental Methods*.
- Przedwojski, B., Blazejewski, R. & Pilarczyk, K.W. (1995) *River training techniques - Fundamentals, Design and Application*, Balkema, Rotterdam.
- Rehbock, T. (1926) *Das Flussbaulaboratorium der Technischen Hochschule in Karlsruhe*, VDI Verlag, Berlin.
- Richardson, E.V., Stevenson, M.A., & Simons, D.B. (1975) The design of spurs for river training. *Proceedings of the 16th IAHR congress*. 382-388. Sao Paulo, Brazil
- Riepe, E. (1930) *Versuche über die Wirkung inklinanter Buhnen in einer konkaven Flusskrümmung*. PHD thesis, Technische Hochschule Braunschweig. 1-234.

- Rusello, P.R., Lohrmann, A., Siegel, E., & Maddux, T. (2006) Improvements in acoustic Doppler Velocimetry. *The 7th International Conference on Hydrosience and Engineering*. Philadelphia, USA
- Schnauder, I., Sukhodolov, A., Uijttewaal, W.S.J., & Labeur, R.J. (2008) Field experiments and numerical modelling of shallow mixing layers at a confluence of two parallel streams. *Proceedings of the International Conference on Fluvial Hydraulics*. Izmir, Turkey
- Shields, F.D., Cooper, C.M. & Knight, S.S. (1995) Experiment in Stream Restoration. *Journal of Hydraulic Engineering-Asce* 121, 494-502.
- Sukhodolov, A., Engelhardt, C., Kruger, A. & Bungartz, H. (2004) Case study: Turbulent flow and sediment distributions in a groyne field. *Journal of Hydraulic Engineering-Asce* 130, 1-9.
- Sukhodolov, A., Schnauder, I., Anlanger, C., Rauch, H.P., & Uijttewaal, W.S.J. (2008) Field experiments on flow hydrodynamics and exchange processes in groyne fields. *Proceedings of the International Conference on Fluvial Hydraulics*. Izmir, Turkey
- Sukhodolov, A. & Sukhodolova, T. (2007) Coherent structures in river flows over submerged vegetation: experimental study in a lowland river. *Proceedings of the Conference on Hydraulic Measurements & Experimental Methods*. 172-177. Lake Placid, USA
- Sukhodolov, A., Thiele, M. & Bungartz, H. (1998) Turbulence structure in a river reach with sand bed. *Water Resources Research* 34, 1317-1334.
- Sukhodolov, A., Uijttewaal, W.S.J. & Engelhardt, C. (2002) On the correspondence between morphological and hydrodynamical patterns of groyne fields. *Earth Surface Processes and Landforms* 27, 289-305.
- Tominaga, A., Ijima, K., & Nakano, Y. (2001) Flow structures around submerged spur dikes with various relative height. *Proceedings of the 29th IAHR Congress*. 421-427
- Uijttewaal, W.S.J. (1999) Groyne field velocity patterns determined with particle tracking velocimetry. *Proceedings of the 28th IAHR Congress*. 226. Graz, Austria
- Uijttewaal, W.S.J. (2001) *New insights in the physical and ecological processes in groyne fields* (eds A. van Mazijk & V. Weitbrecht), TU-Delft, Delft.
- Uijttewaal, W.S.J. (2005) Effects of groyne layout on the flow in groyne fields: Laboratory experiments. *Journal of Hydraulic Engineering-Asce* 131, 782-791.
- Uijttewaal, W.S.J. & Booij, R. (2000) Effects of shallowness on the development of free-surface mixing layers. *Physics of Fluids* 12, 392-402.

- Uijtewaal, W.S.J., Lehmann, D. & van Mazijk, A. (2001) Exchange processes between a river and its groyne fields: Model experiments. *Journal of Hydraulic Engineering-Asce* 127, 928-936.
- Van Prooijen, B.C. & Uijtewaal, W.S.J. (2002) A linear approach for the evaluation of coherent structures in shallow mixing layers. *Physics of Fluids* 14, 4105-4114.
- Verhagen, H.J. (2009) Groynes in the Netherlands. URL:
<http://www.citg.tudelft.nl/live/pagina.jsp?id=3221bf8a-9be6-4a62-823f-378718174057&lang=en>.
- Weitbrecht, V. (2004) *Influence of dead-water zones on the dispersive mass transport in rivers*. PHD thesis, Universität Karlsruhe. 1-145.
- Weitbrecht, V., Socolofsky, S.A. & Jirka, G.H. (2008) Experiments on mass exchange between groin fields and main stream in rivers. *Journal of Hydraulic Engineering-Asce* 134, 173-183.
- Wirtz, C. (2004) *Hydromorphologische und morphodynamische Analyse von Bühnenfeldern der unteren Mittelbe im Hinblick auf eine ökologische Gewässerunterhaltung*. PHD thesis, Freie Universität Berlin. 1-305.
- Wolter, C., Arlinghaus, R., Sukhodolov, A. & Engelhardt, C. (2004) A model of navigation-induced currents in inland waterways and implications for juvenile fish displacement. *Environmental Management* 34, 656-668.
- Yossef, M.F.M. (2005) Morphodynamics of rivers with groynes. *Delft Hydraulics Selected Series* 7, 1-216.
- Zuisen, L., Kohji, M., & Shiro, M. (2007) Hydraulic characteristics of a group of permeable groins constructed in an open channel flow. *Proceedings of the 32th IAHR Congress*. 7-10. Venice, Italy